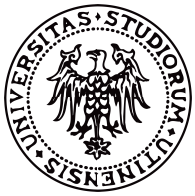

UNIVERSITY OF UDINE

PHD COURSE IN ENVIROMENTAL AND ENERGY
ENGINEERING SCIENCE
XXXVI CYCLE

Methods to improve efficiency of CO_2-based refrigerating systems: Zeotropic mixture, Energy storage, Cycle modifications

Candidate:
Gabriele Toffoletti

Supervisor:
Prof. Giovanni Cortella

A thesis submitted in fulfillment of the requirements for the degree of Doctor of Philosophy

2024

Author's e-mail:

toffoletti.gabriele@spes.uniud.it
gabriele.toffoletti@gmail.com

Author's adress:

Refrigeration and Heat Pumps research group
Polytechnic Department of Engineering and Architecture
University of Udine
via delle Scienze 206
33100 Udine - Italy

Last update

Udine - January 22, 2024

"You're never really done for, as long as you've got a good story and someone to tell it to."

Max Tooney - The legend of 1900

Credits

I, Gabriele Toffoletti, declare that this thesis entitled, "Methods to improve efficiency of CO_2-based refrigerating systems: Zeotropic mixture, Energy storage, Cycle modifications" and the work presented are:

- **Chapter 2**: This work was carried out at the Thermal Engineering Research Group Laboratory at the Jaume I University, Castellò de la Plana (Spain), under the supervision of Prof. Rodrigo Llopis Doménech.
- **Chapter 3**: The experimental part of the work was carried out at the Thermal Engineering Research Group Laboratory at the Jaume I University, Castellò de la Plana (Spain), under the supervision of Prof. Rodrigo Llopis Doménech who made the experimental facility available.
- **Chapter 4**: The experimental part of the work was carried out at the Thermal Engineering Research Group Laboratory at the Jaume I University, Castellò de la Plana (Spain), under the supervision of Prof. Rodrigo Llopis Doménech who made the experimental facility available.
- **Chapter 5**: The experimental part of the work was carried out at the Ray W. Herrick Laboratories at the Purdue University, West Lafayette - Indiana (USA), under the supervision of Prof. Davide Ziviani who made the experimental facility available.
- **Chapter 6**: This work was carried out at the Refrigeration and Heat Pumps research group at the University of Udine.

Udine - January 22, 2024

Abstract

The Heating, Ventilation, Air Conditioning and Refrigeration (HVAC&R) sector plays an essential role into the 21st-century life, silently but significantly influencing numerous domains, including but not limited to food preservation, indoor climate control, healthcare, industrial processes, and energy management. According to the IIR, it is estimated that there are approximately 5 billion refrigeration, air-conditioning, and heat pump systems currently operational around the globe. Still according to IIR, the refrigeration sector, including air conditioning, consumes about 20% of the overall electricity used worldwide with a demand that could be more than double by 2050. The sector is responsible for 7.8% of the world greenhouse gas emissions (4.14 $GtCO_{2,eq}$), from which 37% are caused by direct escapes of refrigerants and 63% are related to indirect emissions due to the use of electricity. This thesis aims to reduce these two sources of environmental impact by presenting a work that involves CO_2 as a refrigerant fluid used as a method to reduce direct emissions, with the focus on improving its utilisation as a solution to indirect emissions. The work is structured in two parts, with the first focusing on the possibility of increasing the efficiency of CO_2 plants through zeotropic mixtures: by doping carbon dioxide or by using these mixtures in a dedicated mechanical subcooling system (DMS). The second focusing on pure CO_2 system, analysing different possible configurations of both the refrigeration cycle and also of the whole plant, in this case with the use of a thermal storage. The order of the chapters follows a structure that focuses on the mixtures at the beginning, enlarging the viewpoint on the different cycles and then further enlarging the viewpoint on the global system connected to the supermarket building.

Several CO_2-doped blends are evaluated theoretically and experimental analysis of the CO_2/R-152a mixture was conducted. Experimental tests show the potential for enhancement of COP in typical CO_2 cycles with the use of mixtures replacing pure CO_2; in particular, the use of CO_2/R-152a [90/10%] and CO_2/R-152a [95/5%] mixtures provided maximum COP improvement of 10.2% and 10.6% respectively for the same heat rejection temperature. On the other hand, for a cycle with internal heat exchanger (IHX), the use of the new mixture decreases energy efficiency with the only exception observed with CO_2/R-152a [95/5%] and an inlet temperature

of 35 °C, which led to a 0.4% improvement in COP. Finally, the use of a zeotropic mixture in a dedicated mechanical subcooling (DMS) system improves efficiency by only 1.4% with the R-600/R-152a [60/40%] blend however confirming the theoretical results trend.

Moving on to the second part, an analysis of commercial CO_2 refrigeration cycles is conducted. Four CO_2 cycles were experimentally compared in the same plant over four ambient conditions, with a maximum improvement by 4.64% and 9.47% when ejector and IHX cycles are used respectively. A variable-diameter nozzle and liquid CO_2 pump were assessed as ejector control methods; The CO_2 pump, once successfully stabilized, can control the ejector, increase its efficiency to a maximum of 11% and increase the cooling capacity to a maximum of 6.2%. Nevertheless, a reduction in COP is measured when the pump is in use; however, unlike the other three different configurations, it was only analyzed under subcritical conditions due to a limited operational envelope. Then a real case of a supermarket with an Ice Thermal Energy Storage (ITES) is analysed, where the storage can be fruitfully used to shave peaks in electricity use. In the particular configuration analysed, the storage shows to be detrimental for the energy efficiency; however, the cost analysis shows that the reduction in size of the reversible heat pump, and the chance to avoid the installation of an electrical transformer in a dedicated room allows saving up to 58699 € in 10 years, thus making the choice of ITES more profitable in the usual lifetime for these plants.

Acknowledgements

Trying to avoid clichés, I would like to thank:

My supervisor Giovanni, thank you for always helping me in every way, in every place and in every time zone. I really envy your leadership style, I am very inspired by your natural way of dealing with problems. Thank you for giving me this opportunity!

Rodri, thank you for hosting me again, and again, and again... thank you for your contagious passion, I hope one day to be able to give back all that I have received.
Carioca&Los Papus, to be honest, I wouldn't know how to translate *De locos, pep!* in English.
Laura, thank you for your help, your advice, your friendship and for your period abroad with us. You will be missed, and not only by the University of Udine.

Prof. Ziviani, thank you Davide for hosting me at the Herrick Labs, having the opportunity to do research in the world's largest academic HVAC laboratory is no small feat, and for this, I am very grateful to you.
Fatih, thank you for your academic and non-academic help and Steven, hearing a Colombian sing Vasco Rossi while repairing the plant, was one of the most satisfying moments of my journey.
I am grateful to all the people who helped me inside, and outside the laboratory! I cannot avoid mentioning among them Laura and the Indian Parveen's crew, thank you for your kindness, and for teaching me humility through squash.

Contents

List of Figures

List of Tables

Nomenclature

A	Area	$[m^2]$
C_p	Specific heat	$[J(kgK)^{-1}]$
e	Electricity price	$[€(kWh)^{-1}]$
$\dot{E}_X$	Exergy	[kW]
F	Binary-specific multiplier	[-]
h	Specific enthalpy	$[[J(kg)^{-1}]]$
h_e	Heat transfer coefficient	$[W(m^2K)^{-1}]$
I	Uncertainty	[Units Vary]
k	Thermal conductivity	$[W(mK)^{-1}]$
$\dot{m}$	Mass flow rate	$[kg(s)^{-1}]$
M	Mass	[kg]
n	Plant service lifetime	[Years]
p	Pressure	[bar]
p_c	Critical Pressure	[bar]
P	Power consumption	[kW]
q'	Heat flow rate per unit length	$[W(m)^{-1}]$
$\dot{Q}$	Heat Flow rate	[kW]
R'	Thermal resistance per unit length	$[W(mK)^{-1}]$
r	Radial position - Discount rate	[m] – [-]
s	Specific entropy	$[J(kgK)^{-1}]$
SH	Superheating degree	[K]
t	Temperature	[°C]
t_c	Critical Temperature	[°C]
U	Internal Energy	[J]
UA	Overall conductance	$[W(K)^{-1}]$
w	Entrainment ratio	[-]
w_s	Specific isentropic compression work	$[J(kg)^{-1}]$
x	Quality or vapour title	[-]
$\dot{V}$	Volumetric flow	$[m^3(h)^{-1}]$

Z	Mass fraction of components	[-,%]
Z_v	Mass fraction of components of saturated vapour	[-,%]
Z_l	Mass fraction of components of saturated liquid	[-,%]
β,γ	REFPROP fitting coefficients	[-]
Δ	Difference	[Units Vary]
ϵ	Thermal effectiveness - Measurement accuracy	[-] - [Units Vary]
ρ	Density	$[\mathrm{kg}(\mathrm{m}^3)^{-1}]$
η	Efficiency	[-,%]
λ	Latent heat	[J/kg]
ν	Specific suction volume	$[\mathrm{m}^3(\mathrm{kg})^{-1}]$
τ	Time	[s]

List of Abbreviations

AC	Air Conditioning
AEC	Annual Energy Cost
BP	Back-Pressure Valve
COP	Coefficient of Performance
CC	Capital Cost
CRU	Commercial Refrigeration Unit
DHW	Domestic Hot Water
DMS	Dedicated Mechanical Subcooling
ECHA	European Chemicals Agency
EG	Ethylene Glycol
EXV	Expansion Valve
FS	Full Scale
FT	Flash Tank
GC	Gas Cooler
GWP	Global Warming Potential at 100 years
HP	Heat Pump
HPV	High Pressure Valve
HR	Heat Recovery
HS	High Stage
HVAC	Heating, ventilation, Air Conditioning
HX	Heat exchanger
IC	Intercooler
IHX	Internal heat exchanger
ITES	Ice Thermal Energy Storage
MT	Medium Temperature
PFAS	Per- and Polyfluoroalkyl Substance
P&ID	Piping and Instrumentation Diagram
LS	Low Stage
LT	Low Temperature

PC	Parallel Compressor
RC	Running Cost
RDG	Reading
VCC	Volumetric cooling capacity
VFD	Variable Frequency Drive

Subscripts

aux	Refers to the auxiliary compressor
base	Refers to CO_2 cycle without subcooling
CO_2	Refers to the CO_2 cycle
comp	Compressor
cool	Cooling capacity
d	Ejector diffuser outlet
dis	Compressor discharge
DMS	Refers to the dedicated mechanical cycle
env	Environment
e	Effective
ev	Evaporation
g	Refers to propylene glycol/water mixture
gc	Refers to gas-cooler
i	Iteration counter
in	Inlet
k	Condenser
l	Saturated liquid
lmtd	Logarithmic mean temperature difference
main	Refers to the main compressor
o	Refers to evaporator
out	Outlet
int	Internal
ITES	Refers to the Ice Thermal Energy Storage
r	Return
sf	Secondary fluid
sub	Subcooling
suc	Compressor suction
trans	Refers to transcritical operation

v	Saturated vapour
w	Refers to water
0	Initial

Dedicated to
Carmofroz, Gioovi, Chino, Jacum and Francesca

Chapter 1

Introduction

1.1 Motivation

One of the main challenges in contemporary refrigeration is the development of environmentally friendly refrigeration technologies, focusing both on efficiency of equipment and the use of low-impact refrigerants. The exponential expansion of the world's population, coupled with industrialisation and globalisation, has elevated global warming to one of mankind's most pressing concerns. Refrigeration is closely linked to modern life and serves a multitude of needs. From essential functions such as preserving food and medical supplies to improving comfort and quality of life through air conditioning, refrigeration plays an indispensable role. It is also crucial in numerous industrial processes and applications. Given the expanding population and widespread use of cooling systems, refrigeration is an area with significant environmental consequences.

According to the International Institute of Refrigeration (IIR), the global number of refrigeration and air conditioning systems is close to 5 billion, consuming about 20% of the world's total electricity consumption [1]. The IIR also states that the refrigeration sector is responsible for about 7.8% of global greenhouse gas emissions, whose 37% attributed to direct emissions (leakage) of fluorinated refrigerants (CFCs, HCFCs and HFCs) and 63% coming from indirect emissions [2]. The Montreal Protocol on Substances that Deplete the Ozone Layer [3], an international treaty designed to safeguard the ozone layer, garnered consensus among the world's economies to eliminate the production and consumption of ozone-depleting substances by 2030. Developed countries committed to an even earlier deadline of 2020.

The Kigali Amendment [4] to the Montreal Protocol, effective from January 1, 2019, accelerated the global reduction of HFC_s (hydrofluorocarbons), fostering the adoption of natural refrigerants, such as CO_2. As of June 2020, 93 countries and the European Union have ratified this amendment, however, this numbers every changing as more countries pledge their commitment to drastically scale down the use of HFC_s.
In Europe, the 2014 F-Gas Regulation [5] is set to phase down the use of HFCs, by 79% by 2030. It has a significant impact on users of HFC refrigerants, since HFCs (GWP > 150) are prohibited in multipack centralized refrigeration systems with a power greater than 40kW with the exception of primary refrigeration circuit of cascade systems where GWP higher than 1500 may be used. Furthermore, on 5 April 2022, the European Commission made a legislative proposal to update the F-gas Regulation, and as a consequence, there is a provisional agreement in October 2023 [6]. The proposal has the objective of preventing almost 500 million tonnes of further emissions by 2050. It might contribute to the EU's 2030 climate targets of at least 55% emission reductions, and help make Europe climate-neutral by 2050. In particular, the proposal agreement tightens the quota system for hydrofluorocarbons (HFC phase-down). The use of hydrofluorocarbons (HFCs) might be reduced by 95% by 2030 compared to 2015, to zero by 2050.

Among the natural refrigerants, Carbon Dioxide (CO_2) offers several advantages, such as excellent transport and thermo-physical properties, being neither toxic nor flammable, and also having a low price and high availability around the world. However, due to its relatively low critical temperature of 30.9 ºC and high critical pressure of 73.9 bar, this refrigerant exhibits distinctive characteristics that need to be taken into account during its application.

It is estimated that there are more than 35000 transcritical CO_2 installation globally today with 29000 located in Europe [7]. In Figure 1.1 the global distribution of installations around the planet is presented where the number of installations is strongly influenced by the environmental policies of the country under consideration. Moreover, with 140 installations in 2008, rising to 35500 in 2020, growth is significant, not only in Europe as is shown in Table 1.1 with data from 2008 to 2020 [7].

Among the transcritical plants in Europe, 90% CO_2-stores implement

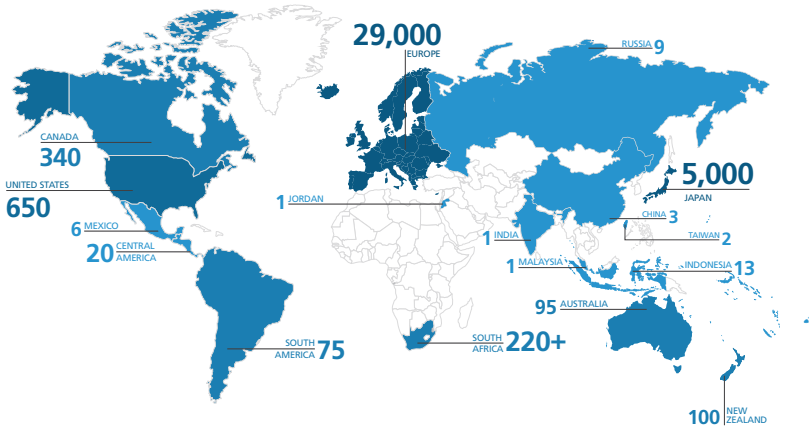

FIGURE 1.1: Global distribution of transcritical CO_2 installation [7]

TABLE 1.1: Growth data of transcritical CO_2 plants over the years [7]

Region	Number of transcritical CO_2 installations in 2008	Number of transcritical CO_2 installations in 2018	Number of transcritical CO_2 installations in 2020	Growth in % from 2018 to 2020
Europe	140	>16000	29000	81%
U.S	-	>370	650	76%
Canada	-	>245	340	39%
Japan	-	>3530	5000	42%
Australia	-	>20	95	375%
New Zealand	-	>40	100	150%
South Africa	-	>110	>220	100%

medium or large-sized architectures (cooling capacity >40kW), 5% are industrial systems and only 5% are systems for low-sized capacities, which are usually known as condensing units. The high percentage of large CO_2 systems is explained by economic reasons, since they allow higher investment rate, so they can rely on advanced refrigeration architectures. However, the investment in high-efficiency CO_2 cycles for low-capacity systems may not always be profitable, so manufacturers usually still rely on condensing units operating with HFC or HFO fluids. In fact, with capacities between 4 to 40kW, penetration of ultra-low GWP solutions is not a fact. While new stand-alone refrigeration systems (cooling capacity lower than 4kW) are based on hydrocarbons (R-600a and R-290), they do not allow reaching sufficient cooling capacity with the current charge limits (Calleja-Anta et al. [8]; International Electrotechnical Commission [9]). Concerning external systems, the limitation of charge depends on the regulation EN 378 [10], following the criteria of distance, positioning and type of system used. As a definition used in this thesis, "large size" refers to rated capacity greater than 40 kW following F-Gas regulation for "centralised refrigeration system" [5], considering the charge limitations on typical stand-alone refrigeration systems just described, "small size" refers to capacity below 4 kW and medium size to rated capacity between 4 and 40 kW.

1.2 Research Context

To reduce the direct global warming impact of refrigerants in HVAC&R applications, low-global warming potential (GWP) refrigerants, including natural refrigerants, have been extensively investigated as alternatives to hydrofluorocarbon (HFC) refrigerants. Among the natural refrigerants, Carbon Dioxide (CO_2) offers several advantages, such as excellent transport and thermo-physical properties, being neither toxic nor flammable (A1 according to the ASHRAE standard [11]), and also having a low price and high availability around the world. However, the high critical pressure and low critical temperature of CO_2 often lead to transcritical operation, conditions in which it is necessary to increase the complexity of the system compared to subcritical cycles in order to achieve high efficiencies. With the aim of achieving high efficiencies for the CO_2 plants, the approaches to be

taken can be from the fluid point of view, or from the cycle point of view.

In this thesis, the state of the art will be divided into sections under the same topic for ease of reading.

1.2.1 Pure CO_2 cycles

Ejector

A significant number of cycle modifications have been proposed to increase the COP of transcritical CO_2 cycles, and within this topic, expansion work recovery has proven to have significant potential. One of the most widely used methods of expansion work recovery in refrigeration is the ejector, which was first introduced by Gay [12] with regard to the two phase ejector type. The past decades have brought about a large amount of numerical and experimental research on ejectors. Liu et al. [13] presented performance enhancement of a transcritical CO_2 air conditioner with a controllable ejector at variable operating conditions and variable compressor frequencies. They show experimentally how the COP of a CO_2 air conditioning system can be enhanced by using an ejector expansion device to replace a conventional expansion valve, with COP improvement up to 36%. Lucas and Koehler [14] evaluated an experimental comparison between the standard CO_2 expansion valve refrigeration cycle and the ejector refrigeration cycle is presented with COP improvements of the ejector cycle of 17% were reached with ejector efficiencies of up to 22%. However, because the primary purpose of an expansion device in a vapor compression cycle is cycle control, active control of the ejector has become a research focus. Elbel and Hrnjak investigated an ejector with a variable-diameter motive nozzle (Elbel and Hrnjak [15]), resulting in COP and cooling capacity improvements of 7% and 8%, respectively, as well as proving the device control could be used to vary the gas cooling pressure of the cycle to achieve a maximum COP. Another strategy for ejector control is the multi-ejector, introduced by Hafner et al. [16] and experimentally investigated by Haida et al. [17]. In the latter work, COP and exergetic efficiency benefits of 7% and 13.7%, respectively, were obtained compared to the standard high-pressure valve expansion mode for a parallel compression cycle R744 refrigeration unit. Moreover, cycle stability was validated through variation of both ambient temperature and

flash tank pressure. Zhu and Elbel [18] found that introducing a tangential flow upstream of a converging-diverging nozzle to impart a swirl could be an effective method to control nozzle performance.

Subcooling methods

Additionally, there has been considerable research on "subcooling" techniques applied at the gascooler outlet in transcritical CO_2 refrigeration systems. As pointed out by S.M. Hojjat Mohammadi [19], for a transcritical refrigeration system, the term subcooling is not suitable to use as there is no real subcooling in the supercritical pressures. However, most research works also consider CO_2 subcooling under subcritical conditions, where, according to Mohammadi [19], the term "subcooling" would be appropriate. Since most research has used the term "subcooling", the same nomenclature has been followed in this thesis. Subcooling has been recognised during the last years as a useful technology to enhance the performance of refrigeration cycles. Subcooling, as reviewed by Park et al. [20] for subcritical cycles, consists in chilling the liquid at the exit of the condenser, thus incrementing the refrigerating effect and, in general, improving the coefficient of performance. However, when subcooling is used in transcritical systems the benefits of this method are taken to an extreme, as analysed by Llopis et al. [21]. In transcritical cycles the decoupling between pressure and temperature in the supercritical region makes it possible, for the subcooling operation, to reduce the enthalpy of the refrigerant at the inlet of the first expansion stage and at the same time to cut down the optimum heat rejection pressure. The combination of both outcomes increases the refrigerating effect per unit mass and at the same time reduces the compression ratio and thus diminishes the power consumption of the compressor, resulting in large increments on capacity and COP. Specifically, using internal heat exchangers increments up to 12% in COP have been measured (Torrella et al. [22]), using economizers (subcooling by expanding a part of the liquid) up to 21% (Cavallini et al. [23]) and using thermoelectric subcoolers up to 9.9% (Sánchez et al. [24]). Concretely, one of the most appealing methods is the subcooling based on an external vapour compression cycle, known as dedicated mechanical subcooler (DMS) (Bertelsen and Haugsdal [25]; Llopis et al. [26]). In this case the subcooling is provided at the exit

of the condenser/gas-cooler using an auxiliary vapour compression cycle with a heat exchanger (subcooler) where a different refrigerant evaporates. The main characteristic of this system is that both cycles, the main and the auxiliary, perform heat rejection at the same temperature level and the DMS operates a low temperature span, thus with high efficiency. Initial experimental tests in single-stage plants measured capacity and COP improvements of 55.7% and 30.3% respectively using R-1234yf as refrigerant in the DMS (Llopis et al. [27]) only with the optimization of the heat rejection pressure. Later, with an updated version of the plant and using R-152a in the DMS (Nebot-Andrés et al. [28]), they demonstrated the existence of optimum working parameters and determined them, heat rejection pressure and subcooling degree, which are the two main variables to control in this cycle. In addition, Dai et al. [29] have also verified from a theoretical approach that the DMS system is also useful to improve the performance of heat pumps for residential heating, with predicted COP increments up to 24.4% (Dai et al. [30]).

Booster systems

The complexity increases with multi-evaporator cycles: they are commonly applied in both supermarket and transport refrigeration due to the need to maintain cooling compartments at different temperatures while using a centralized vapor compression cycle. To offer a transportation container refrigeration perspective, Lawrence et al. [31] numerically assessed the performance of a multi-temperature refrigerated transportation container system using a transcritical CO_2 with an ejector and internal heat exchanger, resulting in a COP of 0.96 at an extreme ambient temperature of 57 °C. Barta et al. [32] also investigated a multi-temperature refrigeration container system numerically, applying an expander and a flash tank upstream of the medium temperature (MT) evaporator, achieving a COP of 1.28 at an ambient temperature of 57.2 °C. These papers numerically displayed the ability of complex cycles to be applied to multi-evaporator transportation container refrigeration systems in an effort to achieve COP values equal to or over unity, motivating further experimental investigation. The cycle architectures applied in transcritical CO_2 supermarket applications vary

in complexity in order to achieve performance benefits over the HFC cycles they seek to replace, depending on the proposed ambient conditions (Karampour and Sawalha, [33]). On the complex end of this spectrum, Minetto et al. [34] experimentally investigated parallel compression, ejector expansion work recovery, and flooded evaporation in a multi-evaporator architecture, reducing compressor power consumption by 13% at an ambient temperature of 16 °C. Numerous technical approaches can be employed to enhance the energy efficiency of the fundamental booster CO_2 system, striving to achieve energy performance at least on par with conventional HFC-based plants. The literature contains various publications that offer comparisons among different solution alternatives. Gullo et al. [35] theoretically evaluated the multi-ejector concept where a drop energy consumption by 19.4% over a R-404A system is calculated and a potential energy saving of 15.6% can be achieved if integrated CO_2 solution were used. Sawalha [36] evaluated a COP improving of 3-7% along the temperature range of 10-40 °C among some possible modifications and improvement on the CO_2 systems solutions for supermarket refrigeration compared to R-404A. A review which provides numerous examples of multi-evaporator architectures, expansion work recovery, and phase separation was written by Gullo et al. for additional reference (Gullo et al. [37]). In relation to the application of the DMS to CO_2 booster systems, Bush et al. [38] tested a lab-scale plant with R-134a in the DMS, measuring a COP improvement of 9.5%. Nonetheless, with other different approaches, the use of the DMS with booster systems has been analysed (Bush et al. [39]; Catalán-Gil et al. [40]; D'Agaro et al. [41]; Gullo et al. [42]). The general conclusion of these investigations is that the application of the DMS cycle to booster systems is as more beneficial as higher the heat rejection temperature (or environment temperature) is. In fact, Catalán-Gil et al. [40] predicts, for a medium-sized supermarket, annual reductions of electricity consumption between 2.9 to 3.4% in warm regions and from 3.0 to 5.1% in hot zones.

All-in-one systems

Furthermore, the management of the supermarket does not only include the cooling capacity, but all the management of the possible heat produced and the electrical energy consumed during the day. In fact heat recovery,

together with flooded evaporation, parallel compression and integration of air conditioning, is one of the most promising features of integrated CO_2 system. In particular, Karampour and Sawalha [33] state how according to the calculation results, heat recovery in two stages is an energy efficient solution to provide tap water heating and space heating demands. Space heating of the CO_2 system was about 10% higher than a stand-alone air source heat pump. Tap water heating was also provided by the CO_2 system with high average COP values of 5.4. In the same paper, the heating provided by CO_2 is about 50% cheaper than purchasing the heat from district heating network, and 20% cheaper than providing the heat by air source heat pump. Polzot et al. [43] report as the global energy consumption is about 10% lower, together with a significant reduction in the investment cost respect to a CO_2 refrigeration system together with two electric heat pumps for space heating and hot water production. With CO_2 systems the high temperature reached at the compressor discharge side and the high heat capacity of the gas at supercritical conditions has opened to new opportunities for heat recovery solutions. Heat rejected by the refrigeration cycle can be recovered at different temperature levels, placing the heat exchanger(s) at the compressor discharge before the gas-cooler, or in place of the gas-cooler (or condenser in subcritical mode), or at the exit of the gas-cooler, acting as a subcooler in subcritical mode (Sawalha [36]; Karampour and Sawalha, [44]).

Furthermore, the profile of electrical power use in a shopping mall is strongly uneven and subject to considerable daily fluctuations. At nighttime the energy demand is very low, thanks to the reduced refrigerating capacity required by food storage equipment and to the HVAC system being idle; during the day, high refrigeration and air conditioning loads occur almost simultaneously, early in the morning or around noon. Thermal energy storage (TES) is therefore suggested to shift loads, in order to achieve a better daily average energy efficiency, to take advantage of time-of-use tariffs, and to allow some reduction in the design capacity of the systems.

Most PCM_s analyzed by researchers and commercial companies with a melting temperature below 0 °C are eutectic solutions of water salts, while above 0 °C are organic PCMs. Eutectic salt solutions are good in terms of thermophysical properties such as enthalpy of phase change (since water is the main component) and are cheap; however, due to the incorporation

of the mixture with salts, they could be chemically unstable and corrosive. On the other hand, most organic PCM_s are non-corrosive and chemically stable, but they have lower thermal conductivity, lower latent heat, greater volume change between solid and liquid phases, and are relatively expensive [45]. The most studied low-temperature PCM is water for obvious reasons: it is cheap, has the best thermal properties and also has good long-term stability. Primarily used in air conditioning systems for peak load shifting since this technology is mature and commercially available. As far as air conditioning is concerned, passive (often PCM) elements on the air side can be used for their simplicity and reliability, but with the main purpose of dumping supply air temperature during on-off cycles or defrosting periods of heat pumps. Higher storage capacity can be easily achieved by using water storage; in some cases, a huge water reservoir for fire prevention is available, and can be effectively used for this purpose. (Polzot et al. [46]) investigated its application to subcool a refrigerating system or to act as a source for a heat pump in heating operation (Polzot et al. [47]). Instead, in the case of air conditioning the typical operating temperatures reduce the feasibility options for a TES. Despite the need to perform cooling at below zero temperature, which seems ineffective when compared to the typical evaporating temperature for air conditioning purposes, such systems have been investigated from both energy and exergy points of view, and encountered some interest (Sanaye and Shirazi [48]; Yau and Rismanchi [49]). However, their performance and energy effectiveness are strictly correlated to their control rules, (Beghi et al. [50], Candanedo et al. [51]) which involve a clear definition of the aim of the system and a thorough prediction of the user demand profile often related to weather forecast.

1.2.2 CO_2 doped blends

Acting on the "fluid point of view", while CO_2 is the standard for medium to large-sized commercial applications, as it combines safety and low environmental impact. Recently, CO_2-doping (the addition of a small quantity of another fluid) has attracted scientific attention, as when CO_2 is mixed with fluids with higher critical temperatures, the optimum operation moves to subcritical, providing COP increments in relation to pure-CO_2 operation. During the last decade, there has been a rising interest in extending the

use of CO_2 to medium-capacity refrigeration systems, trying to implement simple architectures by using refrigerant mixtures. Kim et al. [52] measured that blends of CO_2 with propane were able to improve the performance of an air-conditioning system through glide matching in the heat exchangers, reporting that the mixture CO_2/R-290 [85/15%] offered 8% higher COP than pure CO_2. It was observed that doping CO_2 with small quantities of other fluids also allowed for the reduction of optimum working pressures, though the capacity of the plants was reduced and the blend introduced a large glide in the phase change processes. Similar results were obtained with a similar mixture by Zhang et al. [53]. In light of these studies, several works in the last years have focused on the analysis of CO_2-doped blends in refrigeration systems, the doping agents of which are detailed in Table 1.2. From a theoretical perspective, Wang et al. [54] considered R-41 as a doping agent for its use in a refrigerated MT cabinet, concluding that CO_2/R-41 [50/50%] blend could increase the COP by 28.62%. Kumar and Kumar [55] evaluated the blend with R-290 for chiller applications, reporting that 15% of R-290 allowed the cycle to operate in subcritical conditions due to a high pressure reduction, but they did not report COP increments. Zhao et al. [56] evaluated the use of butane, isobutane and two pure HFOs as CO_2 doping agents for application in single-stage and two-stage cycles with IHX for LT applications. All the combinations offered COP increments in relation to CO_2 and they selected the ternary mixture R-744/R-1234ze(E)/R-1234ze(Z) as best mixture. Xie et al. [57] extended the analysis considering R-152a and R-161 for its application in a single-stage cycle. At the evaluation conditions, they predicted a huge COP increment of 26%. Finally, Vaccaro et al. [58] extended the analysis with three hydrocarbons (R-600a, R-600 and R-290) and three hydrofluoroolefins (R-1234ze(E), R-1234ze(Z) and R-1233zd(E)). This is the widest theoretical evaluation to date, as it covers the application of CO_2-doped blends in the single-stage cycle with an IHX, a flash-gas separator, and an ejector. For an application at an evaporation temperature of -15ºC and a gas-cooler exit temperature of 40ºC, they concluded that CO_2/R-1234yf and CO_2/R-290 were the best blends, reaching COP increments up to 12.8% with R-1234yf and 7.9% with R-290 (base cycle with IHX).

Nevertheless, experimental validation of the theoretical hypothesis is scarce, but Tobaly et al. [59] were able to measure 19.7% COP increment in relation to CO_2 using the mixture CO_2/R-290 [90/10%] as refrigerant

at air-conditioning conditions with a single-stage test rig with IHX and scroll compressor. Later, Yu et al. [60] extended the analysis of CO_2/R-290 mixtures as working fluid in MAC systems measuring 22% COP increments. And finally, Sánchez et al. [24, 61] evaluated R-290, R-1270 and R-32 as doping agents of CO_2 in order to create fluids that were used as refrigerants in a beverage cooler for positive temperature applications. In this case, under fixed climatic chamber conditions, they measured energy consumption reductions in relation to pure-CO_2 up to 17.2% at an environment temperature of 25ºC and up to 12.2% at 30 ºC. These works confirm that it is possible to enhance the performance of basic cycles which use CO_2 as working fluid by using, instead, a blend made by doping the pure CO_2 with a small quantity of another fluid.

TABLE 1.2: Theoretical and experimental works about the use of CO_2-doped blends in refrigeration systems

Author	Character[a]	R-600	R-600a	R-290	R-601	R-1270	R-152a	R-134a	R-161	R-41	R-32	R-1234yf	R-1234ze(E)	R-1234ze(Z)	R-1233zd(E)
Wang et al.[54]	T									■					
Kumar et al.[55]	T			■											
Vaccaro et al.[58]	T		■	■	■							■	■		■
Xie er al.[57]	T						■		■						
Zhao et al.[56]	T	■	■											■	■
Li et al.[62]	T	■	■				■	■		■		■		■	■
Kim et al.[52]	E			■											
Zang et al.[53]	E			■											
Tobaly et al.[59]	E			■											
Yu et al.[60]	E			■											
Sanchez et al.[61]	E					■									
Sanchez et al.[24]	E			■		■					■				

[a]T= Theoretical; E= Experimental

1.3 Identified gaps and research questions

From the research background presented above, various gaps and research questions that require a solution are identified.

The existing works regarding the possible utilization of the CO_2-based blends are focused on air-conditioning systems or small stand-alone refrigeration systems (<4 kW) and no works have been found in relation to condensing unit applicable to medium-sized refrigeration applications.

There is a lack of experimental data for the evaluation of different CO_2 refrigeration cycles with doping agents.

Dai et al. [63] launched a hypothesis about the use of zeotropic refrigerant mixtures with matching glide in the DMS cycle, to reduce the temperature difference in the subcooler and thus to improve the performance of the combination. However, Dai's hypothesis has not been verified experimentally for the moment.

Despite the significant amount of research that has been conducted on the topic of performance enhancing measures to transcritical CO_2 refrigeration cycles, there are very few publications that cover so many cycles compared on the same refrigeration plant, nor are there any papers which conduct an experimental comparison of the use of a CO_2 pump as a method of ejector control.

Clearly defining the potential improvements of a thermal energy storage in a complex system such as a real supermarket is not straightforward, energy and cost parameters over the lifetime of the system must be taken into account and there is a lack of analysis based on real data from the field.

1.4 Contribution to the knowledge

The contribution of this study to the knowledge can be summarized as follows:

- Investigating the effect of several CO_2-doped blends in different architectures, taking into account the fractionation inside the system.
- Filling the existing gap in terms of experimental evaluation of CO_2-doped blends in different refrigeration cycle architectures.

- Experimentally proving the benefits of non-azeotropic mixtures in a Dedicated Mechanical Subcooling system used in a transcritical CO_2 refrigeration cycle.
- Presenting a simulation model for predicting ice formation and melting in an Ice Thermal Energy Storage.
- Exhaustively investigating the energy/cost advantages associated with the use of an ITES in a real supermarket booster system.
- Presenting an experimental evaluation comparing four different architectures in the same plant utilizing intercooling, open economization, an internal heat exchanger and an ejector.
- Presenting an experimental evaluation of two ejector control methods, a variable-diameter motive nozzle and a variable-speed liquid CO_2 pump located directly upstream of the ejector motive nozzle inlet.

1.5 Publications

The outcomes of this thesis have been published in the papers:

1.5.1 Papers for international conferences

- M. Martinez, E. Sicco, **G. Toffoletti**, L. Nebot, R. Cabello, P. D'Agaro, R. Llopis Theoretical assessment of CO_2-based blends as refrigerants. Evaluation in different refrigeration architectures. 26th ICR international congress of refrigeration, Paris, France 21-25 August 2023
- E. Sicco, M. Martinez, **G. Toffoletti**, L. Nebot, G. Sanchez, G. Cortella, R. Llopis Experimental evaluation of different refrigeration system configurations using CO_2-based blends as refrigerants 26th ICR international congress of refrigeration, Paris, France 21-25 August 2023
- **G. Toffoletti**, L. Nebot-Andrés, M. Martinez, G. Cortella, R. Llopis Evaluation of zeotropic mixtures as refrigerants in a dedicated subcooling system of a CO_2 refrigeration plant XI Congreso Ibérico y IX Congreso Iberoamericano de Ciencias y Técnicas del Frío, Cartagena, Spain 17-19 April, 2022

- P. D'Agaro, M. Libralato, **G. Toffoletti**, G. Cortella Demand Coverage and Energy Savings by Combined CO_2 Refrigeration System and HVAC in Supermarkets 7th IIR conference on Sustainability and the Cold Chain, Newcastle (UK) 11-13 April, 2022
- P. D'Agaro, M. Libralato, **G. Toffoletti**, G. Cortella Ice thermal energy storage for electricity peak shaving in a commercial refrigeration/HVAC unit 6th IIR Conference on Thermophysical Properties and Transfer Processes of Refrigerants, Vicenza Italy 1-3 September, 2021

1.5.2 Papers for international journals

- **Toffoletti G.**, Barta R., Grajales M., Liu H., Ziviani D., Groll E. Experimental Comparison of Cycle Modifications and Ejector Control Methods in a Multi-Evaporator Transcritical CO_2 Refrigeration System - International Journal of Refrigeration - (Under review)
- **Toffoletti G.**, Cortella G., D'agaro P. Thermodynamic and economic seasonal analysis of a transcritical CO_2 supermarket with HVAC supply through ice thermal energy storage (ITES) - Journal of Cleaner Production - DOI
- Sicco E., Martinez M., **Toffoletti G.**, Nebot-Andrés L., Sanchez D., Cabello R., Llopis R., Cortella G. Experimental evaluation of CO_2/R-152a mixtures in a refrigeration plant with and without IHX - International Journal of Refrigeration - DOI
- Martinez M., Sicco E., **Toffoletti G.**, Nebot-Andrés L., Sánchez D., Cabello R., Cortella G., Llopis R. Evaluation of CO_2-doped blends in single-stage with IHX and parallel compression refrigeration architectures - International Journal of Refrigeration - DOI
- Llopis R.,**Toffoletti G.**, Nebot-Andrés L., Cortella G. Experimental evaluation of zeotropic refrigerants in a dedicated mechanical subcooling system in a CO_2 cycle - International Journal of Refrigeration - DOI

1.5.3 Supplementary papers published

- **G. Toffoletti**, E. Sicco, P. D'Agaro, R. Llopis, G. Cortella Analysis of different control strategies for improved performance at off design operation in CO_2 heat pump water heater 26th ICR international congress of refrigeration, Paris, France 21-25 August 2023
- P. D'Agaro, M. Libralato, **G. Toffoletti**, G. Cortella Influence of cooling load profile on the prediction of energy use in commercial refrigeration plants 15th IIR-Gustav Lorentzen Conference on Natural Refrigerants, Trondheim, Norway 13-15 June, 2022
- G. Cortella, **G. Toffoletti**, M. Libralato, P. D'Agaro Demand side management through latent thermal storage in HVAC systems coupled with commercial refrigeration units 15th IIR-Gustav Lorentzen Conference on Natural Refrigerants, Trondheim, Norway 13-15 June 2022

1.6 Structure of the thesis

This thesis is divided into two parts: the first focuses on zeotropic mixture and their theoretical and experimental evaluation and the second focuses on CO_2 booster systems and their possible management from a cycle modifications plant and energy management point of view. An outline is presented in the following table.

Chapter 1	Gives an introduction to the CO_2 transcritical refrigeration systems, with a research context. The aim of the thesis as well as the research questions are presented.
	Part I
Chapter 2	A theoretical evaluation of CO_2-doped with the fluids R-152a, R-1234yf, R-1234ze(E) and R-1233zd(E) considering the base cycle with an internal heat exchanger (IHX) and the cycle with parallel compression (PC) where fractionation takes place.
Chapter 3	An experimental evaluation of the blends CO_2/R-152a mixtures, ([90/10%] and [95/5%]), used as refrigerants in a single-stage refrigeration plant with and without internal heat exchanger.
Chapter 4	Theoretical assessment of the most effective compositions of R-600, R-32 and CO_2 with the base fluid R-152a in a DMS. Then, experimental evaluation of blend R-600/R-152a [60/40%] in a dedicated mechanical subcooling system in the CO_2 cycle for constant heat load temperature for three heat rejection temperatures (25.1, 30.3 and 35.1 ºC)
	Part II
Chapter 5	An experimental comparison of cycle modifications and ejector control methods in a multi-evaporator transcritical CO_2 refrigeration system is conducted, where a total of four cycle configurations and two different ejector control strategies are compared in the same plant.
Chapter 6	A real case of an ice thermal energy storage (ITES) application in a supermarket where a CO_2 refrigeration system also provides heating, air conditioning and hot water is considered. A seasonal thermodynamic and economic analysis of a transcritical CO_2 supermarket with HVAC supply through ITES is conducted.
Chapter 7	Includes a brief discussion of the results, the answer to the specific research questions and future work

Part I

Zeotropic mixtures as a method of improving CO_2 plants

Chapter 2

Theoretical Evaluation of CO_2-doped blends

Literature reveals, from a theoretical perspective and with experimental confirmation, that CO_2-doping is a method to enhance the performance of CO_2 refrigeration systems, which application could favour the extension of ultra-low GWP solutions to low and medium capacity applications without the need to use complex advanced architectures. This chapter broadens the analysis, focusing on the evaluation of R-152a, R-1234yf, R-1234ze(E) and R-1233zd(E) as CO_2 doping agents, moreover, as well as the theoretical evaluation of these mixtures, the model aims to identify a promising mixture through the comparison of COP performance. The criteria for the choice of refrigerants as possible CO_2 doping agents are their low GWP (less than 150 in a mixture) their availability, and their potential theoretical increase in COP performance. Hydrocarbons are excluded from this list in order to avoid flammable mixtures. Moreover, there is a restriction proposal by ECHA [64] (European Chemicals Agency) addressing the risks to the environment and human health associated with the use of per- and polyfluoroalkyl substances ($PFAS_s$). $PFAS_s$ are defined as any substance that contains at least one fully fluorinated methyl (CF_3-) or methylene (-CF_2-) carbon atom (without any H/Cl/Br/I attached to it). These substances therefore include the R-1234yf, R-1234ze(E) and R-1233zd(E) refrigerants and therefore additional considerations should be made in case of a possible experimental evaluation.
These mixtures are evaluated in the two most simple and used CO_2 architectures, the cycle with double-stage expansion and internal heat exchanger

and the cycle with parallel compression. The analysis extends the evaluation conditions for an evaporating level of -10 ºC and an environment temperature range from 10 to 40 ºC, where all the optimum conditions (compositions, high and intermediate pressures) are determined. Additionally, and for the first time, the evaluation considers the phenomenon of fractionation of the refrigerant in the parallel compression system, which is another parameter to focus on.

2.1 Properties of doped CO_2

The benefits of using CO_2 as refrigerant contrast with its low critical temperature, which hinders its ability to provide high cooling capacity and good efficiency at high ambient temperature, as well as its high pressure, which increases the design challenge. By doping CO_2 with small proportions of other fluids, the thermodynamic properties can be adjusted. REFPROP v10.0 is generally used to predict the thermophysical properties [65], however, it should be noted that mixture properties are estimated through mixing rules. Lemmon et al. [65] employ mixing rules based on four adjustable parameters to the Helmholtz energy ($\beta_{T,ij}$, $\gamma_{T,ij}$, $\beta_{v,ij}$, and $\gamma_{v,ij}$) and one binary-specific multiplier called "F" [66], which are fitted using published data (experimental or molecular simulation results) by an automatic fitting procedure [67]. When experimental data is not available, the interaction parameters are estimated using the Lemmon and McLinden method [68] or using interaction parameters for "similar" blends. For the mixtures considered in this chapter, the interaction parameters used by REFPROP v10.0 are detailed in Table 2.1.

TABLE 2.1: Method and interaction parameters used by REFPROP v10.0 [65]

Binary Part	**Method/mixing rule**	**Data origin**	$\beta_{T,12}$	$\gamma_{T,12}$	$\beta_{v,12}$	$\gamma_{v,12}$	F_{ij}
CO_2/R-152a	Bell and Lemon/XR0	Experimental	1.0022	1.0065	1.0000	1.0000	0.0000
CO_2/R-1234yf	Bell and Lemon/KW0	Simulation	1.0170	1.0000	1.0000	1.0150	-0.6570
CO_2/R-1234ze(E)	Bell and Lemon/KW0	Simulation	1.0000	1.0230	1.0000	-0.0840	0.0000
CO_2/R-1233zd(E)	Identical to CO_2/R-1234yf	-	1.0170	1.0000	1.0000	1.0150	-0.6570

Table 2.3 summarises some thermophysical properties of different refrigerant blends used in this chapter (evaluated with the interaction parameters detailed in Table 2.1), which are calculated for a phase change temperature of -10 ºC. Calculated t_c (critical temperature) values are higher than CO_2 value and p_c (critical pressure) always rises contrary to the hoped-for behaviour. This could be a deviation caused by REFPROP v10.0 (see binary mixture Type 1, van Konynenburg et al.[69]) or the correct experimental behaviour. For example, experimental data of Juntarachat et al. [70] reports for the mixture CO_2/R-1234yf (89/11% by mass) a p_c of 73.55 bar against 78.41 bar evaluated by REFPROP v10.0, while for CO_2/R-152a (87/13% by mass) the p_c evaluated by the software (75.53 bar) matches fine the experimental measurement (74.75 ± 0-006 bar) [71] (Table 2.2). This indicates that when using REFPROP v10.0 with predicted interaction coefficients to estimate the thermophysical properties of high temperature glide mixtures, some uncertainty is associated, which needs to be considered until experimental validation of the simulations is offered.

TABLE 2.2: Theoretical and experimental critical pressures

Fluid	p_c [bar]	
	Experimental data	REFPROP v10.0 [65]
CO_2/R-152a [87/13%]	74.75 [72]	75.53
CO_2/R-1234yf [89/11%]	73.55 [70]	78.41

TABLE 2.3: Thermophysical properties evaluated with REFPROP v.10.0 [65]

Fluid	t_c (°C)	p_c (bar)	λ^a (kJ/kg)	ν^a (m^3/kg)	Glide (K)
CO_2	30.978	73.77	258.62	0.01405	0
R-152a	113.23	45.17	316.98	0.17090	0
CO_2/R-152a [90/10%]	41.58	78.82	284.61	0.01760	13.3
R-1234yf	94.70	33.82	169.46	0.07962	0
CO_2/R-1234yf [90/10%]	37.85	77.61	256.49	0.01530	7.3
R-1234ze(E)	109.36	36.35	193.35	0.12301	0
CO_2/R-1234ze(E) [90/10%]	39.62	78.78	270.38	0.01618	12.4
R-1233zd(E)	166.45	36.24	208.32	0.54231	0
CO_2/R-1233zd(E) [90/10%]	43.025	83.42	283.08	0.01740	24.2

[a]Properties evaluated at t=-10°C and for ν as saturated vapour

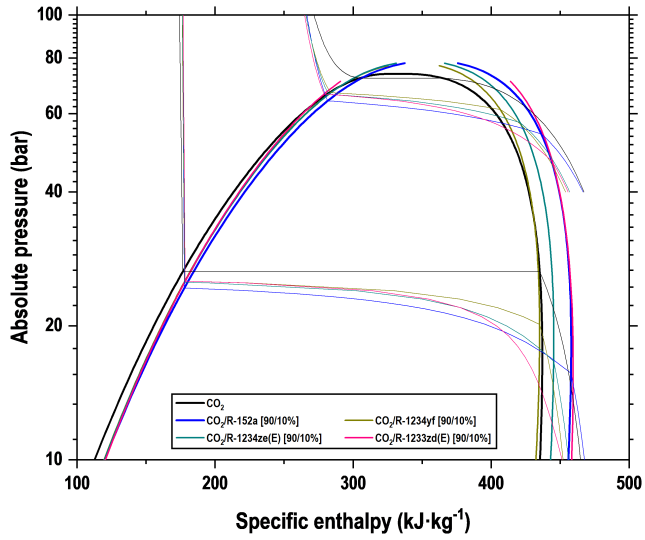

FIGURE 2.1: Pressure enthalpy diagram of selected refrigerant blends

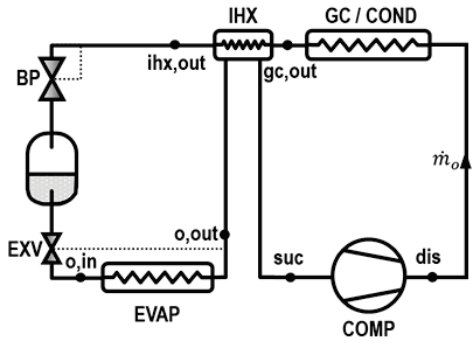

FIGURE 2.2: Base cycle with IHX

Figure 2.1 depicts the pressure-enthalpy diagram of CO_2 and the mixtures with 10% of mass proportion, as well as -10 ºC and 30 ºC isotherms. For the same phase-change temperatures, the doped mixtures have lower pressures than pure CO_2. Except for the blend CO_2/R-1234yf, all blends have larger latent heats of phase change than CO_2 and the specific volume of saturated vapour increases as in Table 2.3. However, an important drawback of the mixtures is the presence of a large temperature glide in the phase-change process; in this case, for a temperature of -10 ºC (pressure evaluated for 50% of vapour quality), the temperature glide varies between 7.3 K for the mixture CO_2/R-1234yf [90/10%] to 24.2 K for CO_2/R-1233zd(E) [90/10%]. In this figure, as in the subsequent ones, iso-therms are identified with the same color as the fluid in the corresponding legend.

2.2 Modelling

To analyse the blends, two reference cycles for medium temperature applications were considered: first, the base cycle used for CO_2 in cold regions (Figure 2.2) that incorporates a double stage expansion system and an IHX; and second, the cycle with PC (Figure 2.3), which is one of the the reference system in warm regions [33].

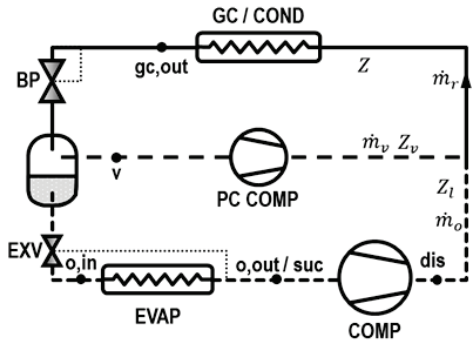

FIGURE 2.3: Cycle with parallel compression

2.2.1 General modelling considerations

Both architectures, using pure-CO_2 and blends, were simulated using a first-law approach at the same operating conditions, neglecting heat losses, pressure drops, and avoiding the modelling of the heat exchangers. For a given evaporating temperature (t_o), the low working pressure (p_o) was computed considering the mean enthalpy in the evaporator to consider the temperature glide effects of the blends, Eq. (2.1).

$$p_o = f\left(t_o, \frac{h_{o,in} + h_v}{2}\right) \tag{2.1}$$

The heat rejection level was related to the environment temperature (t_{env}), differentiating between subcritical (Back-Pressure valve providing a pressure drop to guarantee the subcooling degree generated by the IHX) and transcritical operation. Cycles were simulated in subcritical conditions at low heat rejection temperatures. Therefore, the temperature at the exit of the condenser ($t_{k,out}$) was calculated considering an approach temperature with the environment (Δt_{sub}), Eq.(2.2). The condensing pressure (p_k), fixed by the BP, was considered a degree of freedom and the corresponding condensing temperature (t_k) was evaluated for this pressure and for a quality (x_v) of 50%.

$$t_{k,out} = t_{env} + \Delta t_{sub} \tag{2.2}$$

$$t_k = f(p_k, x_v = 0.5) \tag{2.3}$$

Cycles were computed in transcritical conditions at temperatures close to or above the critical temperature. Therefore, the temperature at the exit of the gas-cooler $t_{gc,out}$ was evaluated using a constant temperature difference with the environment (Δt_{trans}), Eq. (2.4); and the heat rejection pressure (p_{gc}) was a degree of freedom.

$$t_{gc,out} = t_{env} + \Delta t_{trans} \tag{2.4}$$

Temperature at the exit of the evaporator ($t_{o,o}$) was calculated considering a constant superheating degree (SH) taking the saturated vapour temperature at the corresponding pressure ($t_v|_{p_o}$) as reference, Eq. (2.5).

$$t_{o,o} = t_v|_{p_o} + SH \tag{2.5}$$

The expansion process in the main expansion valve was considered isenthalpic, with the enthalpy being identical to that of saturated liquid at the vessel pressure ($h_l|_{p_i}$), as shown in Eq. (2.6).

$$h_{o,in} = h_l|_{p_i} \tag{2.6}$$

The power consumption of the main compressor ($P_{C,main}$) was calculated considering the refrigerant mass flow ($\dot{m}_o$), the specific isentropic compression work ($w_{s,main}$), and the overall efficiency of the compressor (η_g), which was computed using Eq. (2.7). The overall effectiveness of the main compressor was obtained with Eq. (2.8) from manufacturer data [73] of a CO_2 transcritical compressor, with its coefficients detailed in Table 2.4. Eq. (2.8) takes into account the different mixtures through the inlet and outlet conditions, the coefficients are the same for all the mixtures considered.

$$P_{C,main} = \dot{m}_o \frac{w_{s,main}}{\eta_g} \tag{2.7}$$

$$\eta_g = a_o + a_1 p_o + a_2 p_{gc} + a_3 \frac{p_{gc}}{p_o} + a_4 v_{suc} \tag{2.8}$$

TABLE 2.4: Coefficients for overall efficiency of the compressor

a_o	0.76339328
a_1	- 0.00209763
a_2	0.00134440
a_3	- 0.05713840
a_4	0.54246804

2.2.2 Specif considerations for the base cycle with IHX

The IHX was simulated using its thermal effectiveness, Eq. (2.9); thus, through the energy balance in the IHX, Eq. (2.11); and considering isenthalpic lamination, its volumetric cooling capacity (VCC) is expressed by Eq. (2.12) and the COP of this architecture by Eq. (2.13). All subscripts refer to the Figure 2.2.

$$\epsilon = \frac{Q_{IHX}}{Q_{max}} = \frac{h_{gc,out} - h_{ihx,out}}{Q_{max}} = \frac{h_{suc} - h_{o,out}}{Q_{max}} \tag{2.9}$$

$$Q_{max} = min[h_{gc,out} - h_{ihx,out,min},\ h_{suc,max} - h_{o,out}] \tag{2.10}$$

$$h_{gc,out} - h_{ihx,out} = h_{suc} - h_{o,out} \tag{2.11}$$

$$VCC = \frac{h_{o,out} - h_{o,in}}{v_{suc}} \tag{2.12}$$

$$COP = \frac{\dot{Q}_o}{P_{c,main}} = \frac{h_{suc} - h_{gc,out}}{w_{s,main}} \eta_g \tag{2.13}$$

Where $h_{ihx,out,min}$ is the minimum enthalpy value that could be obtained at the outlet of the high pressure zone of the IHX, if the temperature at that point matches the inlet temperature of the low pressure zone of the IHX ($t_{o,out}$) and $h_{suc,max}$ is the maximum enthalpy value that could be obtained at the outlet of the low pressure zone of the IHX, if the temperature at that point equals the inlet temperature of the high pressure zone ($t_{gc,out}$). The optimization parameter for this architecture is the heat rejection pressure for both transcritical and subcritical with forced condensing pressure conditions, since the back-pressure valve provides the necessary pressure drop to ensure the subcooling degree of the IHX and to guarantee the minimum compression ratio in the compressor.

2.2.3 Specific considerations for the parallel compression cycle

A simulation of the parallel compression architecture was conducted, considering steady-state operation of the receiver. The auxiliary compressor removed all the vapor coming from the back-pressure and all the liquid was sent to the evaporator. In this case, the receiver pressure (p_i) was an additional degree of freedom for this cycle. The quality at the inlet of the vessel (x_v) was calculated considering the enthalpy at the gas-cooler outlet and the selected pressure in the vessel according to Eq. (2.14); thus, the vapor mass flow rate can be quantified with Eq. (2.15) and the liquid flow rate with Eq. (2.16).

$$x_v = f(p_i, h_{gc,o}, Z) \tag{2.14}$$

$$\dot{m}_v = \dot{m}_r x_v \tag{2.15}$$

$$\dot{m}_o = \dot{m}_r (1 - x_v) \tag{2.16}$$

Furthermore, a specific consideration for the parallel configuration cycle is required when operating with zeotropic blends, which is the fractionation of the mixture caused by the phase separation in the vessel. For a given refrigerant composition Z of the refrigerant, when it is fractionated in the vessel, the vapor will have a composition Z_v richer in the most volatile component and the liquid Z_l richer in the least volatile component. Fractionation was calculated using Bell & Deiters [72] correlations developed for closed systems, since there are not specific studies about fractionation dealing with steady flow devices such as the ones considered. The rules for fractionation are available in REFPROP v10.0 [65]; thus, the mass compositions of saturated vapour and liquid are a function of the vessel pressure, the enthalpy of the mixture at the exit of the back-pressure, and of the initial composition of the refrigerant Z, as detailed by Eq. (2.17). The same procedure was considered by Vaccaro et al. [58]. Accordingly, all the thermodynamic properties from the exit of the liquid of the vessel up to the joint of the two compressors in Fig. 2.3 were evaluated with the fractionated liquid composition Z_l and those at the auxiliary compressor suction and discharge with the fractionated vapour composition Z_v.

$$[Z_l, Z_v] = f(p_i, h_{gc,out}, Z) \tag{2.17}$$

The volumetric cooling capacity provided by this architecture was evaluated using Eq. (2.12) considering isenthalpic lamination and its COP with Eq. (2.18). To evaluate the power consumption of the auxiliary compressor, the same correlation for the overall effectiveness was used, Eq. (2.9).

$$COP = \frac{\dot{Q}_o}{P_{c,main} + P_{c,aux}} = \frac{h_{o,o} - h_l|_{p_i}}{\frac{w_{s,main}}{\eta_{g,main}} + \frac{x_v}{1-x_v}\frac{w_{s,aux}}{\eta_{g,aux}}} \tag{2.18}$$

The optimization parameters for this architecture are the heat rejection pressure (taking into account forced condensation in subcritical conditions) and the pressure inside the vessel. "Optimum conditions" are defined as those conditions where the heat rejection pressure and the intermediate pressure (if parallel compressor is used) maximize COP. As the method used to maximize COP, having defined the input conditions, all values are calculated for all possible gas cooler and intermediate pressures and later identified the point with the highest COP. The Figure 2.4 shows the simplified flow chart where subscripts "lim" and "min" mean maintaining operational limits that meet the requirements described in the next section. The accuracy limit of pressures is 0.1 bar and the software used for the simulation is MATLAB with an in-house code.

2.2.4 Boundary conditions and component limitations

For the simulations the following parameters were assumed to be constant. They are consistent with experimental data or suggested by other scientists in theoretical studies about CO_2 refrigeration systems:

- Approach temperature in gas-cooler/condenser: the approach temperature, in transcritical and forced condensation conditions, was fixed to 2 K due to the high heat transfer rates (Kim et al. [74]), corroborated in an experimental test bench by Llopis et al. [75]; in subcritical conditions increased to 4 K for all the refrigerants (Sharma et al. [76]).
- Superheating degree in evaporator: it was fixed for all the conditions at 5 K (Purohit et al. [77]), (Vaccaro et al. [58]).
- Minimum compression ratio: in subcritical conditions at low heat rejection temperatures, a minimum compression ratio of 1.5 was fixed to guarantee the operation of the compressor (Catalán-Gil et al. [40]).

For the PC compressor the minimum compression ratio was of 1.5 and maximum suction pressure of 55 bar.

- Minimum pressure drop in the expansion valve of the evaporator: a minimum pressure difference of 3 bar to guarantee the proper operation of this expansion valve (Catalán-Gil et al. [40]).
- Thermal effectiveness of the IHX was fixed to 50% (Torrella et al. [22]).
- Heat losses to the environment and pressure drops in the components were neglected.

Finally, it needs to be mentioned that all the thermodynamic properties were evaluated using REFPROP v10.0 [68], employing the mixing rules for the blends described in Section 2.1.

2.2.5 Model Validation

As mentioned, there are no experimental results dealing with the evaluation of CO_2-doped mixtures in transcritical plants yet, in the next chapter will be discussed extensively on experimentation, nevertheless not all mixtures and their compositions can be tested and verified experimentally. Therefore, at this point, the model was checked using the data provided by Vaccaro et al. [58] for the IHX architecture with two different mixtures. Vaccaro's simulation conditions are established for a plant working at an outlet temperature of the cooled fluid of -10 ºC, with a pinch point with the inlet temperature of the refrigerant of 5 K, and for a gas-cooler outlet temperature of 40 ºC. This simulation condition fits within the operating range of the model considered in this chapter. Table 2.5 summarizes the validation of the model against Vaccaro's results at an inlet temperature of the refrigerant to the evaporator of -15 ºC, gas-cooler outlet temperature of 40 ºC, 5 K of superheating degree in the evaporator, and at the optimum gas-cooler pressure maximizing the COP. Table 2.6 summarizes the deviations of the COP for two cases: First, the model is simulated considering an overall efficiency of the compressor (η_g) of 80% and a thermal effectiveness of the IHX of 80%, as stablished by Vaccaro et al. [58] to verify the model with the same assumptions, ("IHX adjusted model" in Table 2.6 and Table 2.5). Second, COP_s have been calculated using our model, with the overall efficiency of the compressor of Eq. (2.8) and for a thermal effectiveness of the IHX of

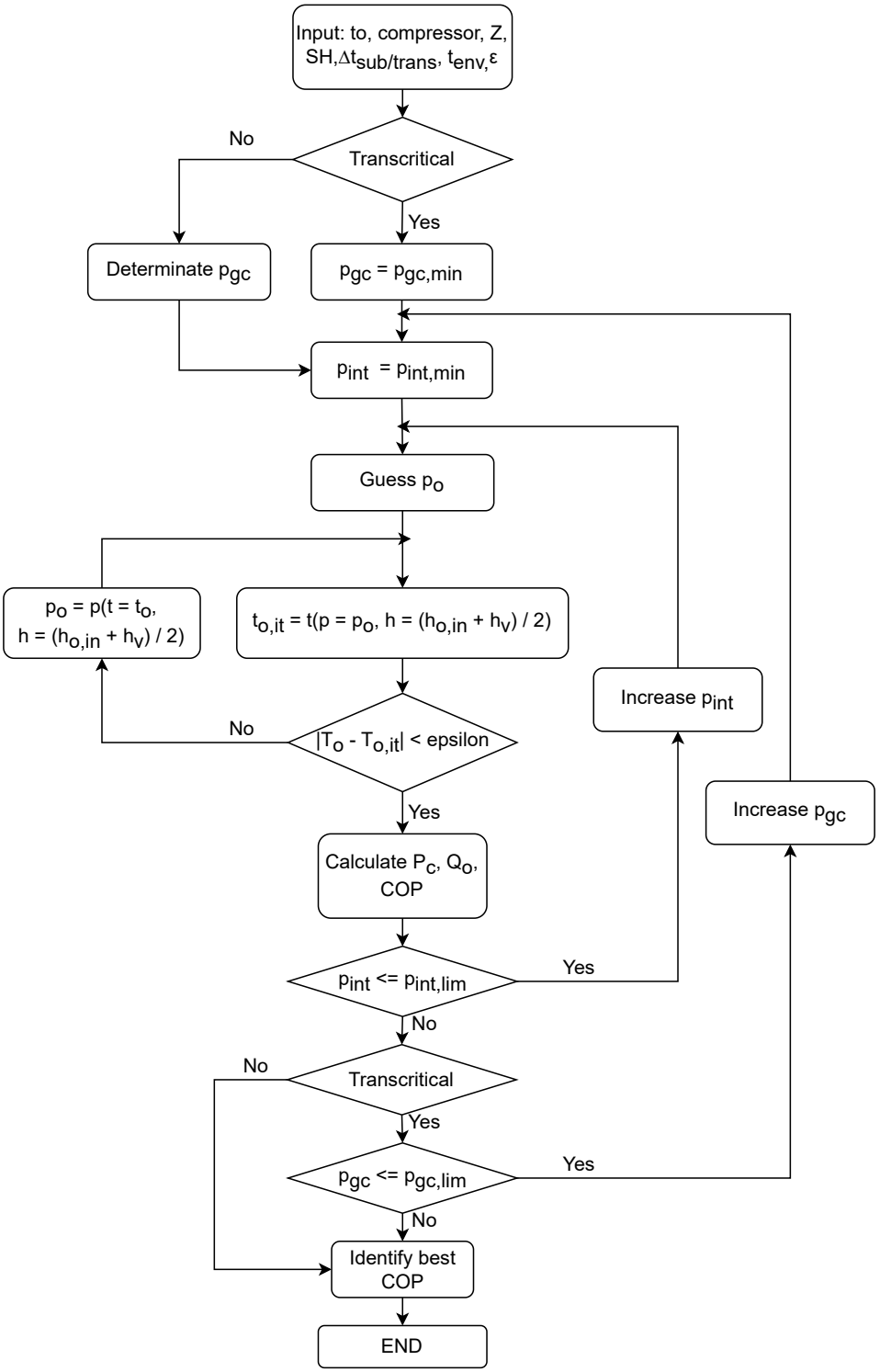

FIGURE 2.4: Simplified flow chart

80%. Table 2.5 also presents the optimum heat rejection pressures, the average evaporating temperatures, and the effective temperature glide in the evaporator. Discrepancies from Vaccaro's COP_s are below 1% for mixtures with R-1234yf and R-1234ze(E) and the ΔCOP discrepancies are also below 1% (Table 2.6). There is also agreement in the effective temperature glide in the evaporator, as Vaccaro et al. [58] select the mixture compositions with a limit of 10 K in the effective temperature glide in the evaporator. The optimum heat rejection pressures reflect a deviation, which could be caused by the superheating degree in the evaporator (the value is not provided in the work of Vaccaro's et al. [58]). Results presented in Table 2.5 indicate that the mean evaporating temperature with the mixtures rises in relation to that of CO_2. Obviously, this increment in temperature would require larger heat transfer areas in the evaporator. Nonetheless, Vaccaro's et al. do not deepen in this aspect. Concluding, it is fair to mention that this comparison is in no way a substitute for experimental validation, however the proposed model fits well with Vaccaro's results, indicating that it is consistent with previous theoretical works.

TABLE 2.5: Model validation against Vaccaro et al. [58] results at $t_{o,in}$=-15 ºC, $t_{gc,o}$=40 ºC, SH= 5 K and at optimum high pressure

			IHX adjusted model				IHX model			
	Vaccaro et al. [58]		$\eta_g = 80\%$, ϵ=80%				η_g= Eq.(2.8), ϵ=80%			
	COP (-)	$p_{gc,opt}$ (bar)	COP (-)	$p_{gc,opt}$ (bar)	t_o (°C)	Glide_o (K)	COP (-)	$p_{gc,opt}$ (bar)	t_o (°C)	Glide_o (K)
CO_2	1.6	94.0	1.603	101.0	-15.0	0.0	1.227	98.6	-15.0	0.0
CO_2/R-1234yf [85/15 %]	1.8	83.5	1.802	84.7	-12.5	10.0	1.378	82.9	-12.5	9.9
CO_2/R-1234ze(E) [92/8 %]	1.72	90.5	1.735	91.3	-13.1	9.9	1.327	89.5	-13.1	9.9

TABLE 2.6: Model deviations against Vaccaro et al. [58] results at $t_{o,in}$=-15 ºC, $t_{gc,o}$=40 ºC, SH= 5 K and at optimum high pressure

		IHX adjusted model		IHX model	
	Vaccaro et al. [58]	$\eta_g = 80\%$, ϵ=80%		η_g= Eq.(2.8), ϵ=80%	
	$\left(\frac{COP-COP_{CO_2}}{COP_{CO_2}}\right)_{\%}$	$\left(\frac{COP-COP_{CO_2}}{COP_{CO_2}}\right)_{\%}$	ΔCOP Discrepancy from Vaccaro et al. [58]	$\left(\frac{COP-COP_{CO_2}}{COP_{CO_2}}\right)_{\%}$	ΔCOP Discrepancy from Vaccaro et al. [58]
CO_2/R-1234yf [85/15%]	12.5	12.4	-0.19	12.3	-0.1
CO_2/R-1234ze(E) [92/8%]	7.5	8.2	-0.11	8.1	-0.1

2.3 Theoretical results

This section synthesizes the simulation results for CO_2 and its doped blends. Subsection 2.3.1 focuses on the results using the cycle with IHX (Fig. 2.2), while subsection 2.3.2 evaluates the mixtures in the cycle with PC (Fig. 2.3) where the phenomenon of mixtures fractionation occurs. Finally, subsection 2.3.3 contrasts the improvements offered by the blends in both architectures. A summary of all theoretical results is presented at the end of the chapter (Table 2.7 - 2.11).

2.3.1 Cycle with internal heat exchanger

For a given operating condition, the energetic performance of the base cycle when doping CO_2 with another fluid tends to enhance the COP. Fig. 2.5 depicts the evolution of this parameter (at t_o=-10 ºC, t_{env}=30 ºC) in transcritical conditions. It has been observed that it increases up to a maximum, beyond which the addition of more additive results in detriments. For low additive proportions, the cycle operates in transcritical conditions and with proportions around 5%, the cycle performs at best conditions in subcritical with forced condensing pressure. There seems to be no clear relation that explains the optimum mass fraction of the additive, not about the energy improvement. Nonetheless, it is clearly observed that CO_2 doping with a small quantity of another fluid (between 10 to 15% for this condition) is a method to enhance the performance of CO_2 refrigeration plants. Optimum mass proportion calculation was extended to a wide range of operating conditions for the pair CO_2/R-152a, the results of which are presented in Fig. 2.6. As it can be observed, the optimum composition of additive refrigerant (Z) is practically a function of the heat rejection temperature, whereas the evaporating temperature has little influence. Only when evaporating at high evaporating temperatures and low heat rejection temperatures does an optimum composition appears, but it is caused by the consideration of a minimum compression ratio in the compressor. Anyway, from Fig. 2.6, it can be affirmed that the use of CO_2-doped mixtures is beneficial at high heat rejection temperatures, especially for environment temperatures higher than 20 ºC, whereas for low heat rejection levels, the use of blends could be even detrimental.

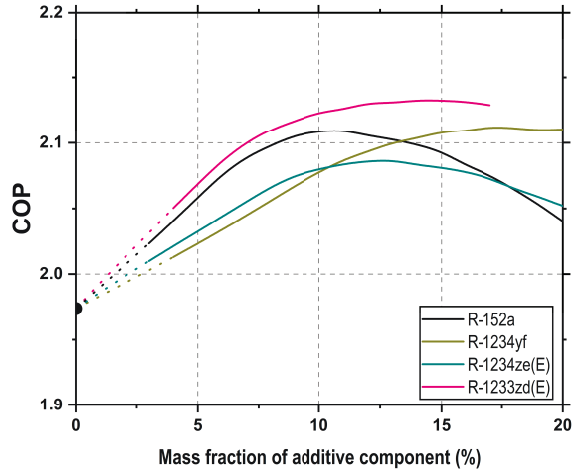

FIGURE 2.5: COP of cycle with IHX at t_o=-10 ºC, t_{env}=30 ºC (dotted line in transcritical; continuous line in subcritical with forced condensing pressure)

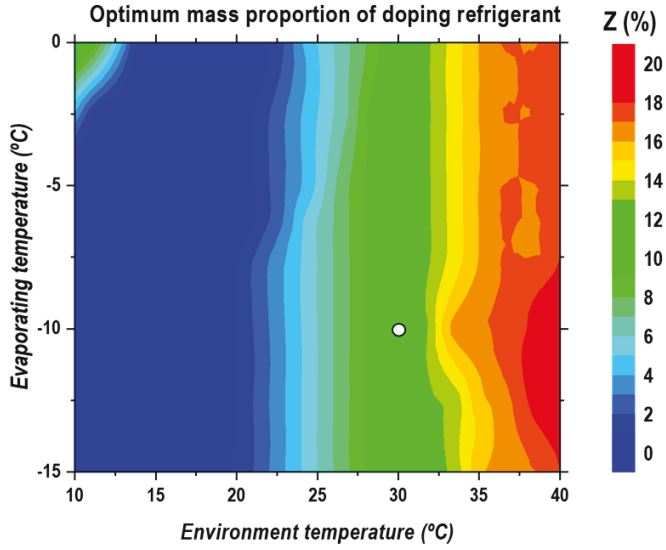

FIGURE 2.6: Optimum proportion of R-152a in CO_2 with the IHX cycle at different operating levels

To understand the cycle modifications when using a mixture (with a fluid having higher critical temperature than CO_2), the focus is on the operation of the cycle at t_o=-10 ºC, t_{env}=30 ºC when blending with R-152a (see white point in Fig. 2.6). To find the composition that maximizes COP, described below as optimum proportion, in each pair of external conditions (environment and evaporating temperature), multiple mass proportions are calculated up to 20 %, and then the composition that results in the highest COP is identified. For this condition, the optimum proportion of R-152a is approximately 10%. Fig. 2.7 depicts the operating cycle of the base system in a p-h diagram at the best performing conditions (heat rejection pressure optimized). As can be observed, the CO_2 cycle operates in transcritical conditions, where the back-pressure regulates the heat rejection pressure. When adding 10% of R-152a, the p_c and the t_c change, and the cycle moves to subcritical operation. In this case, in order to maintain the subcooling degree of the internal heat exchanger, the back-pressure valve forces the condensing level, which is the condition that maximizes the COP. According to the results of Table 2.8 and 2.9, the COP achieved with the blend is 6.9% higher than with CO_2. However, the use of the blend causes a reduction in the VCC of 25.5% because R-152a has lower volumetric capacity than CO_2. In addition, it is important to note the reduction of the operating pressures with the blend. The optimum high pressure is reduced by 10.2 bar and the evaporating level by 5.2 bar. In evaporation, the temperature glide effect can be observed (Fig. 2.7), which is a disadvantage for the heat transfer process in the evaporator. For an evaporating temperature of -10 ºC (see section 2.2.1), the inlet temperature at the evaporator is -13.20 ºC and that of saturated vapour of -1.08 ºC, what means that the evaporator operates with an effective temperature glide of 12.2 K. Obviously, this large temperature glide will require higher heat transfer surfaces in comparison to the operation with CO_2. Finally, another important modification perceived is a high increase of the compressor discharge temperature, in this case of 12.7 K. However, this difference has been calculated considering that the compressor overall efficiency does not depend on the fluid component added, so the experimental behaviour could be different.

Finally, Fig. 2.8 summarizes the COP deviation of the considered blends (with 5 and 10% proportion) in relation to the operation of the cycle with IHX and CO_2. As mentioned, doping is not advisable for low heat rejection temperatures, as all blends present COP reductions. CO_2 cycle works

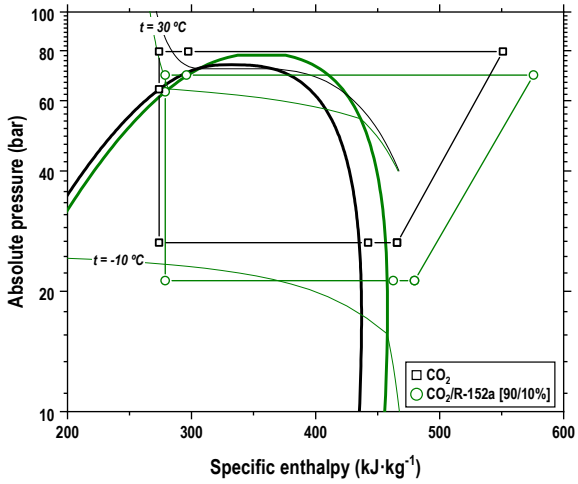

FIGURE 2.7: p-h diagram at optimum conditions IHX cycle with CO_2 and CO_2/R-152a [90/10%] (t_o=-10 ºC, t_{env}=30 ºC)

in subcritical with high efficiency at low temperatures while these blends cause efficiency reductions. Then, at medium heat rejection levels, the COP modification is neutral, coinciding with the transition regime of CO_2 operation. But at high heat rejection levels (25 to 35 ºC), the COP of the system is enhanced using the mixtures, as the doped fluids still operate in subcritical conditions. For the considered fluids, the predicted COP gains at t_o=-10 ºC reach between 3.16% at 27 ºC (CO_2/R-1234yf [95/5%]) to 7.70% at 31 ºC (CO_2/R-1233ze(E) [90/10%]). It can therefore be confirmed as the application of CO_2-doped mixtures could be an opportunity to improve the performance of cycles based on CO_2, particularly at high heat rejection temperatures. In addition, because of a large effective glide in the evaporator (see Table 2.8, 2.9) reaching values higher than 10 K for a 10% of mass proportion of the doping agent, considerations must be made when designing the heat exchanger: higher heat transfer surface areas and limits in the application range of the fluids, i.e., the inlet temperature of the secondary fluid to the evaporator must be higher than that at the exit of the evaporator (for CO_2/R-1233zd/(E) [90/10%] it must be higher than 14.1 ºC).

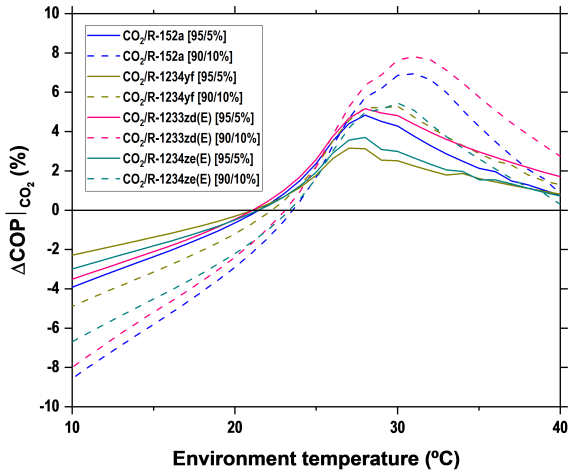

FIGURE 2.8: COP percentage difference from pure CO_2 with base cycle with IHX at t_o=-10 ºC

2.3.2 Cycle with parallel compression

As mentioned, the state-of-the-art cycle for medium and high heat rejection level corresponds to the cycle with parallel compression, wherein the auxiliary compressor's function is to remove the vapour generated in the vessel, increasing the specific cooling capacity and thus enhancing cycle's energy efficiency. When blends are used as refrigerants, this architecture has special features, as the vessel will experience fractionation. Phase-separation in the vessel will provide two currents with different compositions: the saturated vapor will contain a higher proportion of the most volatile component, and the saturated liquid will contain a higher proportion of the least volatile component. Fractionation, first suggested by Vaccaro et al. [58] but not deeply studied, could introduce new ways of improvement, which will be discussed in this section. To illustrate the use of blends in the parallel compression architecture, focusing on the operation of the cycle at t_o=-10 ºC and t_{env}=30 ºC. Fig. 2.9 represents the p-h diagram at optimum conditions for CO_2 and Fig. 2.10 for the mixture CO_2/R-1233zd(E) [90/10%]. Contrasting the operation in both figures, it is observed that, as with the

IHX cycle, CO_2 doping moves the cycle from transcritical (Fig. 2.9) to subcritical operation (Fig. 2.10), introducing the positive effects mentioned in Subsection 2.3.1. In addition, the fractionation produces two different flows: saturated vapour extracted from the vessel has a composition of CO_2/R-1233zd(E) [97.71/2.29%] and saturated liquid of CO_2/R-1233zd(E) [86.39/13.61%]. These numbers reveal that, thanks to the fractionation, two different refrigerants are generated, whose properties can enhance or decrease the performance of the cycle. It would be desirable for the vapour to contain more fluid with lower slope in the isentropic lines; and it would be desirable for the liquid to present higher volumetric cooling capacity, to increase the cooling effect in the evaporator. These effects, which are clear when considered separately, cannot be isolated in the considered cycle; thus, a complete evaluation at optimum conditions is needed. For the considered case (Fig. 2.10), the use of the blend theoretically enhances the COP of the cycle by 1.8% at these conditions (7.7% in IHX cycle), so it appears that the improvements of doping are lower for this architecture. However, as discussed later, the region of improvement changes. For the operation at t_o=-10 ºC and t_{env}=30 ºC, a reduction of 11.1% in the volumetric cooling capacity (18.9% in IHX cycle) and a decrease of 7.5 bar in the optimum heat rejection pressure (10.6 in IHX cycle) are predicted. Also, the effective temperature glide in the evaporator rises due to the fractionation, going from 24.2 K for this mixture in the IHX cycle to 24.8 K in the PC cycle; thus, the use mixtures with high proportion of doping agent in refrigeration applications can be difficult from the point of view of heat transfer, even, their application range can be reduced to high exit temperatures at the exit of the evaporator.

Fig. 2.11 summarizes the COP deviation of the considered blends (with 5 and 10% proportion) in relation to the operation with CO_2. The trends are quite different from the operation with the base cycle. First, at low heat rejection levels (up to t_{env} = 13 ºC) the auxiliary compressor does not operate because the compression ratio is below 1.5. In this region, as well as in the IHX cycle, doping results not to be convenient. From this temperature up to 27 ºC approximately, the auxiliary compressor operates and there is fractionation in the cycle (see Fig. 2.12). In this region there is a clear trend of COP improvement when using CO_2-doped blends. When the auxiliary compressor starts, the vapor line (the one that compresses the auxiliary compressor) contains a higher proportion of the most volatile component, in this case CO_2, and the liquid line higher proportion of the

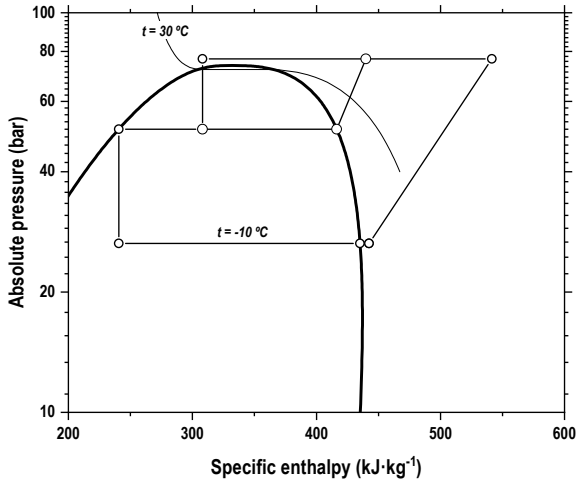

FIGURE 2.9: p-h diagram at optimum conditions PC cycle with CO_2 (t_o = -10ºC, t_{env} = 30ºC)

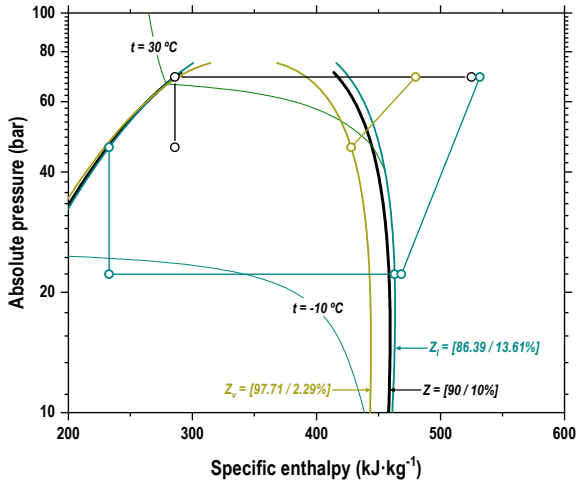

FIGURE 2.10: p-h diagram at optimum conditions PC cycle with CO_2/R-1233zd(E) [90/10%] (t_o = -10ºC, t_{env} = 30ºC)

least volatile component. Calculations predict COP improvements up to 11.98% (CO_2/R-1233zd(E) [95/5%]) at t_{env} = 27 ºC. In this region all the blends offer COP improvements. From 27 to 32 ºC approximately, there is a big reduction in the enhancement. In this region, while the doped-CO_2 blends are operating in subcritical conditions with forced heat rejection pressure (see Table 2.10, Table 2.11), CO_2 operates in transcritical conditions, where it has a quick improvement of the COP, thus the percentage is reduced. Finally, from temperatures above 32 ºC the COP enhancement stabilises, from 2% approximately for CO_2/R-1234yf [95/5%] to 8% approximately with CO_2/R-1233ze(E) [95/5%]. Detailed data can be checked in Table 2.10, 2.11. Again, these results are based on simulations and an experimental validation is needed. Results related to the use of the fluid R-1233zd(E), as detailed in the tables, may vary from the experimental behaviour since there is no validated specific information about the interaction coefficients used to compute the thermophysical properties. Therefore, the energy parameters are subjected to an unknown degree of uncertainty. In addition, if the results are consistent, the use of the mixture CO_2/R-1233zd(E) [90/10%] could result very difficult in practice due to a large effective temperature glide in the evaporator.

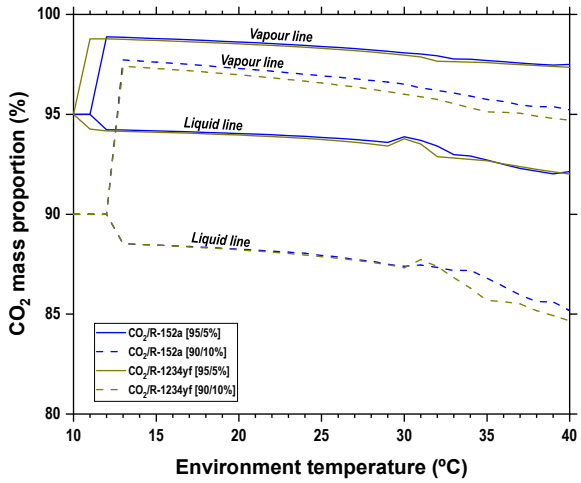

FIGURE 2.12: CO_2 mass proportion in liquid and vapour lines after fractionation for mixtures CO_2/R-152a and CO_2/R-1234yf with PC cycle at t_o = -10 ºC

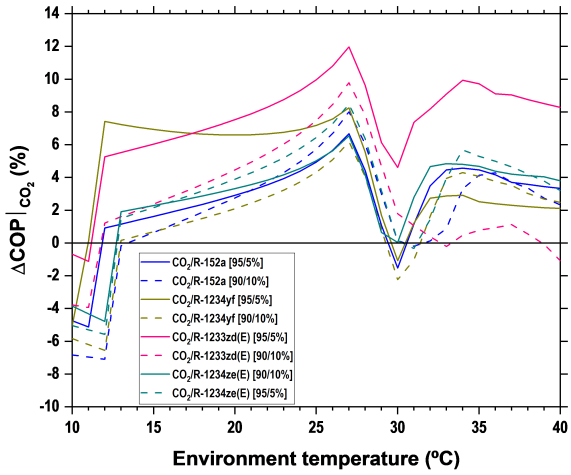

FIGURE 2.11: COP percentage difference from pure CO_2 with PC cycle at t_o = -10 ºC

2.3.3 Performance comparison

This section summarizes the COP improvements when using CO_2-doped blends with the two considered architectures. Fig. 2.13 represents the predicted COP values for both technologies with CO_2 (black symbols) and with the considered mixtures, the data of which is detailed in Table 2.7. It is clearly observed that the energy improvements at t_{env}=25 and 35 ºC using the mixtures is moderate, specifically, the model estimates COP improvements from 1.6% (CO_2/R-1234ze(E) [90/10%] at 25 ºC) up to 5.8% (CO_2/R-1233zd(E) [90/10%] at 35 ºC). However, the use of the parallel compression architecture with the mixtures predicts larger COP improvements, which could be related to the fractionation of the blends in the cycle. In this case, the COP improvements range from 0.8% (CO_2/R-1233zd(E) [90/10%] at 35 ºC) to 10% (CO_2/R-1233zd(E) [95/5%] at 25 ºC).

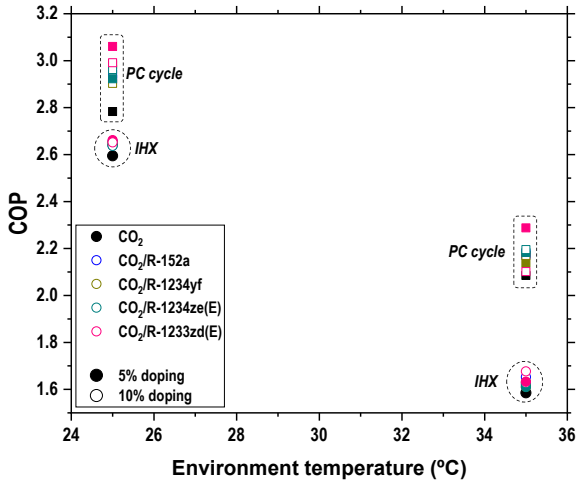

FIGURE 2.13: COP vs. t_{env} (t_o = -10 ºC) for IHX cycle and PC cycle (filled symbol 5% by mass doping, empty symbol 10% doping)

2.4 Chapter conclusions

This chapter employs a theoretical analysis to explore the potential enhancement of two conventional CO_2 cycles: base cycle with (a) the internal heat exchanger and (b) the parallel compressor, through the utilization of CO_2-doped blends. In this context, R-152a, R-1234yf, R-1234ze(E), and R-1233zd(E) are examined as doping agent to influence the performance of these chosen system designs. Results have been based on the use of a comprehensive model using REFPROP v10.0 and its mixing rules as reference.

It has been predicted that 5-10% CO_2 doping tends to enhance the COP of the architectures, but this is accompanied by a reduction of the volumetric cooling capacity. The optimum mass proportion of additive is independent on the evaporating level, being only dependent and positive for environment temperatures above 20 ºC. CO_2 doping with pure fluids which have higher critical temperature than CO_2 allows the optimum condition of the cycle to go to subcritical operation, causing a reduction of the operating pressures in all the cycles.

Considering the IHX architecture, COP improvements are predicted in environment temperatures higher than 25 ºC, reaching maximum improvement around 30 ºC and being attenuated at 40 ºC. For the analysed blends, the COP gains at t_o=-10 ºC reach between 3.16% at 27 ºC (CO_2/R-1234yf [95/5%]) to 7.70% at 31 ºC (CO_2/R-1233ze(E) [90/10%]).

In relation to the PC layout, the use of refrigerant blends deals with the fractionation of the refrigerant in the phase-separation vessel, where two flows with different compositions are generated. The saturated vapour contains a higher proportion of the most volatile component (CO_2 in this work), and the saturated liquid is enriched with the least volatile component (doping agents in this work). This fractionation introduces modifications to the cycle, which can be considered as another mechanism to enhance the performance. For the PC cycle, CO_2-doped has wider range of benefit, approximately from t_{env}=13 ºC to 27 ºC and from 32 to 40 ºC. Also, the COP enhancement is higher with this architecture. Enhancements up to 11.98% were predicted with the mixture (CO_2/R-1233zd(E) [95/5%]) at t_{env} = 27 ºC.

TABLE 2.7: COP comparison at t_{env}=25 and 35 ºC for t_o=-10 ºC

Fluid	COP_{IHX}	$\left(\frac{COP_{IHX}-COP_{IHX,CO_2}}{COP_{IHX,CO_2}}\right)_{\%}$	COP_{PC}	$\left(\frac{COP_{PC}-COP_{PC,CO_2}}{COP_{PC,CO_2}}\right)_{\%}$	$\left(\frac{COP_{PC}-COP_{IHX,CO_2}}{COP_{IHX,CO_2}}\right)_{\%}$
Environment temperature = 25 °C					
CO_2	2.59	-	2.78	-	7.3
CO_2/R-152a [95/5%]	2.66	2.4	2.92	4.9	12.6
CO_2/R-152a [90/10%]	2.64	1.7	2.94	5.7	13.4
CO_2/R-1234yf [95/5%]	2.64	1.8	2.98	7.2	15.0
CO_2/R-1234yf [90/10%]	2.65	2.2	2.90	4.3	11.9
CO_2/R-1234ze(E) [95/5%]	2.65	1.9	2.92	5.0	12.6
CO_2/R-1234ze(E) [90/10%]	2.64	1.6	2.96	6.4	14.2
CO_2/R-1233zd(E) [95/5%]	2.66	2.6	3.06	10.0	17.9
CO_2/R-1233zd(E) [90/10%]*	2.65	2.2	2.99	7.5	15.3
Environment temperature = 35 °C					
CO_2	1.59	-	2.09	-	31.5
CO_2/R-152a [95/5%]	1.62	2.1	2.18	4.5	37.4
CO_2/R-152a [90/10%]	1.65	4.3	2.17	4.1	37.0
CO_2/R-1234yf [95/5%]	1.61	1.6	2.14	2.5	34.9
CO_2/R-1234yf [90/10%]	1.63	2.9	2.17	4.1	36.9
CO_2/R-1234ze(E) [95/5%]	1.61	1.6	2.18	4.7	37.7
CO_2/R-1234ze(E) [90/10%]	1.63	2.6	2.20	5.3	38.5
CO_2/R-1233zd(E) [95/5%]	1.63	3.0	2.29	9.7	44.3
CO_2/R-1233zd(E) [90/10%]*	1.68	5.8	2.10	0.8	32.6

*This condition could be difficult to exploit, as the effective glide in the evaporator is higher than 20 K

TABLE 2.8: Optimum conditions of 5% and 10% CO_2 doped at t_o=-10 ºC and t_{env}=40, 30 and 20 ºC for the base cycle with IHX

Fluid	COP	ΔCOP	VCC	ΔVCC	p_{gc}/p_k	Δp_{gc}	p_o	Δp_o	Glide_o	Mode
		(%)	(kJ/m^3)	(%)	(bar)	(bar)	(bar)	(bar)	(K)	
Environment temperature = 40 ºC										
CO_2	1.317	-	10442	-	104.4	-	26.5	-	0	Transcritical
CO_2/R-152a [95/5%]	1.328	0.8	9449	-9.5	96.5	-7.9	23.7	-2.8	6.4	Transcritical
CO_2/R-152a [90/10%]	1.329	0.8	8499	-18.6	88.2	-16.2	21.0	-5.5	11.8	Transcritical
CO_2/R-1234yf [95/5%]	1.328	0.8	9816	-6.0	99.2	-5.1	24.9	-1.5	3.2	Transcritical
CO_2/R-1234yf [90/10%]	1.335	1.3	9209	-11.8	94.2	-10.2	23.4	-3.1	6.4	Transcritical
CO_2/R-1234ze(E) [95/5%]	1.327	0.7	9614	-7.9	98.5	-5.9	24.5	-2.0	6.2	Transcritical
CO_2/R-1234ze(E) [90/10%]	1.321	0.3	8814	-15.6	92.5	-11.9	22.3	-4.2	11.3	Transcritical
CO_2/R-1233zd(E) [95/5%]	1.340	1.7	9361	-10.4	97.5	-6.9	24.4	-2.1	12.2	Transcritical
CO_2/R-1233zd(E) [90/10%]*	1.354	2.7	8424	-19.3	90.2	-14.2	22.1	-4.4	24.1	Transcritical
Environment temperature = 30 ºC										
CO_2	1.973	-	11455	-	79.8	-	26.5	-	0	Transcritical
CO_2/R-152a [95/5%]	2.058	4.3	10358	-9.6	71.4	-8.4	23.9	-2.6	6.5	Sub. Forced p_k
CO_2/R-152a [90/10%]	2.109	6.9	8529	-25.5	69.6	-10.2	21.3	-5.2	12.2	Sub. Forced p_k
CO_2/R-1234yf [95/5%]	2.023	2.5	10725	-6.4	74.4	-5.3	25.0	-1.5	3.3	Sub. Forced p_k
CO_2/R-1234yf [90/10%]	2.078	5.3	9102	-20.5	69.7	-10.0	23.5	-3.0	6.6	Sub. Forced p_k
CO_2/R-1234ze(E) [95/5%]	2.033	3.0	10564	-7.8	77.5	-2.3	24.6	-1.9	6.3	Transcritical
CO_2/R-1234ze(E) [90/10%]	2.081	5.5	9089	-20.7	69.1	-10.6	22.7	-3.8	11.5	Sub. Forced p_k
CO_2/R-1233zd(E) [95/5%]	2.069	4.8	10291	-10.2	73.6	-6.2	24.5	-2.0	12.3	Transcritical
CO_2/R-1233zd(E) [90/10%]*	2.125	7.7	9292	-18.9	69.2	-10.6	22.6	-3.9	24.2	Sub. Forced p_k

*This condition could be difficult to exploit, as the effective glide in the evaporator is higher than 20 K

TABLE 2.9: Optimum conditions of 5% and 10% CO_2 doped at t_o=-10 ºC and t_{env}=40, 30 and 20 ºC for the base cycle with IHX

Fluid	COP	ΔCOP	VCC	ΔVCC	p_{gc}/p_k	Δp_{gc}	p_o	Δp_o	Glide_o	Mode
		(%)	(kJ/m^3)	(%)	(bar)	(bar)	(bar)	(bar)	(K)	
Environment temperature = 20 ºC										
CO_2	3.381	-	13365	-	60.2	-	26.5	-	0	Sub. Forced p_k
CO_2/R-152a [95/5%]	3.363	-0.5	12380	-7.4	57.0	-3.2	24.1	-2.3	6.7	Sub. Forced p_k
CO_2/R-152a [90/10%]	3.281	-3.0	11416	-14.6	54.2	-6.0	21.9	-4.6	12.6	Sub. Forced p_k
CO_2/R-1234yf [95/5%]	3.374	-0.2	12747	-4.6	58.2	-1.9	25.2	-1.3	3.4	Sub. Forced p_k
CO_2/R-1234yf [90/10%]	3.347	-1.0	12110	-9.4	56.3	-3.9	23.8	-2.7	6.9	Sub. Forced p_k
CO_2/R-1234ze(E) [95/5%]	3.364	-0.5	12560	-6.0	58.1	-2.1	24.8	-1.6	6.5	Sub. Forced p_k
CO_2/R-1234ze(E) [90/10%]	3.309	-2.1	11788	-11.8	56.0	-4.2	23.1	-3.4	11.9	Sub. Forced p_k
CO_2/R-1233zd(E) [95/5%]	3.369	-0.3	12278	-8.1	58.1	-2.1	24.8	-1.7	12.4	Sub. Forced p_k
CO_2/R-1233zd(E) [90/10%]*	3.302	-2.3	11329	-15.2	56.1	-4.0	23.1	-3.4	24.3	Sub. Forced p_k

*This condition could be difficult to exploit, as the effective glide in the evaporator is higher than 20 K

TABLE 2.10: Optimum conditions of 5% and 10% CO_2 doped at t_o=-10 ºC and t_{env}=40, 30 and 20 ºC for the base cycle with parallel compression

Fluid	Z_{vCO_2} (%)	Z_{lCO_2} (%)	COP	ΔCOP (%)	VCC (kJ/m^3)	ΔVCC (%)	p_{gc}/p_k (bar)
Environment temperature = 40 ºC							
CO_2	100.0	100.0	1.82	-	13361	-	93.8
CO_2/R-152a [95/5%]	97.5	92.1	1.88	3.3	11960	-10.5	88.1
CO_2/R-152a [90/10%]	95.2	85.2	1.86	2.3	10419	-22.0	81.7
CO_2/R-1234yf [95/5%]	97.4	92.0	1.86	2.1	12544	-6.1	90.0
CO_2/R-1234yf [90/10%]	94.7	84.7	1.86	2.5	11397	-14.7	85.6
CO_2/R-1234ze(E) [95/5%]	97.7	91.0	1.93	6.3	12144	-9.1	86.1
CO_2/R-1234ze(E) [90/10%]	95.9	84.5	1.88	3.2	10965	-17.9	85.5
CO_2/R-1233zd(E) [95/5%]	98.5	91.1	1.97	8.3	12078	-9.6	89.4
CO_2/R-1233zd(E) [90/10%]*	97.1	85.6	1.80*	-1.1	10417	-22.0	87.6
Environment temperature = 30 ºC							
CO_2	100.0	100.0	2.44	-	13395	-	76.7
CO_2/R-152a [95/5%]	98.1	93.9	2.40	-1.5	12395	-7.5	74.7
CO_2/R-152a [90/10%]	96.5	87.4	2.44	0.1	11788	-12.0	66.8
CO_2/R-1234yf [95/5%]	98.0	93.8	2.41	-1.1	12840	-4.1	75.6
CO_2/R-1234yf [90/10%]	96.0	87.3	2.38	-2.2	12357	-7.7	69.7
CO_2/R-1234ze(E) [95/5%]	98.4	93.7	2.44	0.0	12654	-5.5	75.7
CO_2/R-1234ze(E) [90/10%]	97.0	87.0	2.44	0.1	12139	-9.4	69.1
CO_2/R-1233zd(E) [95/5%]	99.0	93.5	2.55	4.6	12528	-6.5	75.8
CO_2/R-1233zd(E) [90/10%]*	98.1	86.9	2.48*	1.8	11902	-11.1	69.2
Environment temperature = 20 ºC							
CO_2	100.0	100.0	3.47	-	15287	-	60.0
CO_2/R-152a [95/5%]	98.6	94.0	3.57	2.9	14288	-6.5	56.9
CO_2/R-152a [90/10%]	97.3	88.3	3.57	2.8	13073	-14.5	54.1
CO_2/R-1234yf [95/5%]	98.5	94.0	3.70	6.6	14742	-3.6	56.2
CO_2/R-1234yf [90/10%]	97.0	88.2	3.54	2.1	13944	-8.8	56.3
CO_2/R-1234ze(E) [95/5%]	99.0	93.9	3.59	3.3	14589	-4.6	57.9
CO_2/R-1234ze(E) [90/10%]	97.9	88.0	3.61	3.9	13649	-10.7	55.9
CO_2/R-1233zd(E) [95/5%]	99.4	93.4	3.73	7.5	14397	-5.8	58.0
CO_2/R-1233zd(E) [90/10%]*	98.8	87.9	3.63	4.5	13368	-12.6	56.0

*This condition could be difficult to exploit, as the effective glide in the evaporator is higher than 20 K.

TABLE 2.11: Optimum conditions of 5% and 10% CO_2 doped at t_o=-10 ºC and t_{env}=40, 30 and 20 ºC for the base cycle with parallel compression

Fluid	Δp_{gc} (bar)	p_o (bar)	Δp_o (bar)	Glide$_o$ (K)	p_{dep} (bar)	Mode
Environment temperature = 40 °C						
CO_2	-	26.5	-	0	51.4	Transcritical
CO_2/R-152a [95/5%]	-5.8	22.9	-3.6	6.9	49.8	Transcritical
CO_2/R-152a [90/10%]	-12.2	19.7	-6.8	13.0	48.6	Sub. Forced p_k
CO_2/R-1234yf [95/5%]	-3.8	24.4	-2.1	3.5	50.3	Transcritical
CO_2/R-1234yf [90/10%]	-8.2	22.3	-4.1	7.0	49.8	Transcritical
CO_2/R-1234ze(E) [95/5%]	-7.7	23.5	-3.0	6.6	50.5	Transcritical
CO_2/R-1234ze(E) [90/10%]	-8.4	21.1	-5.4	12.2	50.0	Transcritical
CO_2/R-1233zd(E) [95/5%]	-4.4	23.5	-2.9	12.9	50.6	Transcritical
CO_2/R-1233zd(E) [90/10%]*	-6.2	21.2	-5.3	25.1	55.0	Transcritical
Environment temperature = 30 °C						
CO_2	-	26.5	-	0	51.1	Transcritical
CO_2/R-152a [95/5%]	-2.0	23.7	-2.8	6.8	49.8	Sub. Forced p_k
CO_2/R-152a [90/10%]	-9.8	20.9	-5.6	12.3	43.0	Sub. Forced p_k
CO_2/R-1234yf [95/5%]	-1.0	24.9	-1.6	3.5	50.4	Sub. Forced p_k
CO_2/R-1234yf [90/10%]	-6.9	23.2	-3.3	7.0	46.5	Sub. Forced p_k
CO_2/R-1234ze(E) [95/5%]	-0.9	24.5	-2.0	6.6	50.5	Sub. Forced p_k
CO_2/R-1234ze(E) [90/10%]	-7.5	22.3	-4.2	12.1	45.5	Sub. Forced p_k
CO_2/R-1233zd(E) [95/5%]	-0.9	24.4	-2.1	12.6	50.5	Sub. Forced p_k
CO_2/R-1233zd(E) [90/10%]*	-7.5	22.2	-4.3	24.8	46.1	Sub. Forced p_k
Environment temperature = 20 °C						
CO_2	-	26.5	-	0	40.0	Sub. Forced p_k
CO_2/R-152a [95/5%]	-3.1	24.0	-2.5	7.0	37.9	Sub. Forced p_k
CO_2/R-152a [90/10%]	-6.0	21.6	-4.9	13.1	36.0	Sub. Forced p_k
CO_2/R-1234yf [95/5%]	-3.9	25.1	-1.4	3.6	37.4	Sub. Forced p_k
CO_2/R-1234yf [90/10%]	-3.8	23.6	-2.8	7.2	37.5	Sub. Forced p_k
CO_2/R-1234ze(E) [95/5%]	-2.1	24.7	-1.7	6.7	38.6	Sub. Forced p_k
CO_2/R-1234ze(E) [90/10%]	-4.2	22.9	-3.6	12.3	36.8	Sub. Forced p_k
CO_2/R-1233zd(E) [95/5%]	-2.0	24.8	-1.7	12.6	38.7	Sub. Forced p_k
CO_2/R-1233zd(E) [90/10%]*	-4.0	22.9	-3.6	24.7	37.4	Sub. Forced p_k

*This condition could be difficult to exploit, as the effective glide in the evaporator is higher than 20 K.

Chapter 3

Experimental evaluation of the CO_2/R-152a blend in the refrigeration system

This chapter evaluates from an experimental point of view two CO_2/R-152a mixtures, ([90/10%] and [95/5%]), used as refrigerants in a single-stage refrigeration plant with and without internal heat exchanger, and compares the results to those obtained using pure CO_2. In addition, the facility for testing the mixtures will be the same, with no change of components, based on a "drop-in" analysis.

3.1 Materials and methods

3.1.1 Experimental test plant

The experimental tests were realized with a water-to-water single-stage transcritical refrigeration plant with a double-stage expansion system, whose scheme is detailed in Figure 3.1. It is driven by a Dorin CD380H semi hermetic compressor with a displacement of 3.0 m^3/h at nominal speed. Condenser/gas cooler and evaporator brazed plate counter-current heat exchangers with exchange surface area of 4.794 m^2 and 1.224 m^2, respectively. It incorporates a single-pass double pipe IHX arranged in counterflow with a heat transfer surface area of 0.1194 m^2 which can be included or not in the cycle using manual valves. Plant is regulated using two electronic expansion valves, a Carel E2V18 for the back-pressure and a Carel E2V14 for the evaporator. The first regulates the heat rejection pressure using a custom-made

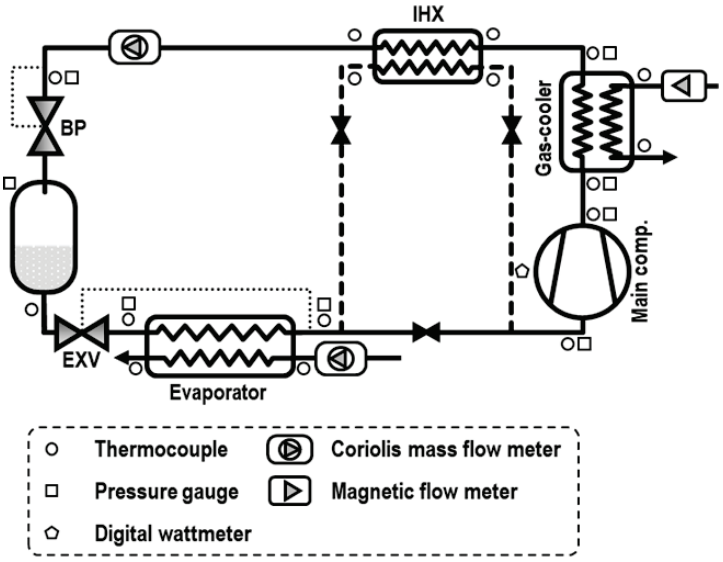

FIGURE 3.1: Schematic diagram of the experimental test bench

PID controller and the second operates as a thermostatic valve with external equalization. The coefficients of the expansion valve of the evaporator are adjusted for the operation of each refrigerant. The plant is fully instrumented to determine its energy performance (see sensor allocation in Figure 3.1). It incorporates 16 T-type thermocouples (immersion thermocouples for the condenser/gas-cooler exit and evaporator, the rest are placed over the pipe surface), 4 high pressure gauges, 1 medium pressure gauge and 3 low pressure gauges. Refrigerant mass flow rate is measured with a Coriolis mass flow meter at the high-pressure line prior to the back-pressure valve, volumetric water flow to the gas-cooler is measured using a volumetric flow meter and the water-propylene glycol mixture (60/40% by volume) mass flow is measured using another Coriolis mass flow meter. The compressor electric power is measured using a digital wattmeter. The calibration range and measurement error of the instrumentation are detailed in Table 3.1 and main components are summarized in Table 3.2

TABLE 3.1: Calibration range and measurement error of instrumentation

Measured variable	Device	Range	Calibrated error
Temperature	T-type thermocouple	-40.0 to 145.0 ºC	± 0.5 K
High pressure	Pressure gauge	0.0 to 160.0 bar	± 0.96 bar
Medium pressure	Pressure gauge	0.0 to 100.0 bar	± 0.6 bar
Low pressure	Pressure gauge	0.0 to 60.0 bar	± 0.36 bar
Refrigerant mass flow rate	Coriolis mass flow meter	0.0 to 0.5 kg·s-1	± 0.1% of reading
Glycol mass flow rate (Evaporator)	Coriolis mass flow meter	0.0 to 13.88 kg·s-1	± 0.1% of reading
Water volume flow rate (Gas-cooler)	Magnetic flow meter	0.0 to 5.0 m3·h-1	± 0.3% of reading
Power consumption	Digital wattmeter	0.0 to 5.0 kW	± 0.5% of reading

TABLE 3.2: Main component of the experimental plant

Equipment	Type	Tech. info
Compressor	Semi hermetic	$\dot{V} = 3.0 m^3/h$
Gas cooler	Brazed plate	$A = 4.794 m^2$
Evaporator	Brazed plate	$A = 1.224 m^2$
IHX	Double pipe	$A = 0.1194 m^2$

3.1.2 Selected refrigerant mixtures and preparation

The theoretical simulations of Xie et al. [57] and Martínez-Ángeles et al. [78] and the results from the previus chapter, concluded that CO_2/R-152a mixtures could improve the performance of transcritical cycles in relation to pure CO_2. In addition, the interaction coefficients of the equations of state of CO_2/R-152a mixtures were fitted from experimental data by Bell and Lemmon [67]; thus REFPROP v10.0 (Lemmon E. W. et al. [65]), which is the software used to predict the thermophysical properties of the fluids, presents validated equations of state. Moreover, the mixture CO_2/R-152a from the theoretical analysis in the previous chapter has one of the lowest temperature glide, and therefore easiest to test experimentally and finally, it is a mixture excluded from the list of PFAS substances [64]. For these reasons, the fluid R-152a is selected as doping agent of CO_2 to perform the experimentation covered by this chapter. The work evaluates the use of CO_2 and CO_2/R-152a mixtures with 5 and 10% mass percentage of R-152a. The pressure enthalpy diagrams of the three fluids are depicted in Figure

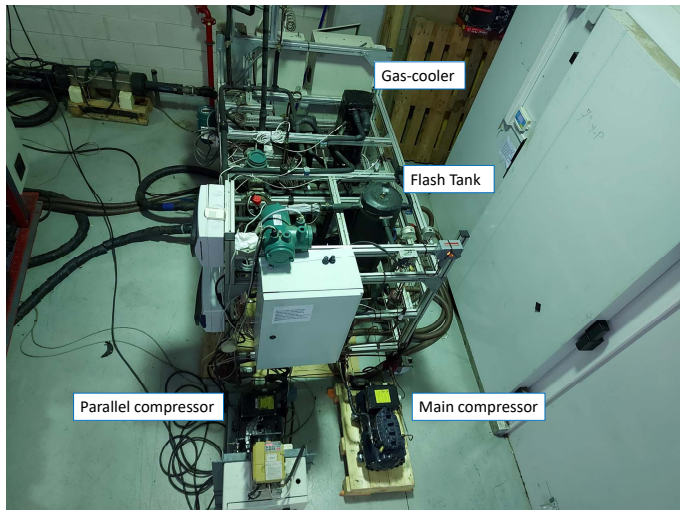

FIGURE 3.2: Experimental transcritical CO_2 system

3.3 and some selected thermophysical properties are presented in Table 3.3. R-152a is a refrigerant with higher critical temperature and lower critical pressure than CO_2. Addition of a small proportion of R-152a to CO_2 induces small changes in the thermophysical properties, as seen in Figure 3.3. In relation to the benefits, the critical temperature increases 10.6 K for 10% R-152a addition, thus the region at which the plant operates in transcritical conditions is reduced. The working pressures at the low- and high-pressure sides decrease (for 10% addition: 3.6 bar at -10ºC and 10.7 at 30 ºC) and the latent heat of vaporization widens (for 10% addition: 10.0% more at -10ºC and 150.5% more at 30 ºC). However, the addition of R-152a introduces two important drawbacks: R-152a has high specific volume, therefore the mixtures increment the specific volume (for 10% addition: 86.4% more) and it could reduce the volumetric cooling capacity (VCC) of the plant; also, since R-152a has a different normal boiling point, it introduces a temperature glide in the phase change temperatures (for 10% addition: 13.3K at -10 ºC and 6.6 K at 30 ºC), which reduces the thermal effectiveness of evaporator and condenser (when operating in subcritical conditions). Nonetheless, the temperature glide in the gas-cooler could be beneficial. As mentioned, there are drawbacks and benefits of doping CO_2 with R-152a, however, they had not been evaluated using an experimental approach yet. In relation

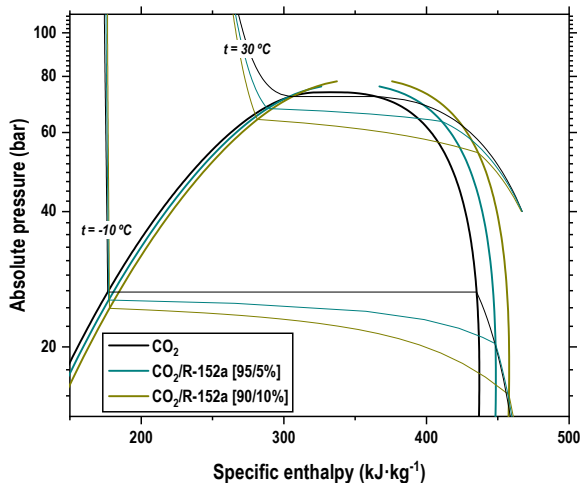

FIGURE 3.3: Pressure-enthalpy diagram of the three tested fluids

to the mixture preparation, the charge of refrigerant was always 12 kg, guaranteeing that at the exit of the vessel the refrigerant was in saturated liquid conditions. It was verified visually through a sight glass in the vessel. Fluids used to prepare the mixtures were certified 99.9% purity gases. To avoid errors in the mixture preparation, first a vacuum procedure was made in the plant; then, the corresponding quantity of R-152a was introduced in the plant (1.2 kg of R-152a for 10%); and finally, the plant was filled with CO_2 until 12 kg (10.8 kg of CO_2 for 10%). The charging procedure was controlled using a certified mass balance with a measurement error of 5 g. The uncertainty of the refrigerant compositions was $\pm 0.04\%$ for both mixtures. Regarding the choice of lubricant, no change was made from pure CO_2 since the amount of R-152a is at most 10% by mass.

FIGURE 3.4: Experimental water/propylene glycol mixture supply system

TABLE 3.3: Thermophysical properties evaluated with REFPROP v10.0

Fluid	t_c (ºC)	p_c[a] (bar)	p (bar)	$\lambda_{-10°C}$[b] (kJ/kg)	$\nu_{-10°C}$[b] (m^3/kg)	Glide$_{-10\,°C}$ (K)	p[a] (bar)	$\lambda_{30°C}$[b] (kJ/kg)	Glide$_{30\,°C}$ (K)
CO_2	30.98	73.77	26.49	258.6	0.0140	0	72.14	60.6	0
R-152a	113.26	45.17	1.81	317.0	0.1709	0	6.90	273.2	0
CO_2/R-152a [95/5%]	36.58	76.93	24.65	272.6	0.0195	7.1	66.58	119.7	2.7
CO_2/R-152a [90/10%]	41.58	78.82	22.84	284.6	0.0261	13.3	61.45	151.8	6.6

a t=30 ºC x_v=0.5

b Properties evaluated for pressure corresponding to the temperature and vapour title of 50%

TABLE 3.4: Enthalpy difference due to the use of the IHX.

$t_{w,in}$	Δh_o (kJ/kg)					
20 ºC	CO_2	8.02	CO_2/R-152a [95/5%]	11.69	CO_2/R-152a [90/10%]	6.86
25ºC		15.23				5.53
30ºC		13.42		11.77		11.73
35ºC		13.70		5.84		5.92

3.1.3 Experimental methodology

Fluids comparison was made setting the plant to the same inlet conditions of secondary fluids. In the evaporator, the secondary fluid used was a water/propylene glycol mixture (60/40% by volume), with a constant volumetric flow of 0.7 m^3/h and a constant inlet temperature of 2.5 ºC, while the secondary fluid used in the condenser/gas-cooler was water, with a constant volumetric flow of 1.17 m^3/h. Condition of the secondary fluid are guaranteed by an external refrigeration system (Figure 3.4). The plant was run with the compressor at the nominal speed (50 Hz) and was tested at water inlet temperatures to the condenser/gas-cooler from 20 ºC to 40 ºC with 5 ºC steps for the base configuration and up to 35 °C for the IHX to keep the discharge temperature below 140 °C. A couple of tests with the mixture CO_2/R-152a [95/5%] at 20 °C could not unfortunately be performed due to limits in the dissipation system. For each test condition, the high-pressure of the plant was optimized to reach the maximum COP value. In addition, each point is tested in steady state condition: waiting for 5 to 10 minutes to obtain stable conditions, and then successively recording the data for 5 to 10 minutes for each point tested.

3.2 Results

This section presents and discusses the experimental results obtained with the experimental test campaign. Subsection 3.2.1 focuses on the evaluation of the plant without IHX (i.e. "base" configuration), subsection 3.2.2 with IHX, and subsection 3.2.3 synthetizes the energy improvements obtained by the use of CO_2-doped mixtures.

3.2.1 Base configuration

Cooling capacity is calculated as the product of refrigerant mass flow rate in the evaporator and the enthalpy difference between the outlet and the inlet of the evaporator. Nonetheless, inlet enthalpy of the evaporator is calculated as the enthalpy at the back-pressure valve, considering an isenthalpic expansion and neglecting heat loss:

$$\dot{Q}_o = \dot{m}_{ref}(h_{o,out} - h_{bp,in}) \tag{3.1}$$

The value of cooling capacity is expressed by, taking into account the uncertainty:

$$\dot{Q}_o = \dot{Q}_o \pm I_{\dot{Q}_o} \tag{3.2}$$

Where the uncertainty is evaluated as Eq. (3.3) and detailed in Appendix A.

$$I_{\dot{Q}_o} = \sqrt{((h_{o,out} - h_{bp,in})\epsilon_{\dot{m}})^2 + (\dot{m}_{ref} I_{h_{o,out}})^2 + (\dot{m_{ref}} I_{h_{bp,in}})^2} \tag{3.3}$$

Apart from the previous equation, cooling capacity can also be calculated through the secondary fluid performing a heat balance as outlined in Eq. (3.4). Both calculated cooling capacities are compared, to validate the obtained results (Table 3.5 and Table 3.6)

$$\dot{Q}_{o,sf} = \dot{V}_g \rho \overline{c_p} (t_{g,in} - t_{g,out}) \tag{3.4}$$

The COP of the system is the ratio between the cooling capacity and the electrical power of the compressor, as exposed in Eq. (3.5)

$$COP = \frac{\dot{Q}_o}{P_c} \tag{3.5}$$

Its uncertainty is evaluated with:

$$I_{COP} = \sqrt{\left(\frac{1}{P_c} I_{\dot{Q}_o}\right)^2 + \left(\frac{-\dot{Q}_o}{P_c^2} \epsilon_{p_c}\right)^2} \tag{3.6}$$

In the condenser/gas-cooler, the heat transfer rate has been calculated both on the refrigerant side as shown in Eq. (3.7) and on the water secondary loop side, using Eq. (3.8).

$$\dot{Q}_{gc} = \dot{m}_{ref} (h_{gc,in} - h_{gc,out}) \tag{3.7}$$

$$\dot{Q}_{gc,sf} = \dot{m}_w \overline{c_p} (t_{w,out} - t_{w,in}) \tag{3.8}$$

As an optimization method, various pressures at the gas cooler are experimentally tested for each external condition, and subsequently the point that maximizes COP is identified. This is a method that is used throughout

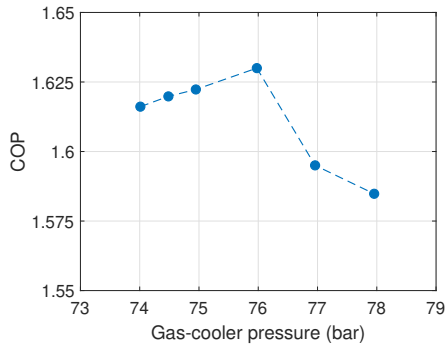

FIGURE 3.5: IHX COP with gas cooling pressure variation for CO_2/R-152a [95/5%]

the thesis where an experimental test is conducted, and the conditions (in this specific case the pressure at the gas cooler only) that allow the maximum COP to be obtained are called "optimal conditions". An example of the identification of optimal conditions is presented in Figure 3.5, where the search for a pressure at the gas cooler that maximizes COP (1.63 in this case) is performed in the case of CO_2/R-152a [95/5%] mixture with IHX.

Figure 3.6, Figure 3.7 and Figure 3.8 show the (p-h) diagrams of the base cycle configuration obtained at the highest COP conditions for each evaluated refrigerant, represented for a water inlet temperature to the gas cooler of 30 ºC. In the three diagrams it can be observed that the critical temperature of the fluid increases with the addition of R-152a. While the cycle that uses pure CO_2 as refrigerant works in supercritical conditions, the cycles which use the mixtures as working fluid work in the critical zone or even subcritical conditions for the blend with 10% of R-152a. This is due to the fact that the critical pressure of the mixtures is higher if compared to the one of the pure CO_2, and the optimum working pressure is reduced when the evaluated mixtures are used instead of the CO_2. Therefore, the use of mixtures gives place to subcooled liquid at the exit of the condenser.

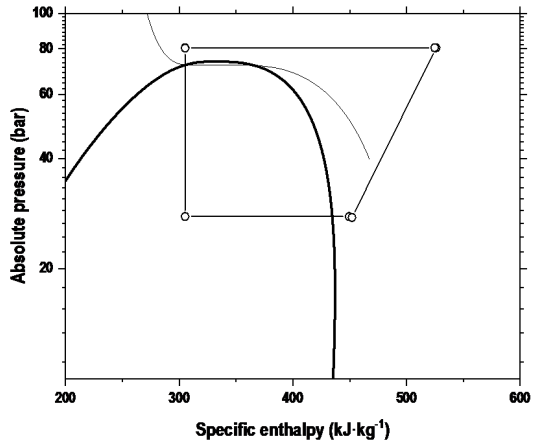

FIGURE 3.6: Real refrigerating cycle sketched in the p-h diagram of CO_2 for base configuration at $t_{w,in}$=30 ºC, at optimum conditions

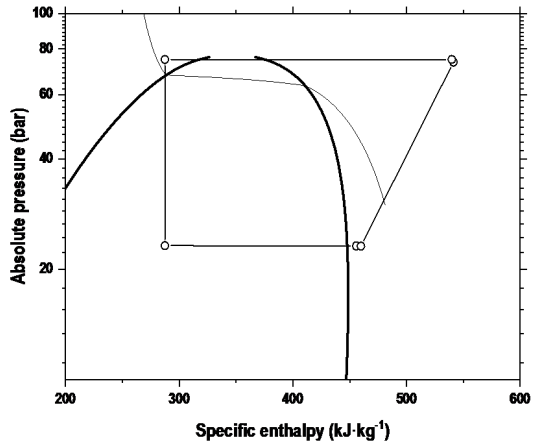

FIGURE 3.7: Real refrigerating cycle sketched in the p-h diagram of CO_2/R-152a [95/5%] for base configuration at $t_{w,in}$=30 ºC, at optimum conditions

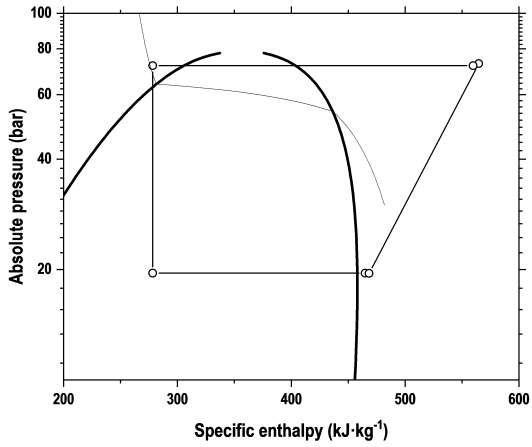

FIGURE 3.8: Real refrigerating cycle sketched in the p-h diagram of CO_2/R-152a [90/10%] for base configuration at $t_{w,in}$=30 ºC, at optimum conditions

COP

For the base cycle, the measured COP values and their uncertainties for each condition using the three tested fluids are displayed in Figure 3.9. As it can be seen, there are different trends that must be noted. With the use of mixture CO_2/R-152a [95/5%] better COP values are obtained, when compared to the COP measured using pure CO_2, which is the reference for this work. The use of the blend CO_2/R-152a [90/10%] shows a different behaviour, as COP values calculated for temperatures below 25ºC are lower than the ones obtained with the use of pure CO_2. However, above the mentioned temperature the COP values obtained using this mixture are higher than the ones given by the use of pure CO_2 and at the highest temperature its performance overcomes even the one given by using CO_2/R-152a [95/5%]. All the COP values and their uncertainties are presented in Table 3.5. These considerations are all made with reference to the averaged results, it is fair to mention that uncertainty makes the data often similar to each other. However, it can be seen that at high temperatures (40 °C water inlet to gas cooler for e.g.) the improvement is clear even taking into account the uncertainty.

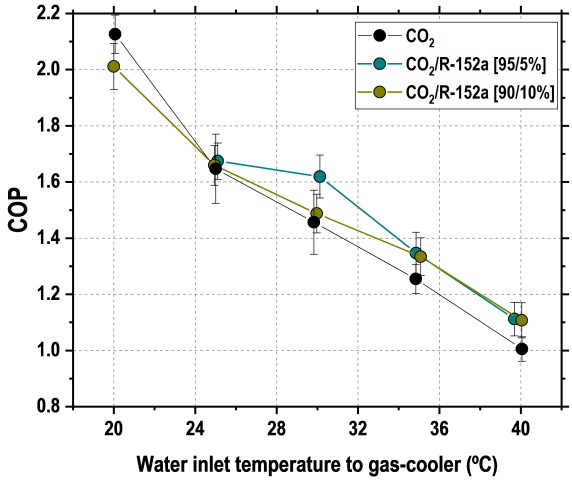

FIGURE 3.9: Evolution of the maximum COP for optimal conditions vs condenser/gas-cooler water inlet temperature for Base configuration

Cooling capacity

Analysing the cooling capacity obtained for the use of the three tested fluids at optimal working conditions, it can be seen that the cooling capacity obtained with the use of pure CO_2 is higher than that obtained by using both the evaluated mixtures, due to the lower volumetric cooling capacity of the blends. As a matter of fact, the higher the mass proportion of R-152a, the lower cooling capacity is generated, as it can be seen in Figure 3.10. However, this slight reduction in cooling capacity can be offset thanks to a proper size design of the plant or even controlling the compressor's rotation speed depending on the needs. In addition, there is one point at 30.1 °C (CO_2/R-152a [95/5%]) that seems not to follow the trend of the other two refrigerants also affecting the COP in Figure 3.9. One possible explanation is that the points tested are under optimal conditions, and thus optimized to maximize COP, and therefore the cooling capacity trend may not follow this logic. In fact, this may have happened with the CO_2/R-152a [90/10%] mixture, where the cooling capacity is similar for 30.0 C° and 35.1 °C water inlet temperature. Another possible explanation is the behavior of

the exchanger, which is limited in its size, and therefore might be more or less efficient under conditions that do not necessarily follow a linear trend.

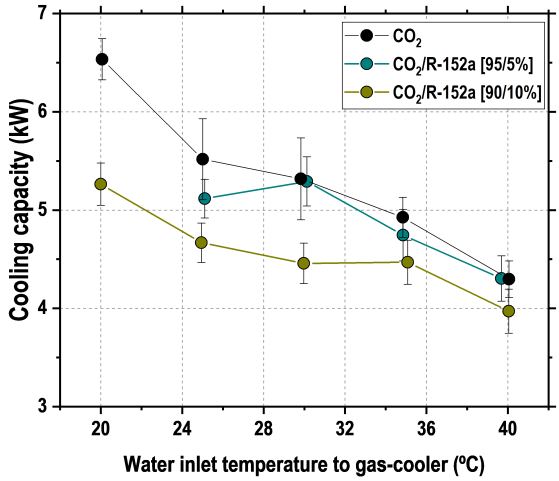

FIGURE 3.10: Evolution of the maximum cooling capacity for optimal conditions vs condenser/gas-cooler water inlet temperature for base configuration

Optimum working parameters

Gas-cooler pressure has a major effect on the performance of the plants and has to be optimized in CO_2 transcritical cycles. The use of a blend instead of pure CO_2 in the system changes the value of the optimum pressure, as shown in Figure 3.11. For all the three tested fluids the trend is towards a lower gas-cooler pressure when increasing the mass fraction of R-152a. This is a positive effect for the reliability of the system. It can be observed that the trend of the optimum gas-cooler pressure depending on the environment temperature is very linear, which makes it easy to be controlled thanks to the expansion valve with a simple PID control. The horizontal line represents the pressure corresponding to the critical point. Figure 3.12 represents the evolution of the compressor discharge temperature for the different conditions: using the tested blends instead of pure CO_2 increased the measured

discharge temperature and this phenomenon was more significant at higher concentration of R-152a.

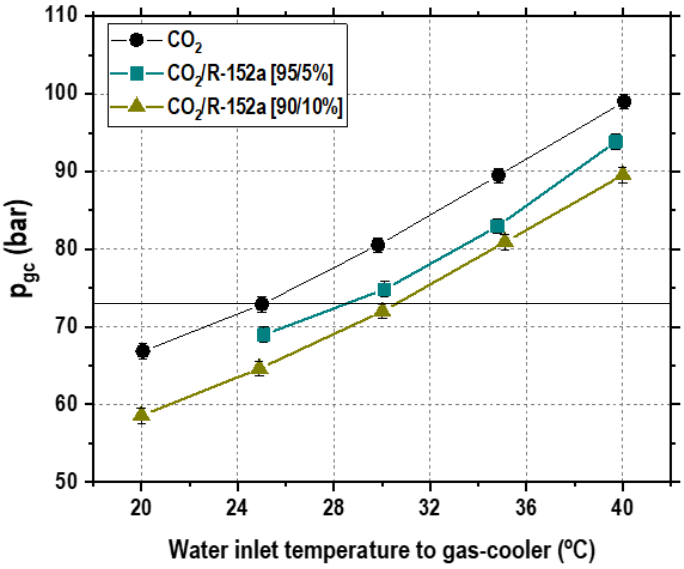

FIGURE 3.11: Optimum gas-cooler pressure vs condenser/gas-cooler water inlet temperature for base configuration

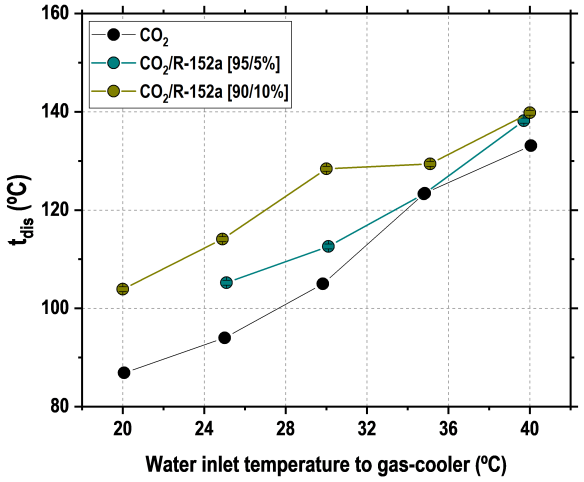

FIGURE 3.12: Compressor discharge temperature for optimal conditions vs condenser/gas-cooler water inlet temperature for base configuration

3.2.2 IHX configuration

The cooling capacity of this configuration is calculated the same way as the base cycle configuration exposed in Eq. (3.1). The calculation of the COP and the heat balances in the gas-cooler/condenser and the evaporator are performed following Eqs. (from(3.1) to (3.5)). The difference between this cycle and the base cycle is the addition of an internal heat exchanger (IHX) that subcools the working fluid downstream the exit of the gas-cooler and heats up the fluid upstream the inlet of the compressor. Heat transfer analysis is performed in both currents flowing through the IHX as shown in Eq. (3.9) and Eq. (3.10) and the efficiency of the internal heat exchanger is calculated by Eq. (3.11).

$$\dot{Q}_{IHX} = \dot{m}_{ref}(h_{gc,out} - h_{IHX,h,out}) \tag{3.9}$$

$$\dot{Q}_{IHX,l} = \dot{m}_{ref}(h_{IHX,b,out} - h_{IHX,b,in}) \tag{3.10}$$

$$\epsilon_{IHX} = \frac{t_{IHX,v,out} - t_{IHX,v,in}}{t_{IHX,l,in} - t_{IHX,v,in}} 100 \tag{3.11}$$

COP

Figure 3.13 shows the COP values obtained with the use of the tested fluids for different conditions of the secondary fluid at the inlet of the gas-cooler/condenser. It can be observed that the best energy performance is carried out using pure CO_2. The introduction of a second component in the mixture worsens significantly the COP of the system at temperature below 30 ºC, while above the mentioned temperature the COP obtained with the use of all three tested fluids are very similar. This is mostly due to the variations in the cooling capacity.

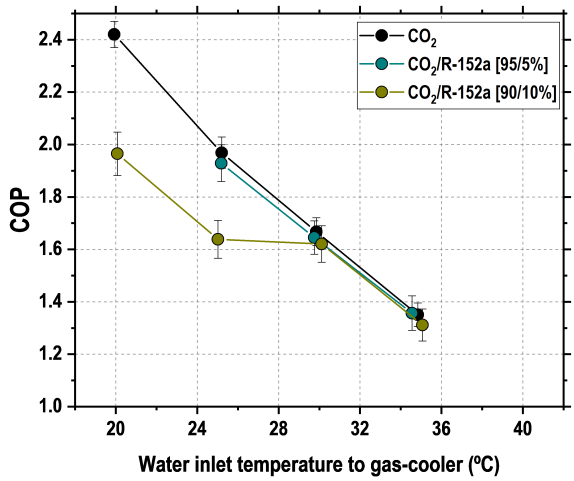

FIGURE 3.13: Maximum COP for optimal conditions vs. condenser/gas-cooler water inlet temperature for IHX configuration.

Cooling capacity

Cooling capacity for optimal conditions are displayed in Figure 3.14. It can be inferred that the introduction of R-152a as an additive in the pure CO_2 causes a reduction in the cooling capacity and this phenomenon is more significant as the mass composition of R-152a increases also due to the reduction in the VCC. The main conclusion extracted from these results

is the decrease of cooling capacity of the cycle working with CO_2/R-152a mixtures in comparison with the $\dot{Q}_o$ obtained with the use of pure CO_2 for both architectures. For the CO_2/R-152a composition [90/10%] at 25 °C of heat rejection temperature, a sharp decrease in the cooling capacity is observed compared to one obtained with an inlet temperature of the secondary fluid at the condenser/gas-cooler of 30 °C. The reason for this decline may be the change of operation conditions. At a heat rejection temperature of 25 ºC the plant works under subcritical conditions, with a temperature approach to the hot sink of almost 4 K, while when the plant is run with a heat rejection temperature of 30 °C the approach is less than 1 K, due to the better heat transfer properties. Since the point at 25 ºC is subcritical, the plant operates with the BP fully open. Forcing the condensing pressure could in this case improve the cooling capacity of the plant. As it can be seen in Figure 3.15, the enthalpy difference in the evaporator for 25 ºC and 30 ºC of the secondary fluid at the inlet of the condenser/gas-cooler is nearly the same while the mass flow circulating at 30 ºC is higher, so the cooling capacity is also higher for this condition.

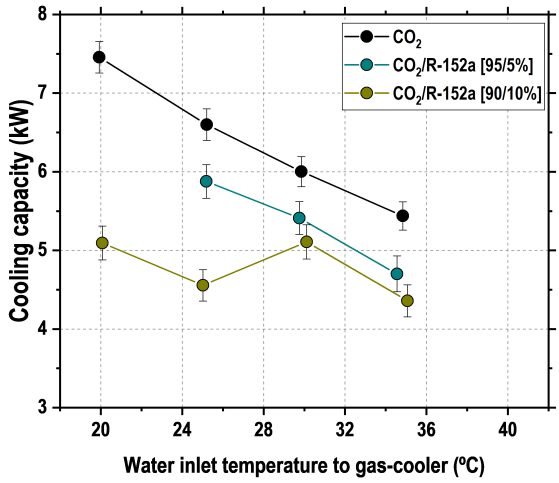

FIGURE 3.14: Cooling capacity for optimal conditions vs. condenser/gas-cooler water inlet temperature for IHX configuration

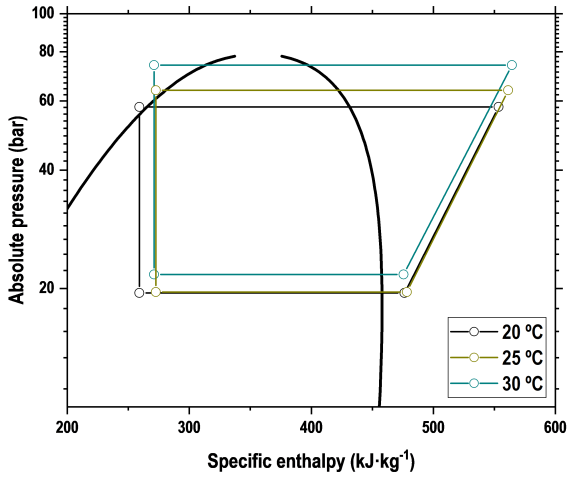

FIGURE 3.15: Ph diagram of CO_2/R-152a [90/10%] for IHX configuration at $t_{w,in}$=20, 25 and 30 ºC at optimum condition

Optimum working parameters

Figure 3.16 and Figure 3.17 present the behaviour of the condenser/gas-cooler pressure and the compressor discharge temperature, at different conditions for the IHX cycle. The thermal effectiveness of the IHX (Eq. (3.11)) calculated for the tested conditions is between 35% and 45%. It seems that the addition of R-152a enhances slightly the thermal effectiveness of the heat exchanger, nonetheless, the measurement uncertainty is too significant to arrive at a definitive conclusion regarding this enhancement. The values of electrical power and compressor discharge temperature can be consulted in Table 3.6. As it can be seen in Table 3.4, the increment of the enthalpy difference due to the use of the IHX is higher when working with pure CO_2 and decreases with the addition of R-152a which makes that the use of the IHX is not so profitable when working with mixtures. Figure 3.18, Figure 3.19 and Figure 3.20 show the IHX cycles at optimum conditions depicted in the (p-h) diagrams of the three tested fluids, for a fixed heat rejection temperature of 30 ºC. With higher concentrations of R-152a in the working fluid, the optimal heat rejection pressure is lower and, at the same time, the critical pressure of the fluid, obtained by REFPROP v10.0, is higher.

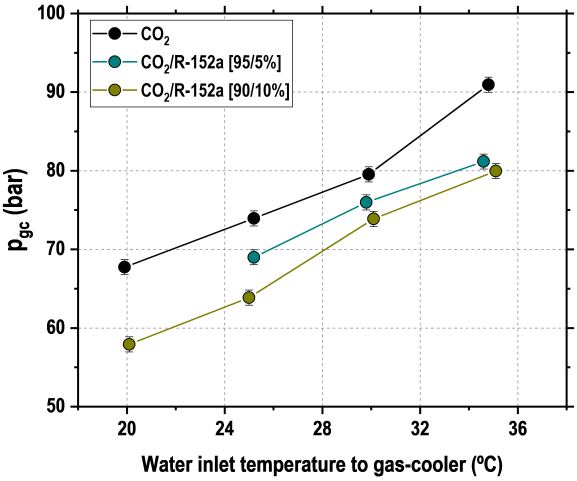

FIGURE 3.16: Optimum condenser/gas-cooler pressure vs water inlet temperature for IHX configuration

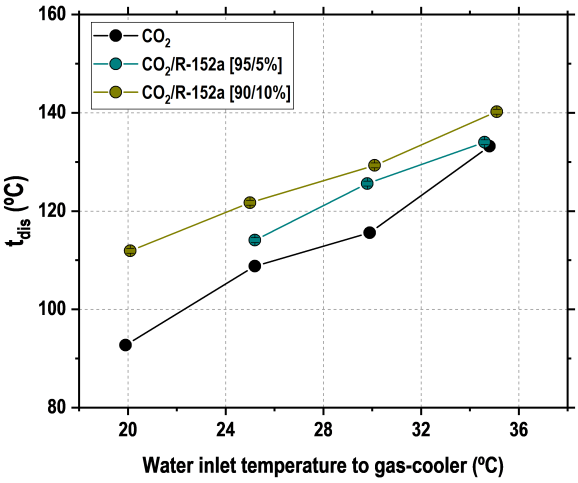

FIGURE 3.17: Compressor discharge temperature vs water inlet temperature for IHX configuration

These two phenomena caused by the use of blends make the cycle work in subcritical conditions.

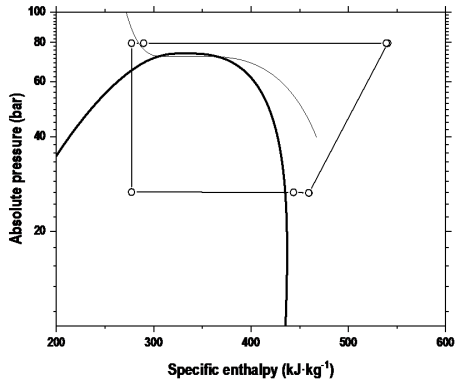

FIGURE 3.18: Real refrigerating cycle sketched in the p-h diagram of CO_2 for IHX configuration at t_w, in=30 ºC, at optimum conditions

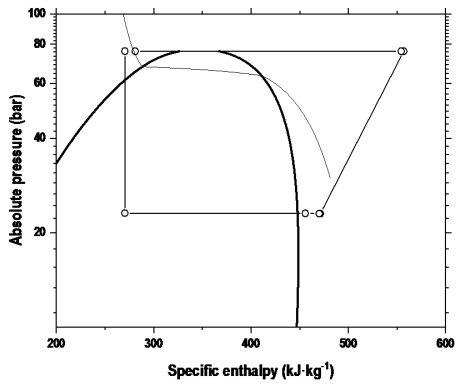

FIGURE 3.19: Real refrigerating cycle sketched in the p-h diagram of CO_2/R-152a [95/5%] for IHX configuration at t_w, in=30 ºC, at optimum conditions

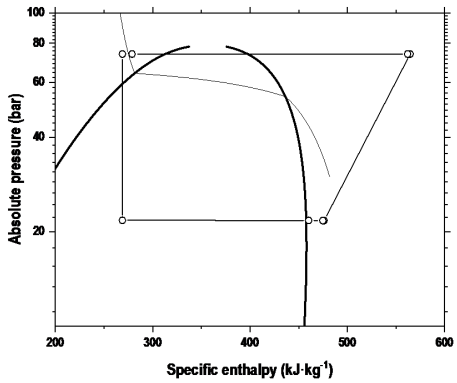

FIGURE 3.20: Real refrigerating cycle sketched in the p-h diagram of CO_2/R-152a [90/10%] for IHX configuration at t_w, in=30 ºC, at optimum conditions

3.2.3 Energy improvement

Table 3.7 and Table 3.8 compare the COP at best performing conditions obtained by the use of each fluid. It shows the COP increments or decrements as defined in the table for all three tested fluids and both base cycle and IHX cycle. It can be noted that at lower gas-cooler water inlet temperatures the use of pure CO_2 outperformed the use of CO_2/R-152a mixtures. On the contrary, at higher gas-cooler water inlet temperatures, using the mixtures allowed a slight improvement in the COP compared to that with the use of pure CO_2. Figure 3.21 shows the COP increments obtained in the base cycle using mixtures making reference to the use of pure CO_2. As it can be observed, for heat rejection temperature higher than 25 ºC, the mixtures always provide a COP improvement. This improvement is higher for the mixture CO_2/R-152a [95/5%] where the increments are 1.6% for 25.0 ºC, 11.2 for 30.0 ºC, 7.3% for 35.0 ºC and 10.6% for 40.0 ºC. Figure 3.22 depicts the COP variation accomplished in the IHX configuration. As it can be seen, the use of mixtures significantly decreases the COP of pure CO_2. With the blend CO_2/R-152a [95/5%] the reductions are lower than 2% but for the composition with 10% of R-152a, the COP decrements are important, reaching -18.6% at the lower temperature.

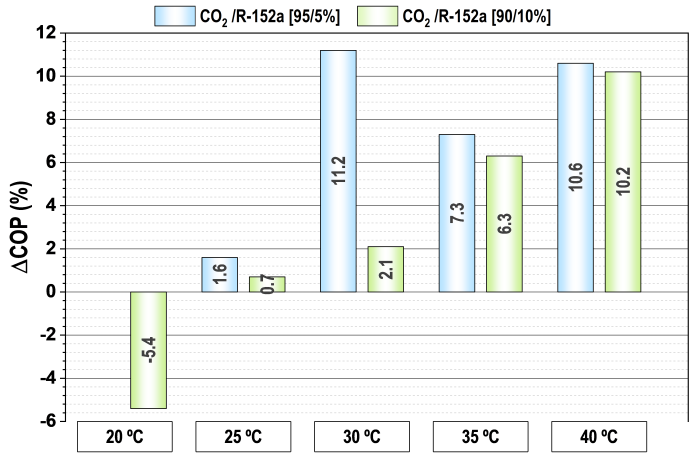

FIGURE 3.21: COP variations for base configuration

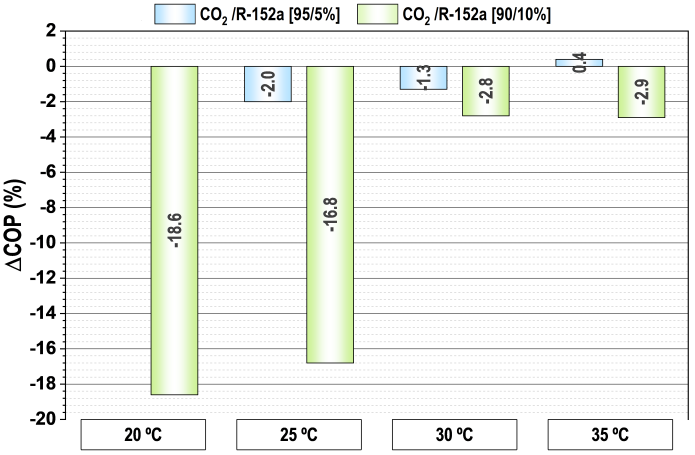

FIGURE 3.22: COP increments for IHX configuration

3.2.4 Theoretical model comparison

In this section, a comparison in terms of COP with the model presented in Chapter 2 of this thesis is presented as an example. The results presented are of the configuration with IHX, and the model was readjusted with the polynomial coefficients provided by the manufacturer for the Dorin CD380H compressor, used in the experimental facility of this chapter. Comparisons of CO_2, CO_2/R-152a [95/5%] and CO_2/R-152a [90/10%] refrigerants are presented in Figure 3.23, Figure 3.24 and Figure 3.25 respectively. As expected, the absolute value of COP is substantial and increases with the percentage of R-152a because of all those simplificative assumptions listed in the previous chapter. Nevertheless, the ability of the model, even if simplified, to predict trends (at least for this mixture) is demonstrated. Once the experimental data are known, combined with plant characteristics, they can be used to correct the model, allowing the behavior of the exchangers and compressor to be simulated in a more accurate and precise manner. However, this is a sucessive step that is beyond the scope of the theoretical model analyzed for mixture selection.

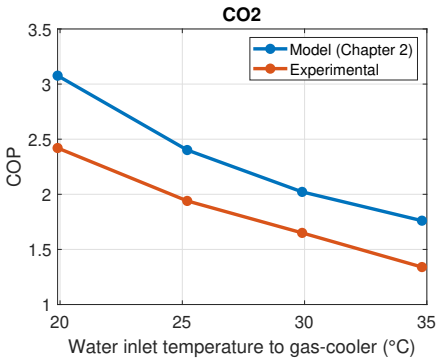

FIGURE 3.23: IHX model comparison

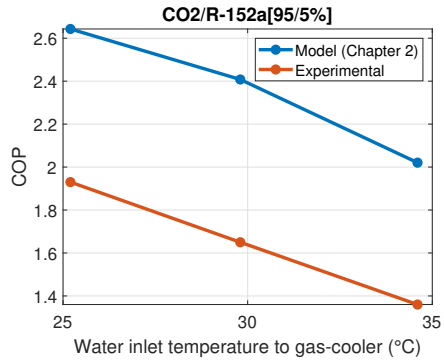

FIGURE 3.24: IHX model comparison

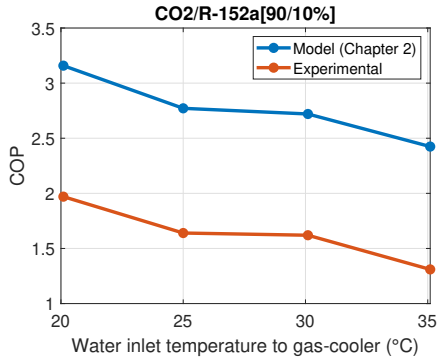

FIGURE 3.25: IHX model comparison

3.3 Chapter conclusions

This chapter presents experimental results and comparison of a CO_2 base refrigeration cycle with and without internal heat exchanger (IHX) working with CO_2/R-152a mixtures at 5% and 10% mass composition of R-152a as refrigerants. The experimentation is performed along heat rejection levels of 20 ºC, 25 ºC, 30 ºC, 35 ºC and 40 ºC and at one inlet temperature in the evaporator of 2.5 ºC, at steady-state conditions. The compressor run at nominal speed and the optimization parameter for both cycles was the gas-cooler pressure controlled with the back-pressure valve. All the obtained results have been validated by energy balances in the heat exchangers (see Table 3.5 and Table 3.6).

The experimental campaign has allowed to demonstrate the enhancement of COP in typical CO_2 cycles with the use of mixtures replacing pure CO_2. Using CO_2/R-152a blends instead of pure CO_2 as refrigerants in a base cycle improved the COP at high heat rejection temperatures. The use of CO_2/R-152a [90/10%] mixture provided COP improvements of 6.3% and 10.2% for $t_{w,in}$= 35ºC and $t_{w,in}$= 40ºC, respectively. Using CO_2/R-152a [95/5%] gave improvements of 7.3% and 10.6% for the same heat rejection temperatures and a maximum COP improvement of 11.2% for $t_{w,in}$=30 ºC. On the other hand, for cycle with IHX, using the evaluated mixtures as working fluids instead of pure CO_2 was always detrimental for the energy efficiency, except for the case of the use of the blend CO_2/R-152a [95/5%]

with $t_{w,in}$=35 °C, which improved the COP by 0.4%.

The COP of the cycle is the main parameter studied, however, other parameters such as cooling capacity, heat rejection pressure or discharge temperature of the compressor have been considered as well. As a consequence of the use of blends, some disadvantages were found: cooling capacity is reduced and the discharge temperature of the compressor is increased. However, the optimum heat rejection pressure is reduced, which is an advantage of using mixtures because it allows the cycle to work in subcritical conditions, where the control is easier, and it can allow to avoid using the liquid receiver.

TABLE 3.5: Test and optimum conditions and energy parameters of Base configuration

	Test conditions				Optimum cycle conditions						Energy parameters and uncertainty								
	$t_{w,in}$ (ºC)	$V_{w,in}$ (m^3/h)	$t_{g,in}$ (ºC)	$V_{g,in}$ (m^3/h)	p_h (bar)	p_{ves} (bar)	p_o (bar)	Δt_{gc} (K)	SH (K)	t_{dis} (ºC)	$\dot{m}_{ref}$ (kW)	$\dot{Q}_o$ (kg/s)	$\dot{Q}_{o,sf}$ (kW)	P_C (kW)	$\dot{Q}_{gc}$ (kW)	$\dot{Q}_{gc,sf}$ (kW)	COP (-)	I_{Q_o} (%)	I_{COP} (%)
CO_2	20.1	1.17	2.55	0.69	66.83	63.08	26.05	5.8	5.7	86.9	0.0392	6.53	6.46	3.07	9.23	9.25	2.13	3.2	3.2
	25.0	1.17	2.49	0.70	72.88	67.03	27.50	4.3	4.8	94.0	0.0398	5.52	5.51	3.35	8.96	8.77	1.65	7.5	7.5
	29.8	1.17	2.52	0.70	80.51	70.24	27.80	2.5	6.4	105.0	0.0391	5.32	5.31	3.65	8.86	8.52	1.46	7.8	7.8
	34.8	1.17	2.52	0.70	89.49	62.48	26.66	0.1	7.1	123.4	0.0343	4.93	4.85	3.93	8.35	8.50	1.25	4.1	4.2
	40.0	1.17	2.49	0.70	99.00	63.47	27.14	0.3	7.4	133.1	0.0332	4.30	4.18	4.27	7.93	8.09	1.01	4.3	4.3
CO_2/R-152a [95/5%]	25.1	1.17	2.52	0.70	68.99	65.24	22.74	1.9	6.2	105.2	0.0313	5.12	5.02	3.06	8.23	8.07	1.67	3.4	3.4
	30.1	1.17	2.53	0.70	74.83	71.96	23.23	1.3	6.2	112.6	0.0312	5.29	5.18	3.27	7.89	7.68	1.62	3.6	3.6
	34.8	1.17	2.49	0.70	82.94	80.65	23.65	0.3	6.3	123.3	0.0302	4.74	4.63	3.52	7.54	7.37	1.35	3.9	3.9
	39.7	1.18	2.54	0.70	93.83	91.68	24.13	0.2	6.2	138.2	0.0291	4.30	4.23	3.87	7.39	7.32	1.11	3.9	4.0
CO_2/R-152a [90/10%]	20.0	1.17	2.48	0.70	58.54	57.16	19.56	3.4	5.8	103.9	0.0266	5.26	5.19	2.62	7.49	7.44	2.01	4.0	4.0
	24.9	1.17	2.54	0.70	64.59	63.20	19.62	2.5	5.8	114.1	0.0256	4.67	4.62	2.81	7.11	7.08	1.66	4.2	4.2
	30.0	1.17	2.47	0.70	71.98	66.32	19.57	0.6	5.9	128.4	0.0240	4.46	4.32	3.00	6.77	6.75	1.49	4.3	4.3
	35.1	1.18	2.49	0.70	80.90	74.77	21.73	0.5	2.1	129.4	0.0270	4.47	4.41	3.35	7.17	6.97	1.33	4.0	4.0
	40.0	1.17	2.49	0.70	89.54	83.64	21.99	0.4	2.1	139.8	0.0261	3.97	3.95	3.58	6.85	6.52	1.11	4.2	4.3

TABLE 3.6: Test and optimum conditions and energy parameters of IHX configuration

	Test conditions				Optimum cycle conditions						Energy parameters and uncertainty											
	$t_{w,in}$ (°C)	$V_{w,in}$ (m^3/h)	$t_{g,in}$ (°C)	$V_{g,in}$ (m^3/h)	p_h (bar)	p_{ves} (bar)	p_o (bar)	Δt_{gc} (K)	SH (K)	t_{dis} (°C)	$\dot{m}_{ref}$ (kW)	$\dot{Q}_o$ (kg/s)	$\dot{Q}_{o,sf}$ (kW)	P_C (kW)	$\dot{Q}_{gc}$ (kW)	$\dot{Q}_{gc,sf}$ (kW)	$\dot{Q}_{ihx}$ (kW)	$\dot{Q}_{ihx,l}$ (kW)	ϵ_{ihx} (%)	COP (-)	I_{Q_o} (%)	I_{COP} (%)
CO_2	19.9	1.17	2.54	0.70	67.74	54.65	26.00	1.3		92.7	0.0378	7.46	7.49	3.08	9.99	10.43	0.499	0.523	39.4	2.42	2.9	2.9
	25.2	1.17	2.48	0.71	73.93	59.05	25.80	1.2	5.9	108.8	0.0353	6.50	6.60	3.35	9.25	9.12	0.498	0.512	36.0	1.94	3.0	3.0
	29.9	1.17	2.51	0.70	79.54	67.53	26.70	1.1	5.9	115.6	0.0356	5.93	6.00	3.60	8.88	8.71	0.502	0.575	35.4	1.65	3.2	3.2
	34.8	1.17	2.49	0.70	90.95	72.49	27.34	0.1	6.1	133.2	0.0338	5.39	5.44	4.03	8.66	8.63	0.496	0.607	35.9	1.34	3.3	3.3
CO_2/R-152a [95/5%]	25.2	1.17	2.56	0.70	69.00	59.21	22.71	1.6	6.2	114.1	0.0299	5.88	5.81	3.05	8.18	8.22	0.343	0.386	39.9	1.93	3.5	3.5
	29.8	1.17	2.51	0.70	75.98	62.89	23.12	0.6	6.2	125.6	0.0289	5.41	5.31	3.29	7.91	7.99	0.351	0.415	40.2	1.65	3.6	3.6
	34.6	1.17	2.50	0.70	81.17	73.68	23.71	0.3	6.2	134.0	0.0285	4.70	4.59	3.47	7.48	7.40	0.249	0.292	42.9	1.36	3.9	3.9
CO_2/R-152a [90/10%]	20.1	1.17	2.48	0.70	57.92	56.64	19.59	3.8	5.8	111.9	0.0255	5.09	5.07	2.59	7.39	7.23	0.091	0.260	43.4	1.97	4.1	4.1
	25.0	1.17	2.54	0.70	63.87	62.58	19.66	2.7	5.8	121.7	0.0248	4.56	4.52	2.78	7.06	6.86	0.053	0.303	44.0	1.64	4.3	4.3
	30.1	1.17	2.55	0.70	73.88	62.24	21.76	0.9	4.1	129.3	0.0267	5.11	4.99	3.15	7.56	7.79	0.250	0.351	39.8	1.62	3.9	3.9
	35.1	1.17	2.48	0.70	79.96	70.07	21.58	0.1	4.5	140.2	0.0251	4.36	4.32	3.32	6.98	6.74	0.150	0.443	45.4	1.31	4.2	4.2

TABLE 3.7: BASE configuration and fluids comparison

BASE					
	CO_2	CO_2/R-152a[95/5%]		CO_2/R-152a[90/10%]	
$t_{w,in}$ (°C)	$COP_{CO_2,Base}$	$COP_{mix,Base}$	$\left(\frac{COP_{mix,Base}-COP_{CO_2,Base}}{COP_{CO_2,Base}}\right)_{\%}$	$COP_{mix,Base}$	$\left(\frac{COP_{mix,Base}-COP_{CO_2,Base}}{COP_{CO_2,Base}}\right)_{\%}$
20	2.13	-	-	2.01	-5.4
25	1.65	1.67	1.6	1.66	0.7
30	1.46	1.62	11.2	1.49	2.1
35	1.25	1.35	7.3	1.33	6.3
40	1.01	1.11	10.6	1.11	10.2

TABLE 3.8: IHX configuration and fluids comparison

IHX								
	CO_2		CO_2/R-152a[95/5%]			CO_2/R-152a[90/10%]		
$t_{w,in}$ (°C)	$COP_{CO_2,IHX}$	$\left(\frac{COP_{mix,IHX}-COP_{CO_2,Base}}{COP_{CO_2,Base}}\right)_{\%}$	$COP_{mix,IHX}$	$\left(\frac{COP_{mix,IHX}-COP_{CO_2,Base}}{COP_{CO_2,Base}}\right)_{\%}$	$\left(\frac{COP_{mix,IHX}-COP_{CO_2,IHX}}{COP_{CO_2,IHX}}\right)_{\%}$	$COP_{mix,IHX}$	$\left(\frac{COP_{mix,IHX}-COP_{CO_2,Base}}{COP_{CO_2,Base}}\right)_{\%}$	$\left(\frac{COP_{mix,IHX}-COP_{CO_2,IHX}}{COP_{CO_2,IHX}}\right)_{\%}$
20	2.42	13.6	-	-	-	1.97	-7.6	-18.6
25	1.97	19.5	1.93	15.2	-2.0	1.64	-0.5	-16.8
30	1.67	14.4	1.65	1.6	-1.3	1.62	11.2	-2.8
35	1.35	7.7	1.36	0.8	0.4	1.31	4.5	-2.9

Chapter 4

Zeotropic refrigerants in a dedicated mechanical subcooling system

Regarding dedicated mechanical subcooling systems, researches have performed the evaluation of the cycles using pure fluids as refrigerants in the DMS. As Dai et al. [79] and Nebot-Andrés et al. [80] point out, the optimum subcooling degree (the precise conditions that maximise COP are called "optimum conditions" in this thesis) in CO_2 transcritical cycles is relatively high, reaching values as high as 16.5 ºC (t_o=5 ºC, t_{tenv}=30 ºC). This large subcooling implies a poor temperature match between CO_2 and the refrigerant when a pure fluid is used as refrigerant in the subcooler. It implies the operation at a low evaporation temperature in the DMS cycle and thus a reduction of the overall thermal efficiency of the cycle combination. In an attempt to enhance even more the combination of a DMS and a transcritical CO_2 cycle, Dai et al. [63] launched a hypothesis about the use of zeotropic refrigerant mixtures with matching glide in the DMS cycle, to reduce the temperature difference in the subcooler and thus to improve the performance of the combination. With a thermodynamic model with pressure dependent overall efficiencies of the compressors and using REFPROP v9.1 [81], they evaluated the performance of zeotropic binary combinations in the DMS. They selected R-32 as base fluid and then evaluated theoretically mixtures with R-290, R-1234yf, R-152a, R-1234ze(E), R-600a and R-1234ze(Z). They determined the optimum working conditions for each refrigerant mixture and concluded that theoretically the COP of a DMS-CO_2 cycle can be improved, and that the optimum heat rejection pressure is further reduced

compared to the case of a pure refrigerant. In Dai's study they found that the mixture R-32 with R-152a promised the best results in comparison with the use of R-152a as pure fluid, reaching an increment in COP of about 6%. An experimental evaluation based on this hypothesis is presented in this chapter. The evaporation test conditions in this chapter are different from the previous ones since the aim is to experimentally prove the use of the zeotropic mixture, and the conditions are adapted from previous tests with pure R-152a for comparison. Furthermore, the previous study conducted by Nebot-Andrés et al. [28] on the same plant shows that the evaporation temperature has little impact on the search for optimum pressure compared to the water inlet temperature at the gas-cooler.

Finally, the main objective of the work in this chapter, is to verify whether a zeotropic mixture in the DMS can improve the overall efficiency and to analyze first theoretically and then experimentally the impact on the temperature glide in the subcooler. As in Chapter 3, the facility for testing the mixtures will be the same, with no change of components, based on a "drop-in" analysis.

4.1 Thermodynamic selection of zeotropic blends

4.1.1 Thermodynamic model

To select the binary mixtures for the experimental evaluation, the thermodynamic model suggested by Dai et al. [63] has been adapted to the existing experimental plant (Fig. 4.2). The first modification is the introduction in the model of the overall efficiencies of the compressors, which were obtained from previous experimental campaigns by Sánchez et al. [82] (Eq. (4.1)) for the CO_2 compressor and by Llopis et al. [27] (Eq. (4.2)) for the DMS compressor with R-152a.

$$\eta_{g,CO_2} = 0.736 - 0.052\frac{p_{dis}}{p_{suc}} \tag{4.1}$$

$$\eta_{g,DMS} = 0.632 - 0.037\frac{p_{dis}}{p_{suc}} \tag{4.2}$$

Then, the simulating conditions were adapted to the known performance of the plant, they being:

- Approach temperature in gas-cooler of 1.5 K, since the plant is a water-to-water system.
- Approach temperature in subcooler of 5 K.
- Approach temperature in the DMS condenser of 8 K.
- DMS condenser subcooling degree of 2 K.
- Superheating degree in CO_2 evaporator of 10 K and in subcooler of 6 K.

Finally, using the model, the COP of the CO_2 transcritical cycle with the DMS system (Eq. (4.3)) was optimized in terms of subcooling degree and heat rejection pressure at a water inlet temperature to the gas-cooler and DMS condenser of 35 ºC and at an evaporating temperature of -14 ºC, which were the experimental conditions with the R-152a evaluation by Nebot-Andrés et al. [28], used as initial reference.

$$COP = \frac{\dot{Q}_o}{P_{C,CO_2} + P_{C,DMS}} \tag{4.3}$$

The optimization covered binary mixtures of R-152a with R-32, R-600 and CO_2 in steps of 10% of mass fraction variation. For each fluid and at each operating condition, an optimization to find the best combination of gas-cooler pressure and subcooling degree was performed, with the aim to quantify the best energy efficiency. The COP at such conditions is named "Maximum COP" as in previous chapters. REFPROP v10.0 was used to evaluate the thermophysical properties of the fluids (Lemmon E. W. et al. [65]).

4.1.2 Theoretical results

Figure 4.1 summarizes the maximum overall COP values with the different evaluated refrigerant mixtures at a water inlet temperature of 35 ºC and an evaporating level of -14 ºC. With R-152a the maximum COP reaches 1.53, whereas for the mixtures it varies depending on the R-152a mass fraction. First, it needs to be mentioned that for the existing plant and for the mixture R-152a/R-32 the COP does not present a maximum value, as observed in the theoretical results of Dai et al. [63]; and furthermore, this binary mixture

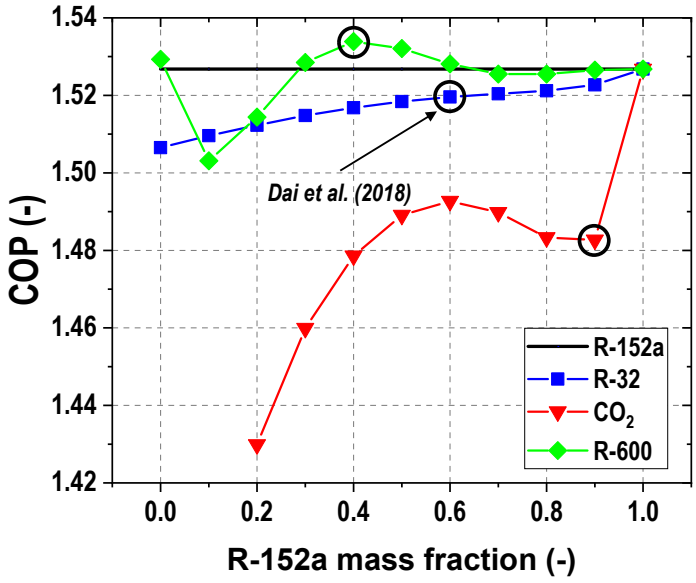

FIGURE 4.1: Maximum theoretical COP at t_o=-14 ºC and $t_{w,in}$=35 ºC, as a function of R-152a mass fraction

does not overperform the base fluid. Second, the mixture of R-152a/CO_2 presents a maximum value, but lower in terms of efficiency to the base fluid. Finally, the unique binary combination that offers COP improvements in relation to the base fluid is R-600/R-152a, which presents a maximum of 1.534 at 0.4 mass fraction of R-152a. Thus, at least with one mixture the theoretical model indicates that there is room for improvement.

4.1.3 Selected refrigerant mixture

According to the simulations, three binary mixtures were tested in the DMS experimentally, whose main characteristics are reflected in Table 4.1, obtained for a CO_2 evaporation temperature of -14 ºC, a CO_2 condensing temperature of 50 ºC ($t_{k,DMS}$), SH=5 K and SUB=2 K.

- R-152a: Selected as the reference fluid for the DMS, since it was completely tested in a previous investigation (Nebot-Andrés et al. [83]).
- R-600/R-152a [60/40%]: it was selected from the theoretical simulation (Fig. 4.1) as the best performing mixture. It was prepared using n-butane with purity of 99.9% and R-152a at 99.9%, with an uncertainty in the mass composition below 0.1%. This fluid presents lower phase-change pressures than R-152a, 18% higher specific volume, 14% reduced volumetric cooling capacity, 2% lower COP_{DMS} and a moderate effective glide in the subcooler of 5.1K.
- R-152a/R-32 [60/40%]: Although it does not obtain good theoretical results, it was considered as suggested by (Dai et al. [63]), since it was the best proportion for the combination of R-152a and R-32 in their study. Presence of R-32 increases the phase-change pressures, the suction volume is 31% lower, the COP_{DMS} is similar and it presents 5.9 K effective glide in the evaporator. The mixture was prepared in the lab with a mass uncertainty below 0.1%.
- R-152a/CO_2 [90/10%]: Finally, although not obtaining good results, this mixture was selected to investigate the effect of using a high-effective-glide fluid in the subcooler. Proportion of CO_2 was limited to 10% to be able to operate with the existing plant. In this case, with 12.3 K glide in the subcooler, the mixture presents 35% higher volumetric cooling capacity, 3% higher COP_{DMS} and 17% reduced specific suction volume. The mixture was prepared in the lab using CO_2 with 99.9% purity. The uncertainty of the composition is below 0.1%.

Mixture preparation was made using high purity fluids. Composition uncertainty is below 0.1% in mass. As mentioned above all the mixtures have been simulated in the theoretical model using REFPROP v10.0 using the suggested mixing coefficients, which could lead to uncertainty in evaluating thermophysical properties. The model, therefore, is not able to supply the necessary accuracy to define the exact behaviour of the mixtures in the system giving rise to the need of an experimental approach.

TABLE 4.1: Selected refrigerants for experimental evaluation and ideal-single-stage cycle performance data of the DMS at t_o=-14 ºC, t_k=50 ºC, SH=5 K and SUB=2 K

Fluid	M (g/mol)	GWP (-)	p_o (bar)	p_k (bar)	v_{suc} (m/kg)	λ (kJ/kg)	VCC_{DMS} (kJ/m^3)	COP_{DMS} (-)	$Glide_o$ [K]	$Glide_k$ [K]
R-152a	66.1	137	4.39	11.77	0.075	291.1	3142	7.03	0.0	0.0
R-152a/R-32 [60/40%]	59.6	353	6.97	18.31	0.051	302.9	4776	6.79	5.9	6.5
R-600/R-152a [60/40%]	61.1	55	4.05	10.60	0.089	308.8	2697	6.87	5.1	5.9
R-152a/CO_2 [90/10%]	62.9	123	5.63	15.38	0.062	327.0	4257	7.25	12.3	19.9

TABLE 4.2: Main component of the experimental plant

Equipment	Type	Tech. info
Main compressor	Semi hermetic	$\dot{V} = 3.48.m^3/h$
DMS compressor	Semi hermetic	$\dot{V} = 4.06.m^3/h$
Gas cooler	Brazed plate	$A = 4.794m^2$
Evaporator	Brazed plate	$A = 1.224m^2$
Subcooler	Brazed plate	$A = 0.576m^2$

4.2 Experimental test bench

4.2.1 Test bench description

To evaluate the zeotropic binary mixtures a research plant previously built was used (Fig. 4.2). The plant is almost the same as Chapter 3 with a single-stage CO_2 compression cycle, a double-stage expansion system that incorporates brazed-plate subcooler (0.576 m^2) and a different type of compressor with a displacement of 3.48 m^3/h at 1450 rpm. Both, back-pressure and expansion valves are electronic and allow controlling the heat rejection pressure and the superheating degree in the evaporator. The subcooling is provided coupling thermally another single-stage vapour compression system through the subcooler, in which the DMS refrigerant evaporates. This cycle is composed of a semi-hermetic compressor (4.06 m^3/h at 1450 rpm), a shell-and-tube condenser and an electronic expansion valve that is customized for each refrigerant. Heat dissipation in gas-cooler and DMS condenser is performed with a water loop, allowing the volumetric flow and inlet temperature to be controlled. The heat load is provided with a loop working with a propylene-glycol mixture (see Figure 3.4 in Chapter 3), also allowing to regulate the volumetric flow and inlet temperature. It is important to note that the CO_2 compressor is different from Chapter 3, and therefore the coefficients for its simulation in the first section of this Chapter are different. For the calibration range and measurement error of instrumentation see Table 3.1 and main components are summarized in Table 4.2.

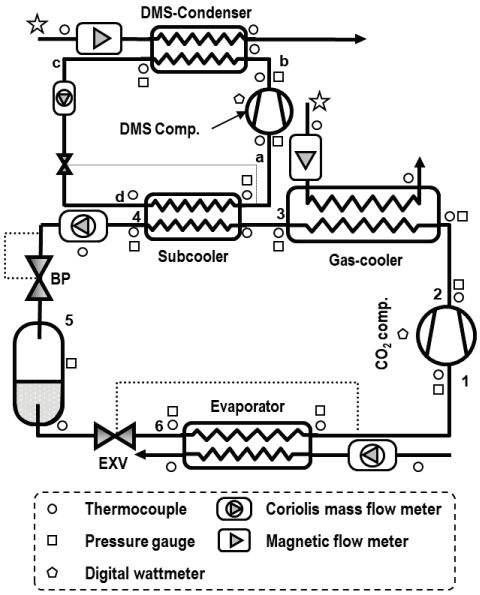

FIGURE 4.2: Scheme of the experimental test bench

4.2.2 Experimental procedure

The experimental tests were conducted in steady-state conditions according to the following constraints:

- Heat rejection: system was evaluated for all the mixtures at three water dissipation temperatures of 25.1, 30.3 and 35.1 ºC. This temperature was warranted (±0.2 K) at the inlet of the DMS condenser and at the inlet of the gas-cooler (see stars in Fig. 4.2). The volumetric flow of water was of 1.16 m^3/h at the gas-cooler and of 0.61 m^3/h at the DMS condenser.

- Heat load: the plant was tested only at one evaporating condition, that was fixed using an inlet temperature of the glycol-mixture in the evaporator at -1.2 ºC ± 0.2 K, with constant volumetric flow rate of 0.71 ± 0.02 m^3/h.

- Heat rejection pressure: it was regulated with the electronic back-pressure using an own PID controller implemented in the monitoring system.

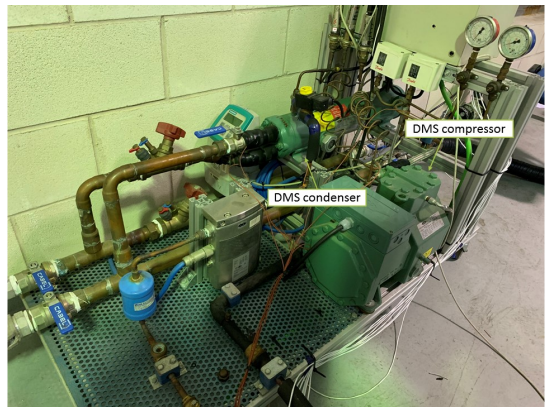

FIGURE 4.3: DMS experimental plant

- Subcooling degree: the subcooling degree in the subcooler was regulated with speed variation of the DMS compressor. The CO_2 compressor was always kept at nominal speed (1450 rpm).
- Superheating degree: In the CO_2 evaporator 10 K and in subcooler 5 K were maintained.

In order to obtain the optimum conditions of the subcooled CO_2 transcritical cycle, the plant was subjected to optimization of heat rejection pressure and subcooling degree. The maximum COP value was obtained from cooling capacity calculation, Eq. (4.4), and the direct measurements of compressor power consumption, according to Eq. (4.3). In Fig. 4.4, it can be observed the optimization process as function of gas-cooler pressure and subcooling degree (Eq. (4.5), where the black points correspond to the experimental measurements. The optimum conditions determination ended when the COP value from a point to another changed less than 1%.

$$\dot{Q}_o = \dot{m}_{CO_2}(h_{o,out} - h_{exp}) \tag{4.4}$$

$$SUB = t_{sub,in} - t_{sub,out} \tag{4.5}$$

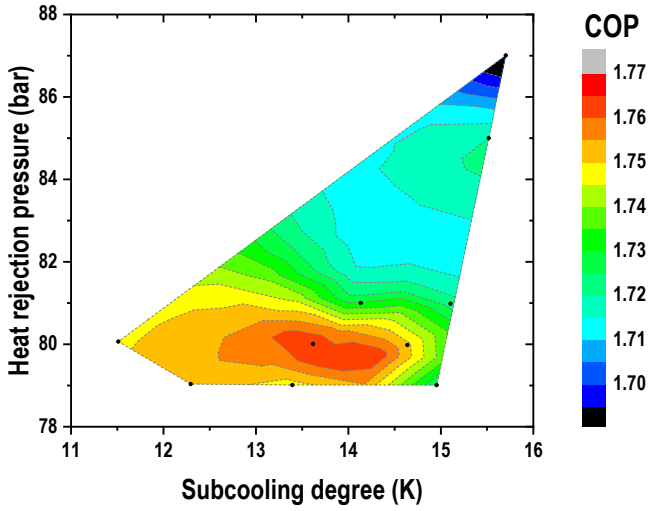

FIGURE 4.4: Experimental optimization of CO_2–R-600/R-152a [60/40%] at $t_{w,in}$=30.3 ºC

4.2.3 Data Validation

Considering the calibrated accuracy of the measurement devices, (Table 3.1, the uncertainties of cooling capacity, Eq. (4.4), and COP, Eq. (4.3), were evaluated using Moffat's method [84] (see Appendix A), reaching maximum uncertainties of 0.84% and 0.95%, respectively. Furthermore, the heat transfer balance in subcooler was considered to check experimentally the consistency of measurements and to contrast that the evaluation of thermodynamic properties of mixtures with REFPROP v10.0 does not introduce large computation errors. Table 4.3 reflects the percentage deviation between the heat transferred by CO_2 and the mixture in the subcooler, reaching maximum deviations of 3.7%, which are considered good for the purpose of this investigation.

4.3 Results

4.3.1 Optimum conditions

Optimum conditions, in terms of COP, Eq. (4.3), for the three heat rejection levels and for the four refrigerants used in the DMS cycle are summarized

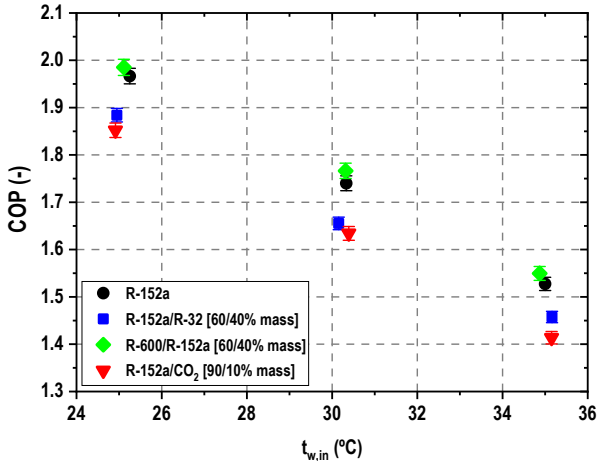

FIGURE 4.5: Maximum experimental COP at $t_{g,in}$ = -1.25 ºC

in Fig. 4.5. It can be observed that a zeotropic mixture is able to overperform the reference fluid (R-152a). Concretely, the energy improvement achieved by the mixture R-600/R-152a [60/40%] is between 1.1 to 1.4% higher than with R-152a. However, the two other refrigerant blends present COP reductions. R-152a/R-32 [60/40%] mixture presents an overall COP decrease between 4.1 to 5% and the R-152a/CO_2 [90/10%] mixture a COP cut between 5.6 to 7.%. Although the test conditions are different, the measured trends (Fig. 4) coincide with the theoretical simulations summarized in Fig. 4.1. Thus, it is demonstrated experimentally that it is possible to improve the performance of a dedicated mechanical subcooling system by the use of a zeotropic mixture in the auxiliary cycle, as suggested by Dai et al. [63]. At optimum conditions (Fig. 4.5), the partial contribution to the cooling capacity of each refrigeration cycle is presented in Fig. 4.6, where $\dot{Q}_{sub}$ represents the enhancement of capacity due to the subcooling, Eq. (4.6), and $\dot{Q}_{base}$ the capacity provided by the CO_2 cycle, Eq. (4.7).

$$\dot{Q}_{sub} = \dot{m}_{CO_2}(h_{sub,out} - h_{gc,out}) \tag{4.6}$$

$$\dot{Q}_{base} = \dot{Q}_o - \dot{Q}_{sub} \tag{4.7}$$

On the one side, as it can be observed in Fig. 4.6, the contribution corresponding to the base cycle is similar for each test condition between the different DMS refrigerants. Small variations of this parameter are linked to the different optimum heat rejection pressures, which are lower as higher the subcooling degree is (see Table 4.3). At reduced heat rejection pressures, the capacity provided by the CO_2 itself is lower. However, large differences are found in the partial contribution to the cooling capacity provided by the subcooler, Eq. (4.6). For the mixture R-152a/R-32 [60/40%] this contribution is between 16.2 and 41.1% higher than with the use of R-152a at optimum conditions, for R-600/R-152a [60/40%] ranges between -5.1 to -7.1% and for R-152a/CO_2 [90/10%] from 0.4 to 9.1%. These variations are not directly correlated with the VCC_{DMS} parameter (Table 4.1). Nonetheless, it is important to note that the use of the DMS cycle always intensifies the capacity provided by the cycle. On the other side, the contribution to the power consumption of each compressor is presented in Fig. 4.7. It is observed that the power consumption of the CO_2 compressor remains similar between all the refrigerants unlike R-152a/R-32 [60/40%] with $t_{w,in}$=35.1 °C that, due to the large optimum subcooling degree, allows the CO_2 cycle to work at a lower optimum pressure; on the contrary there are large differences at all conditions with the auxiliary compressor. In this case, refrigerants with high VCC_{DMS} (R-152/R-32 and R-152a/CO_2) show greater cooling capacity and thus have larger power consumption in the DMS compressor. It is worth focusing on the R-600/R-152a [60/40%] mixture, that presents a very low power consumption in the DMS compressor, it being between 8.9 and 11.2% in relation to the power absorbed by the CO_2 one and between 15.2 and 21.0% lower than that absorbed with the use of R-152a in the DMS cycle. The behaviour of R-600/R-152a [60/40%] mixture and thus the optimum conditions when working coupled to the CO_2 cycle are bounded to the high COP_{DMS} values achieved by the mixture (Table 4.3) which are higher than the values reached with R-152a. Although theoretical COP_{DMS} are higher for R-152a than for R-600/R-152a [60/40%] mixture (see Table 4.1), the experimental COP_{DMS} have an opposite trend, because the working conditions (blend phase-change temperatures) vary, as it is analysed in the following section.

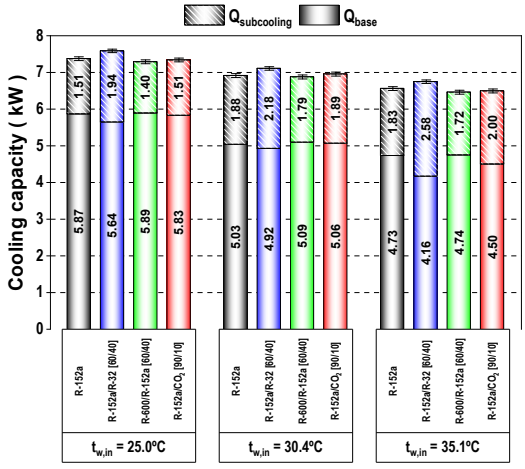

FIGURE 4.6: Cooling capacity at optimum condition at $t_{g,in}$ = -1.25 ºC

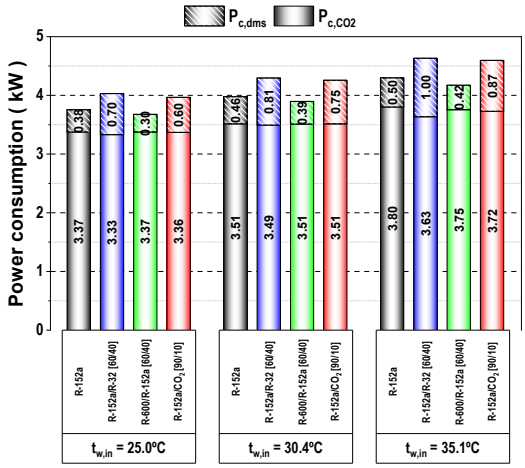

FIGURE 4.7: . Power consumption at optimum condition at $t_{g,in}$ = -1.25 ºC

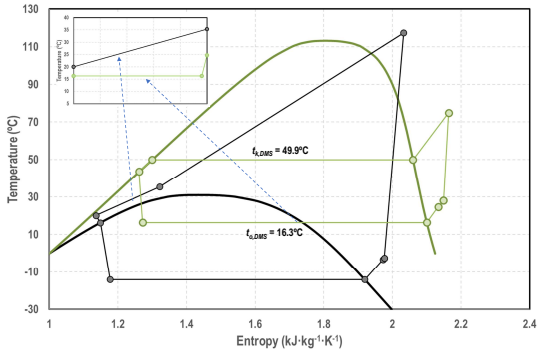

FIGURE 4.8: t-s diagram of CO_2 – R-152a at $t_{w,in}$=35.1 ºC and $t_{g,in}$ =-1.25 ºC

4.3.2 Operating parameters

As mentioned before, the optimum working condition of the dedicated subcooling cycle, in terms of heat rejection pressure and subcooling degree, is different between the different refrigerant blends. This section analyses closely the working conditions of each combination at dissipation water inlet temperature of 35.1 ºC. Fig. 4.8 to Fig. 4.11 represent the t-s diagram of the different refrigerants, where the estimated temperature profiles in the subcooler are highlighted. For the sake of a graphical representation, they are considered linear without affecting the conclusions of this investigation. Fig. 4.12 illustrates the phase-change temperatures of the DMS refrigerant. Furthermore, Table 4.4 summarizes the key parameters of the most representative elements of the plant. As it can be observed in Fig. 4.8 to Fig. 4.11, the use of a zeotropic refrigerant mixture in the DMS cycle introduces a temperature difference through the phase-change temperature. During condensation the temperature decreases, whereas during the evaporation increases. The temperature change or effective temperature glide in the evaporator, Eq. (4.8), depends upon the components of the blend.

$$Glide_{e,o,DMS} = t_{o,v,DMS,out} - t_{o,DMS,in} \tag{4.8}$$

Analysing results of Table 4.4, it is observed that the mixture R-600/R-152a presents the highest effective glide in the subcooler. R-152a/CO_2,

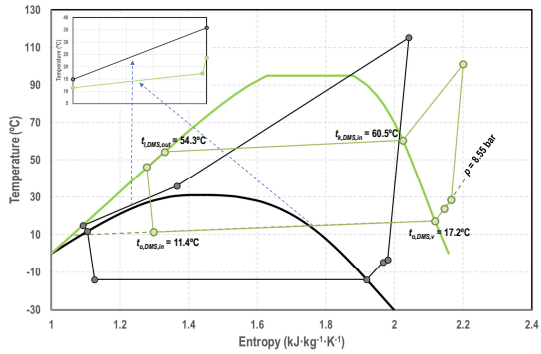

FIGURE 4.9: t-s diagram of CO_2 – R-152a/R-32 [60/40%] at $t_{w,in}$=35.1 ºC and $t_{g,in}$ =-1.25 ºC

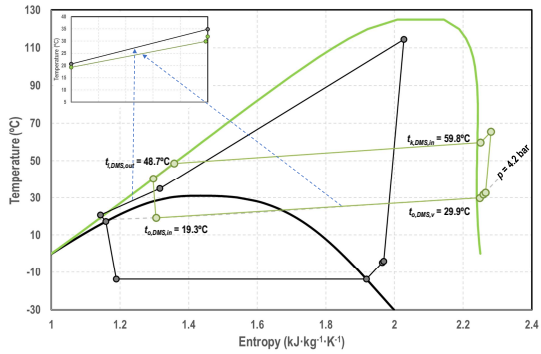

FIGURE 4.10: t-s diagram of CO_2 – R-600/R-152a [60/40%] at $t_{w,in}$=35.1 ºC and $t_{g,in}$ =-1.25 ºC

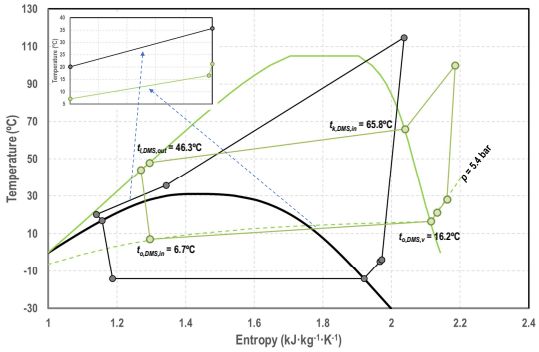

FIGURE 4.11: t-s diagram of CO_2 – R-152a/R-CO_2 [90/10%] at $t_{w,in}$=35.1 ºC and $t_{g,in}$ =-1.25 ºC

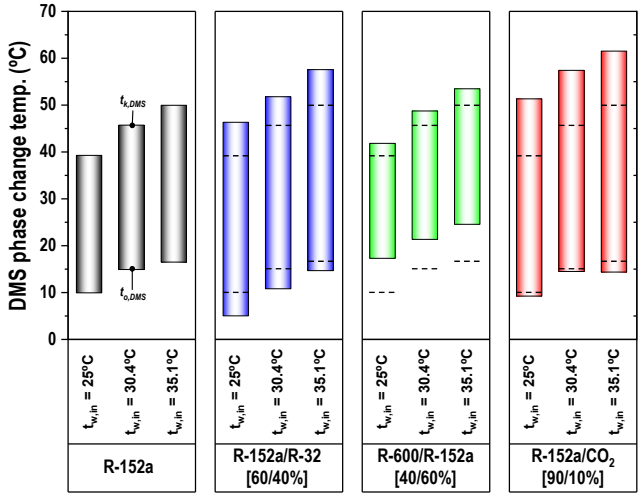

FIGURE 4.12: Phase change temperatures of DMS cycle at optimum conditions at $t_{g,in}$=-1.25 ºC

whose total glide is higher, does not have a large effective glide in the subcooler, since the main change in temperature during the phase-change is produced at lower vapour quality conditions (see isobaric line in Fig. 4.11), which are out of the operation of the subcooler. The best temperature match between R-600/R-152a [60/40%] and the CO_2 temperature profile along the subcooler influence the rest of parameters of the subcooler (Table 4.4). The thermal effectiveness of subcooler, Eq. (4.8), reaches even higher values than that with the use of a pure fluid; the pinch at the exit/inlet of the subcooler, Eq. (4.10), reaches lower values than that with R-152a; and the logarithmic mean temperature difference, Eq. (4.11), also reaches lower values than with the reference fluid. For the rest of the blends, which do not have a good temperature match with CO_2, the parameters of the subcooler are worse than with the use of R-152a. Thus, as suggested by Dai et al. [63], if the refrigerant mixture has a good matching temperature glide with CO_2 temperature profiles, the performance of the system can be improved. It should be noted that the subcooler size was fixed, thus, if the subcooler is resized for each mixture the results could change. In relation to working temperatures (Fig. 4.12), it can be observed that for the blends R-152a/R-32 and R-152a/CO_2 the difference between condensation and evaporation temperature increases due to the low thermal performance of the subcooler (Table 4.4). However, for the mixture R-600/R-152a this difference decreases, and what is more important, the thermal improvement in the subcooler makes the evaporating temperature in the subcooler to be higher and thus, it allows the DMS cycle to work with higher COP_{DMS} values, resulting in a net increment of the COP of the combination, as seen in Fig. 4.5.

$$\epsilon_{sub} = \frac{t_{gc,out} - t_{sub,out}}{t_{gc,out} - t_{o,DMS,in}} \tag{4.9}$$

$$\Delta t_{sub} = t_{DMS,out} - t_{o,DMS,in} \tag{4.10}$$

$$\Delta t_{lmtd} = \frac{(t_{DMS,out} - t_{o,DMS,in}) - (t_{gc,out} - t_{o,v,DMS,out})}{ln\left(\frac{t_{DMS,out} - t_{o,DMS,in}}{t_{gc,out} - t_{o,v,DMS,out}}\right)} \tag{4.11}$$

Finally, to illustrate the energy improvement achieved using zeotropic blends in the DMS cycle, irreversibilities in subcooler, Eq. (4.12) have been evaluated. They are presented in a normalized form in Fig. 4.13. To normalize the irreversibilities, total exergy destruction in the subcooler has

been divided by the cooling capacity of the CO_2 cycle, Eq. (4.4), and by the death state temperature, which has been considered to be -14 ºC.

$$\Delta \dot{E}_{X,sub} = t_d[\dot{m}_{CO_2}(s_{sub,out} - s_{sub,in}) + \dot{m}_{DMS}(s_{DMS,in} - s_{DMS,out})] \quad (4.12)$$

Fig. 4.13 reflects that a good matching temperature glide with CO_2 temperature profile in subcooler allows to reduce the irreversibilities in the subcooler. In this case, the blend R-600/R-152a [60/40%] presents a reduction of irreversibilities in relation to R-152a from -2.9 to 18.9%. In addition, also mixture R-152a/CO_2 [90/10%] reduces irreversibilities in some operating conditions.

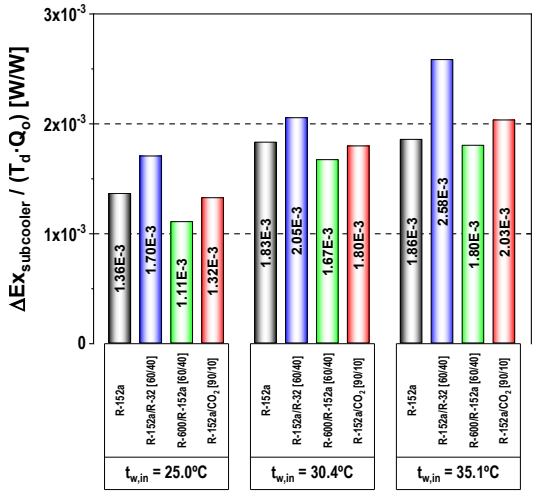

FIGURE 4.13: Normalized exergy destruction in subcooler at $t_{g,in}$=-1.25 ºC

4.4 Chapter conclusions

In this chapter the possibility to enhance the performance of a transcritical CO_2 refrigeration plant using a dedicated mechanical subcooling system with zeotropic refrigerant mixtures has been addressed theoretically and experimentally.

Using Dai et al. [63] model adapted to an existing test plant, the performance of three blends composed of R-32, R-600 or CO_2 with the base fluid R-152a has been evaluated. It has been observed that, theoretically, it is possible to obtain higher COP values in relation to the use of pure fluids. However, trends presented by Dai et al. [63] have not been reproduced in the simulations. The difference, whose cause cannot be defined, could be associated to the different used overall compressor efficiencies and with updated tool for refrigerant properties prediction, which differ from the previous works. Theoretical simulation has identified the blend R-600/R-152a [60/40%] as the best performing one, with theoretical COP improvements up to 0.46%.

Three refrigerant blends, R-152a/R-32 [60/40%], R-600/R-152a [60/40%] and R-152a/CO_2 [90/10%] have been tested experimentally against the operation with R-152a as refrigerant in the dedicated subcooling system. The evaluation was made at fixed conditions of the secondary fluids and covered three heat rejection levels, achieved varying the water inlet temperature to gas-cooler and DMS condenser (25.1, 30.3 and 35.1ºC). Experimental campaign has identified the optimum conditions, in terms of subcooling degree and heat rejection pressure, of the plant.

It has been verified that the mixture R-600/R-152a [60/40%] is able to enhance the COP of the plant, with COP increments between 1.1 and 1.4%. Nevertheless, given the type of mixture, there is also an issue of flammability in a practical utility and this must be taken into account. The mixture R-152a/CO_2 [90/10%], which has good matching temperature profiles in the subcooler, could also improve the performance of the plant if the subcooler was resized. However, the other mixtures did not show good performance. The experimental results indicated that the improvements are higher for blends with low volumetric cooling capacity. At optimum conditions, these mixtures work with a moderate subcooling degree and have low power consumption in the auxiliary compressor. Furthermore, as suggested by Dai et al. [63], the mixtures which effective temperature glide matches with the CO_2 temperature evolution in the subcooler, enhance the thermal performance of the subcooler. Consequently, the evaporating level in the subcooler with the mixture can be higher than with the pure fluid and enhance the performance of the auxiliary cycle and thus of the cycle

combination.

Finally, it needs to be mentioned that the use of zeotropic blends in the subcooler allows to reduce the irreversibilities in this heat exchanger.

TABLE 4.3: Summary of test conditions, main cycle and DMS cycle indicators at optimum working conditions

	Test conditions					Cycle indicators				DMS cycle indicators			
	$t_{w,in}$ (ºC)	$V_{w,gc,in}$ (m^3/h)	$V_{w,DMS,in}$ (m^3/h)	$t_{g,in}$ (ºC)	$V_{g,in}$ (m^3/h)	COP (-)	Q_o (kW)	p_{gc} (bar)	SUB (K)	ϵ_{sub} (%)	COP_{DMS} (-)	$Q_{o,DMS}$ (kW)	$\left(\frac{Q_{o,DMS}-Q_{SUB}}{Q_{SUB}}\right)_{\%}$ (%)
R-152a	25.3	1.10	0.62	-1.2	0.70	1.97	7.4	74.9	14.3	87.5	3.98	1.5	-2.6
	30.3	1.15	0.63	-1.1	0.72	1.74	6.9	79.2	14.5	85.7	4.07	1.9	-2.8
	35.0	1.19	0.61	-1.3	0.73	1.53	6.6	90.0	15.3	80.4	3.69	1.8	-3.6
R-152a/R-32 60/40%	24.9	1.16	0.60	-1.4	0.71	1.88	7.6	74.9	20.0	82.0	2.78	1.9	-1.1
	30.2	1.15	0.62	-1.2	0.71	1.66	7.1	79.9	19.9	83.5	2.71	2.2	-3.5
	35.2	1.15	0.60	-1.3	0.71	1.46	6.7	85.8	21.0	86.0	2.59	2.6	-1.8
R-600/R-152a 60/40%	25.1	1.18	0.61	-1.2	0.72	1.99	7.3	74.9	12.5	75.0	4.65	1.4	-3.2
	30.3	1.16	0.62	-1.2	0.71	1.77	6.9	79.8	13.6	76.0	4.60	1.8	-3.2
	34.9	1.15	0.63	-1.2	0.71	1.55	6.5	89.4	14.2	78.9	4.11	1.7	-2.6
R-152a/CO_2 90/10%	24.9	1.16	0.60	-1.2	0.71	1.85	7.3	74.9	14.0	60.7	2.53	1.5	-1.9
	30.4	1.16	0.59	-1.3	0.71	1.63	7.0	79.9	15.0	63.7	2.54	1.9	-3.3
	35.2	1.16	0.59	-1.2	0.70	1.41	6.5	87.9	15.5	57.1	2.30	2.0	-3.7

TABLE 4.4: Performance operating parameters of key elements at optimum conditions

	$t_{w,in}$ (ºC)	η_{G,CO_2} (-)	$\eta_{G,DMS}$ (-)	t_{CO_2} (-)	t_{DMS} (-)	$Glide_{e,o,DMS}$ (K)	ϵ_{sub} (%)	Δt_{sub} (K)	Δt_{lmtd} (K)
R-152a	25.3	55.0	43.2	3.3	2.4	-	87.5	2.0	6.8
	30.3	54.2	49.1	3.5	2.5	-	85.7	2.4	7.4
	35.0	53.7	48.5	3.8	2.6	-	80.4	3.7	9.4
R-152a/R-32 60/40%	24.9	54.5	45.2	3.4	3.4	5.1	67.0	9.9	16.2
	30.2	53.6	45.6	3.5	3.2	5.4	66.6	10.0	16.1
	35.2	53.3	47.9	3.7	3.2	5.6	67.9	9.9	16.5
R-600/R-152a 60/40%	25.1	54.8	30.4	3.3	2.1	10.9	87.5	1.8	2.5
	30.3	54.5	44.8	3.4	2.3	10.7	87.7	1.9	3.2
	34.9	53.5	47.1	3.8	2.3	10.6	91.0	1.4	2.8
R-152a/CO_2 90/10%	24.9	54.6	42.4	3.3	3.6	8.4	61.1	8.9	11.5
	30.4	54.6	47.6	3.5	3.5	8.5	64.1	8.4	11.3
	35.2	53.5	49.4	3.7	3.9	7.8	57.4	11.5	15.0

Part II

Cycle modifications and thermal energy storage as a method of improving CO_2 commercial refrigeration plants

Chapter 5

Experimental comparison of commercial refrigeration cycle modifications

This chapter presents a comprehensive experimental comparison of modifications to a multi-stage two-evaporator transcritical CO_2 refrigeration cycle. The system was already built and validated in a previous work conducted by Barta et al. [85]. Nevertheless, some modifications were made from the lessons learned from the previous work and to expand the possible configurations of the system, all of which are described in detail below. Among the cycle comparisons there are two methods for ejector control. The first control method is a variable motive nozzle and the second is the addition of a variable-speed pump located at the gas cooler outlet to vary the ejector motive nozzle inlet pressure. The results of a comprehensive comparison parametric study are presented, as is an assessment of the effectiveness of both proposed control methods.

5.1 System overview

5.1.1 Test stand design

The experimental test stand utilized in this work is comprised of two evaporation temperatures, three stages of compression, intercooling between the second and third compression stages, a flash tank at the medium-temperature (FT) evaporator inlet, an IHX, a CO_2 pump located between the gas cooler outlet and ejector motive nozzle inlet, and either an electronic

expansion valve (EXV) or an ejector for expansion. An ejector harnesses expansion work by accelerating the high-pressure flow from the gas cooler outlet via a motive nozzle into a high-velocity motive flow, which entrains low-pressure flow from the evaporator outlet through a suction nozzle. The two flows then mix and diffuse at a pressure greater than the evaporation pressure, which reduces the amount of pressure lift required of the compressor and thus, the required compressor input power. Open economization is conducted with a flash tank, which is a large vessel into which two-phase flow enters and flashes into separate phases as a result of the sudden increase in volume. Gravity then further separates the phases such that the saturated vapor flows out the top of the tank to bypass the evaporator while the saturated liquid exits the bottom of the tank to enter the evaporator at a lower specific enthalpy than the evaporator would receive without the use of a flash tank. This can result in an increased cooling capacity if the impact of the larger change in specific enthalpy across the evaporator outweighs the disadvantage of the reduced mass flow rate passed through the evaporator.

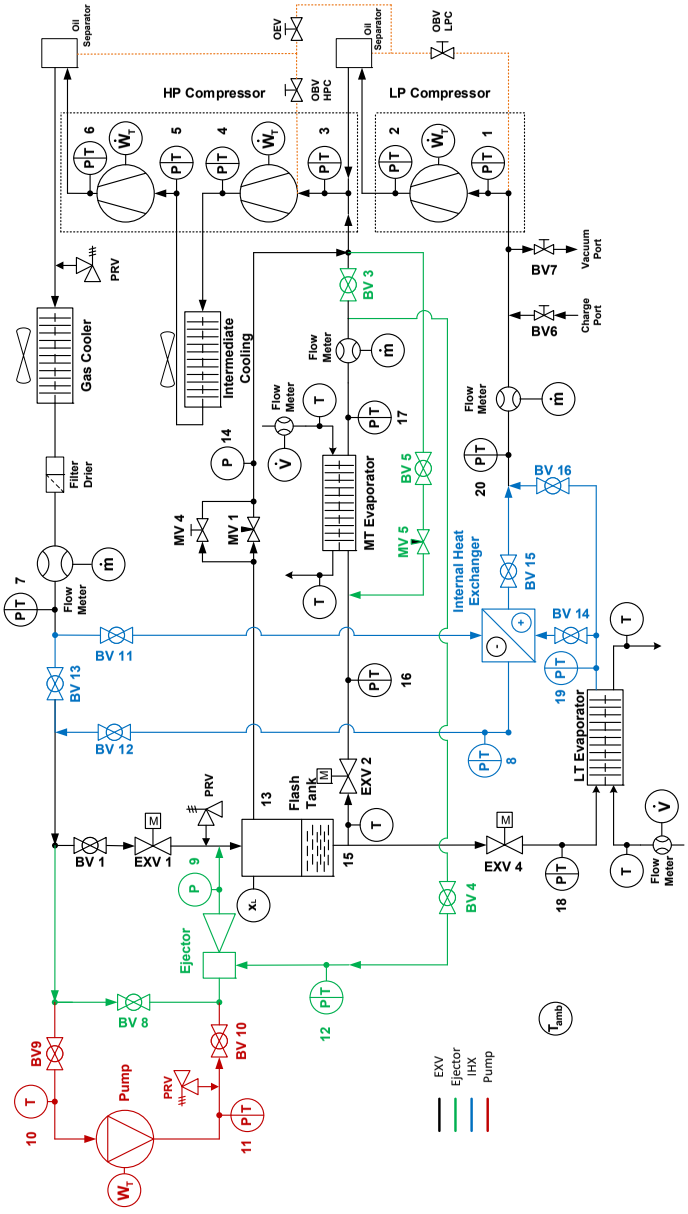

FIGURE 5.1: P&ID of the utilized test stand

In the test stand utilized in this work, four cycle architectures were assessed over a range of operating conditions. The first cycle (Configuration 1) was treated as the baseline and consists of isenthalpic expansion through an EXV with a flash tank applied upstream of the MT evaporator to facilitate open economization, where saturated liquid is throttled to the evaporator inlet and the vapor bypasses the evaporator. The second cycle utilized an ejector with motive flow from the gas cooler outlet and suction flow from the MT evaporator outlet (Configuration 2). The ejector diffuser outlet flow then enters the flash tank where the same open economization process as in configuration 2 takes place occurs. The third cycle is similar to the first configuration but utilizes an IHX (Configuration 3) to further cool the gas cooler outlet flow before it is expanded into the flash tank and also to further superheat the compressor suction flow. Finally, a pump was added between the gas cooler outlet and the motive nozzle inlet (Configuration 4) to increase the cycle efficiency by providing additional pressure differential across the motive nozzle and thus, additional potential work for expansion work recovery. The idea behind applying a pump was that it requires less work to increase the pressure of a liquid than a gas due to the smaller change in specific volume for a given pressure rise associated with less-compressible fluid states. Therefore, the work required by the pump would result in an increase in ejector pressure lift, and, theoretically, decrease the work input required by the compression process by a larger amount than was consumed by the pump. A further advantage of the pump was to facilitate modulation of the motive nozzle input state to provide control of the ejector efficiency, pressure lift, and entrainment ratio without needing variable ejector geometry. The ejector utilized in this work was developed and tested in Liu et al. [13], and the motive nozzle diameter was varied manually during testing through rotation of a threaded needle which moved in and out of the motive nozzle throat, actively varying the effective motive nozzle flow diameter. The main differences and changes made from the previous system are:

- The installation of an internal heat exchanger (IHX), with piping designed for its possible bypassing of the cycle independently (Figure 5.2)
- Removal of the low-pressure flash tank, due to the problems of instability and increased control complexity of the system, especially when

the two flash tanks are used at the same time

- Change of positioning of a Coriolis flow meter, allowing the simultaneous measurement of the 3 mass flows of the plant at the same time for each type of configuration allowing the mass balance to be closed
- Expansion valve size reduction in the medium temperature line

(A) IHX without insulation

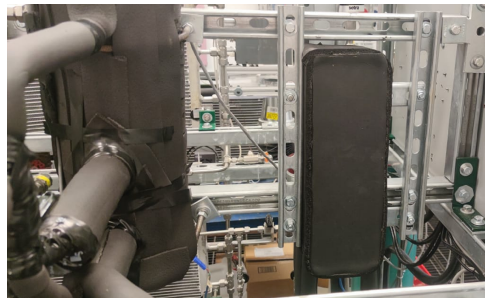

(B) IHX installed

FIGURE 5.2: Photo of the IHX installed in the CO_2 test stand

The new piping and instrumentation diagram (P&ID) of the test stand utilized in this work is shown in Figure 5.1, and a photo of the pump installed in the test stand is shown in Figure 5.4. The LP compressor used in the setup is a reciprocating compressor with a displacement volume of 16.7 cm^3. The HP compressor is a two-stage reciprocating compressor with displacements volume of 33.3 cm^3 and 20.0 cm^3 for the first and second stage, respectively. The chosen air to refrigerant HXs were micro-channel, with stainless steel construction and aluminum louvers between passes. Given that the heat exchangers had a nominal capacity of 5 kW, one was

selected to perform as the intercooler (IC) between the two stages of the HP compressor and three were used in series for the gas cooler of the cycle. The fans mounted on the HX surfaces were rated at 3420 m^3/h each, with one installed on each HX. 24, 26 and 10 plate HX designs were chosen for the LT evaporator, MT evaporator and the IHX, respectively. The volumetric CO_2 pump is an HAMMELMANN High Pressure Process pump with a capacity of 12.16 l/min at 500 rpm.

All of the configurations taken into account in this work are summarized in Table 5.1. The ambient conditions are controlled with the psychrometric chamber where the test stand is located, and both evaporators are controlled by independent Ethylene-Glycol (EG) baths (see Figure 5.3).

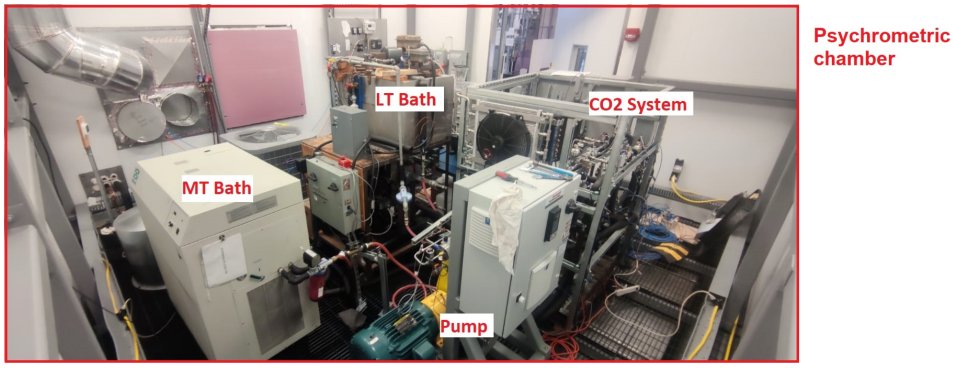

FIGURE 5.3: Photo of experimental setup

TABLE 5.1: Experimentally-investigated cycle configurations

Configuration 1	EXV+Flash tank economization
Configuration 2	Ejector
Configuration 3	EXV+Flash tank economization+IHX
Configuration 4	Ejector+IHX+CO_2 pump

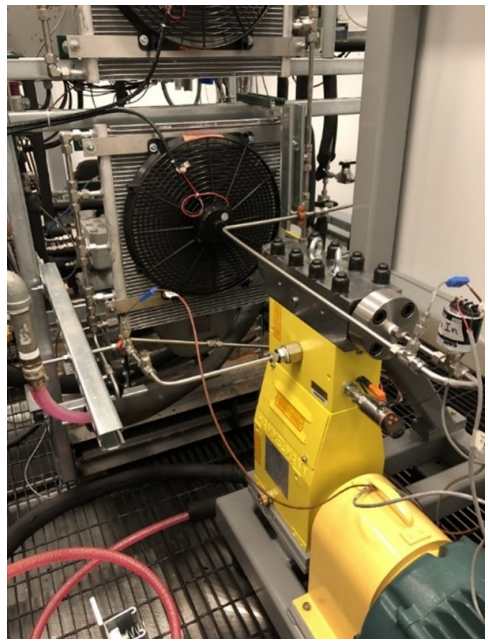

FIGURE 5.4: Photo of pump installed in the CO_2 test stand

5.1.2 Measurement and instrumentation

All single-phase states were measured using calibrated in-line thermocouples and pressure transducers. Many two-phase states were assessed with both temperature and pressure for redundancy. Three Coriolis mass flow meters were used to measure refrigerant mass flow rates, and one turbine flow meter was placed in each EG loop to measure volumetric flow rates. The EG temperature was measured at the inlet and outlet of each evaporator with in-line thermocouples placed in the EG flow. Mass concentrations of 34% and 50% EG were utilized in the MT and LT temperature baths, respectively. Both of the compressors and the pump were controlled with variable frequency drives (VFD), and the power consumption for each device was measured between the power source and the VFD. Fan power for the intercooler and gas coolers was measured via watt transducer. The flash tank liquid level was monitored by both a sight glass and capacitive liquid level sensors to pass the liquid level signal to the data acquisition system. The P&ID shown in Figure 5.1 provides a visual reference for the location

TABLE 5.2: Summary of sensors and corresponding uncertainty

Physical Parameter	Description	Model	Accuracy
Temperature	Ungrounded TC	Omega T-Type	0.5±K
Pressure (MT Side)	PT, 0-20684 kPa	Setra 206	±26.9 kPa
Pressure (LT Side)	PT, 0-6895 kPa	Setra 206	±9 kPa
Mass Flow ($\dot{m}_{motive}$)	Coriolis Flow Meter	Micromotion CMFS050	±0,1% RDG
Mass Flow ($\dot{m}_{suction}$)	Coriolis Flow Meter	Micromotion F025	±0.2% RDG
Mass Flow ($\dot{m}_{LT}$)	Coriolis Flow Meter	Micromotion F025	±0.2% RDG
Volume Flow ($\dot{V}_{EG}$)	Turbine Volume Flow Meter	Omega FTB-1424	±0.1% FS
Liquid Level	Capacitive Liquid Sensor	SWI CS02	±0.5% Linearity
Compressor Power	Watt Transducer	Ohio Semitronics GW5-015E	±0.04% RDG
Fan Power	Watt Transducer	Ohio Semitronics PC8-001	±1.0% FS

of the measurement devices, and details of the various measurements are provided in Table 5.2 where RDG is the reading value and FS full scale. All of the accuracy of instrumentation are used to determine the uncertainty of independent variables as calculated in Equation (A.21) from Taylor and Kuyatt [86].

$$I_y = \sqrt{\sum \left(\frac{\partial Y}{\partial X_i} I_{x_i} \right)^2} \tag{5.1}$$

where Y is the calculated quantity, X is the measured quantity, and I is the uncertainty (see Appendix A).

5.2 Comparison of architecture performance

5.2.1 Experimental procedure

The results of this chapter are comprised of 53 steady-state data points consisting of between five to ten minutes of steady measurement for each point. In every test, the gas cooler pressure was varied in order to find the pressure that resulted in the maximum COP at each ambient condition. The back pressure was regulated with an EXV using a PID controller that was developed in-house and implemented within the monitoring system.

Steady-state results were collected for all four investigated architectures. Experimental tests were conducted at ambient temperatures of 19 °C, 24 °C, 28 °C and 30 °C, and the fans, three of which were used for the gas-cooler and one for the intercooler, were kept at a fixed speed. The heat load was provided by two EG baths: one evaporator inlet temperature target was 3 °C to simulate refrigeration applications (MT), and the low-temperature (LT) EG-side evaporator inlet temperature target was -21 °C to simulate freezer applications; both EG flow rates were set to 10 liter per minute to balance a meaningful temperature difference that would reduce the impact of the thermocouple uncertainty while still falling within the turbine flow meter measurable range. The applied test matrix is provided in Table 5.4. Ambient relative humidity was set at 30% and a target compressor suction superheat of approximately 15 K was chosen. Due to the different cycle configurations, 15 K refers to the superheating at the outlet of the MT evaporator when the ejector is used. When testing the plant in Configurations 3 and 4, where the IHX is used, the superheating at the LT evaporator outlet is set at 10 K in order to avoid excessive LP suction compressor superheating and to maximize the benefit of the IHX. The system refrigerant charge was held constant at a value of 7.9 kg for all tests. In all the test conducted where open economization was achieved, the pressure in the flash tank was fixed at 35 bar via the flash gas valve in order to simulate a common supermarket refrigeration plant. A summary of the cycle parameters is presented in the Table 5.3.

TABLE 5.3: Test stand peripheral operating parameters

Parameter	Units	Value
LT suction(evaporator outlet) superheat	[K]	15, (10) if IHX
MT suction(evaporator outlet) superheat	[K]	15, (15) if Ejector
Ambient Temperature	[°C]	19, 24, 28, 30
Ambient relative humidity	[-]	30%
Ethylene-Glycol inlet temperature, LT evaporator	[°C]	-21
Ethylene-Glycol inlet temperature, MT evaporator	[°C]	3
Ethylene-Glycol volumetric flow rate, LT evaporator	[l/min]	10
Ethylene-Glycol volumetric flow rate, MT evaporator	[l/min]	10
Flash Tank Pressure (open economization)	[bar]	35

TABLE 5.4: Overview of conducted tests

Test	Description	Ambient temperature [°C]
1	Baseline - EXV, FT Economization (Configuration 1)	24
2		28
3		30
4	Ejector (Configuration 2)	24
5		28
6		30
7	IHX, FT Economization (Configuration 3)	24
8		28
9		30
10	Ejector, CO_2 pump, IHX (Configuration 4))	19

Configuration 4 (with the CO_2 pump) was tested only at an ambient temperature of 19 °C, which will be discussed in-depth in the following section. The calculation of COP is shown in Equation (5.2).

$$COP = \frac{\dot{Q}_{cool,LT} + \dot{Q}_{cool,MT}}{P_{comp,LT} + P_{comp,MT} + P_{pump} + P_{fans}} \tag{5.2}$$

Where $\dot{Q}_{cool,LT}$ and $\dot{Q}_{cool,MT}$ are the cooling capacity from the LT and MT evaporators (CO_2 side), respectively. In the denominator, power consumption of the low-pressure compressor, high-pressure compressor, CO_2 pump

and fans are considered. The power consumption of water pumps is neglected, and no additional electrical power is added (for example to simulate a real application with air-source evaporators, where an additional fan power consumption could be considered).

5.2.2 Experimental results

In all tested configurations, conditions that corresponded to a maximum COP have been identified and the resulting COP values with gas cooling pressure variation for configurations 1, 2 and 3 at all four ambient conditions are shown in Figure 5.5, 5.6 and 5.7, respectively.

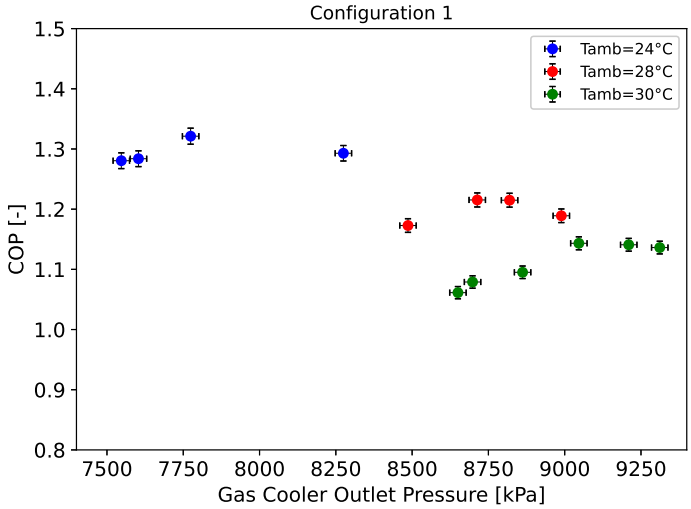

FIGURE 5.5: EXV economization cycle COP with gas cooling pressure variation - Baseline

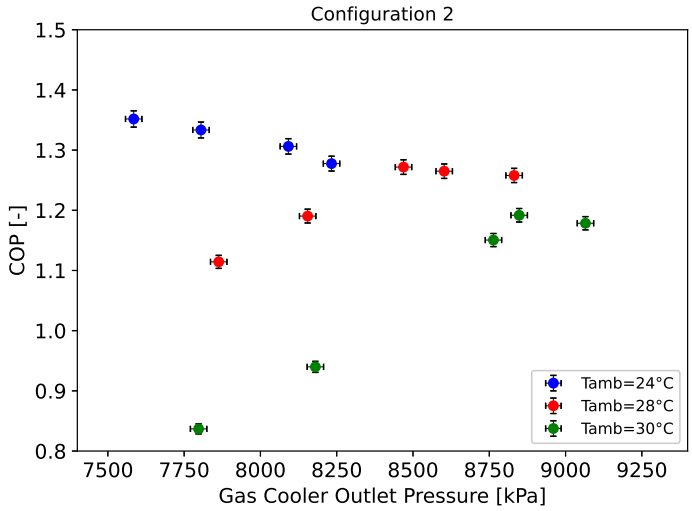

FIGURE 5.6: Ejector cycle COP with gas cooling pressure variation

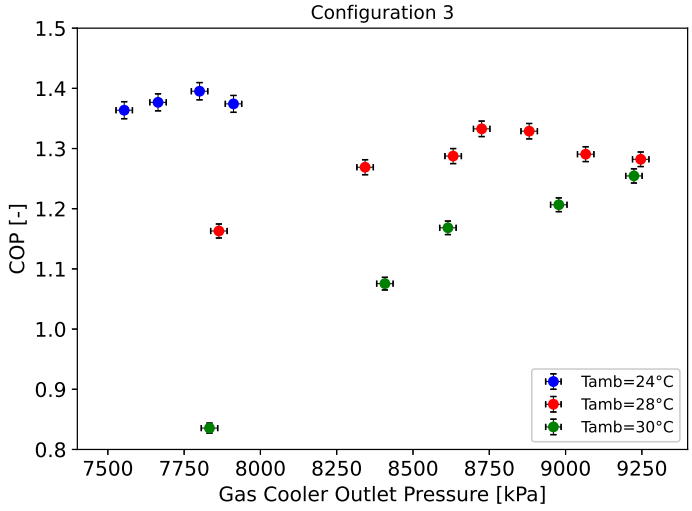

FIGURE 5.7: IHX COP with gas cooling pressure variation

The ejector was originally sized for a 15 kW air conditioning system,

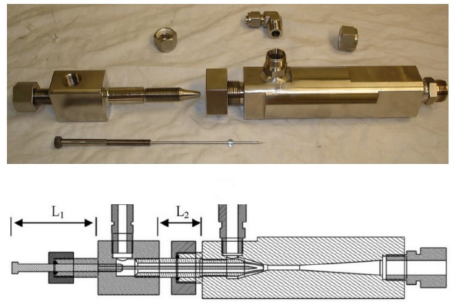

FIGURE 5.8: Photo of the adjustable ejector with technical drawing of the ejector [87]

and was therefore oversized for the test stand at refrigeration conditions, as the test stand utilized herein has an approximate total capacity of 8 kW. This led to reduced ejector efficiency, but the motive nozzle was still able to be modulated to provide adequate control of the gas cooling pressure. In addition, it is an ejector that has been readapted to resist high pressures, passing a water pressure test of 1400 psi (96.53 bar), while retaining the ability to change geometry without leakage. The last characteristic was necessary due to the pressures involved when used in conjunction with the CO_2 pump. For all tests with the ejector, analogous to tests with the EXV, the pressure at the gas cooler needs to be stable; therefore after 5-10 minutes of stable measurements, the point is measured for another 5-10 minutes. To regulate the pressure at the gas cooler during the ejector configuration, the position of a threaded rod was manually varied, changi ng the ejector geometry and its behaviour (see Figure 5.8).

The COP trends followed the expected result of attaining a maximum value for a given ambient condition at a higher pressure with increasing ambient temperature. The point that corresponds to the maximum COP is clear for all configurations. At 24 °C, the minimum pressure is fixed at 75 bars to avoid the vapor dome and, regarding Configuration 3 at 30 °C, the maximum pressure is taken as optimum pressure even though an optimum was reached due to limits on the maximum safety pressure at the gas cooler. From this point onwards, the entire point analysis for each configuration is to be considered at the gas cooler pressure which

results in the maximum COP. Logarithmic pressure-specific enthalpy (p-h) diagrams in the maximum COP at investigated ambient temperatures for Configurations 1, 2 and 3 are presented in Figures 5.9, 5.10, 5.11 respectively.

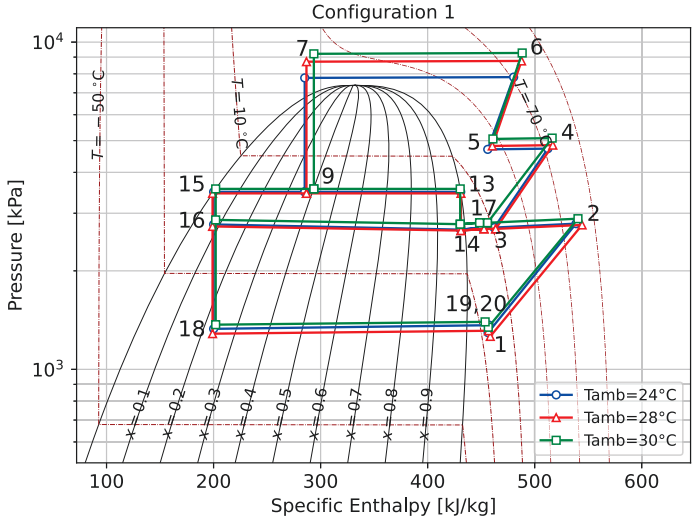

FIGURE 5.9: p-h diagram of EXV and FT economization cycle.

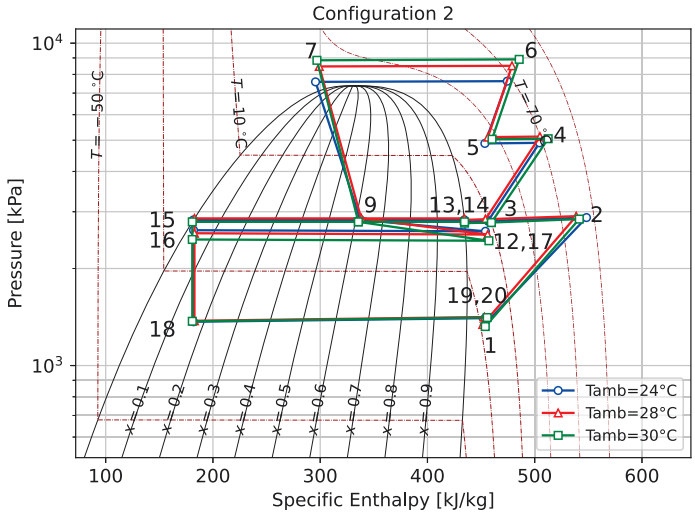

FIGURE 5.10: p-h diagram of ejector cycle

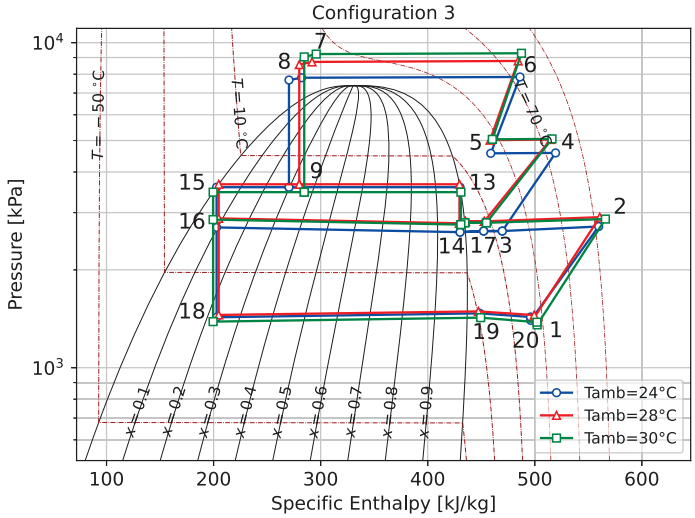

FIGURE 5.11: p-h diagram of IHX cycle

The maximum COP values for each cycle and ambient temperature at the corresponding gas cooler outlet pressure are plotted in Figure 5.12 for

an overall comparison.

Compared with Configuration 1 as baseline, Configuration 2 improves the system COP for all investigated conditions, which also allowed the optimum gas cooler outlet pressure to be lowered by 1.9 bar, 2.45 bar and 3.62 bar at 24 °C, 28 °C and 30 °C ambient conditions, respectively. The maximum COP improvement is 2.33%, 4.64% and 3.67% at 24 °C, 28 °C and 30 °C ambient temperatures, respectively. In this specific test stand, the configuration that was found to increase efficiency the most was Configuration 3, as using the IHX was found to lead to COP increases of 5.60%, 9.47%, and 8.89% at 24 °C, 28 °C and 30 °C, respectively. The effect at 30 °C ambient is still positive, but not as much as might be expected, since, in those conditions, the tested pressure at the gas cooler was limited to approximately 92 bar. This limitation is due to the safety valve in the test stand being set at a maximum pressure of 95 bar, and therefore, the configurations being compared are not as meaningful as at lower temperatures conditions. It is fair to mention that the position chosen for the IHX did not allow for an appreciable optimum pressure-reducing effect due to the significant difference in specific heat capacity and mass flow rate between the flow in the high and low pressure line, which allows subcooling of the high pressure side by approximately 2-3 K, while, on the vapor side, a superheating of 60 K was reached. Therefore, the IHX should be applied on the MT line and not the LT line in applications as well as further investigations using this test stand.

A summary of COP, gas cooler outlet pressure, cooling capacities, and compressor power consumption for all points shown in Figure 5.12 is provided in Table 5.5 where the measured fan power is constant at 0.57 kW.

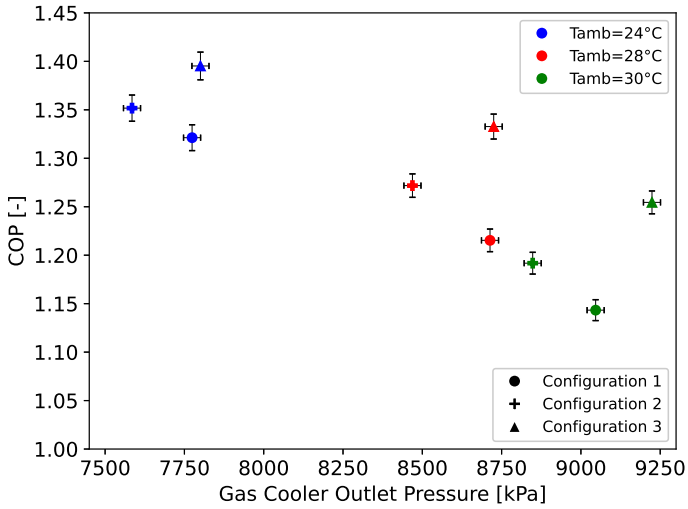

FIGURE 5.12: Summary of maximum achieved COP for Configurations 1, 2 and 3

TABLE 5.5: Summary of data at maximum COP conditions for all tests for Configurations 1, 2 and 3

t_{amb} [°C]	Configuration [-]	$p_{gc,out}$ [kPa]	COP [-]	$\dot{Q}_{cool,LT}$ [kW]	$\dot{Q}_{cool,MT}$ [kW]	$P_{comp,LT}$ [kW]	$P_{comp,MT}$ [kW]
30	1 - Flash Tank Economization	9046 ± 26.9	1.14 ± 0.011	2.60 ± 0.008	3.83 ± 0.011	1.01 ± 0.035	4.05 ± 0.032
	2 - Ejector	8847 ± 26.9	1.19 ± 0.011	2.84 ± 0.008	3.85 ± 0.010	1.04 ± 0.032	4.00 ± 0.032
	3 - IHX	9224 ± 26.9	1.25 ± 0.012	2.35 ± 0.007	4.73 ± 0.012	0.98 ± 0.032	4.10 ± 0.032
28	1 - Flash Tank Economization	8713 ± 26.9	1.22 ± 0.012	2.46 ± 0.007	4.22 ± 0.011	1.00 ± 0.032	3.93 ± 0.032
	2 - Ejector	8468 ± 26.9	1.27 ± 0.012	2.82 ± 0.008	4.26 ± 0.011	1.04 ± 0.032	3.95 ± 0.032
	3 - IHX	8725 ± 26.9	1.33 ± 0.013	2.50 ± 0.008	4.81 ± 0.013	0.99 ± 0.032	3.93 ± 0.032
24	1 - Flash Tank Economization	7774 ± 26.9	1.32 ± 0.013	2.59 ± 0.008	4.31 ± 0.011	1.02 ± 0.032	3.64 ± 0.032
	2 – Ejector	7584 ± 26.9	1.35 ± 0.014	2.61 ± 0.008	4.51 ± 0.011	1.07 ± 0.032	3.63 ± 0.032
	3 - IHX	7800 ± 26.9	1.40 ± 0.014	2.53 ± 0.008	4.65 ± 0.012	0.96 ± 0.032	3.62 ± 0.032

5.3 Ejector control and performance assesment

Two methods of ejector control were assessed in this section. The first was a variable-diameter motive nozzle and the second was a variable-speed

pump located between the gas cooler outlet and motive nozzle inlet. An energetic and ejector performance analysis of the variable-diameter method is presented herein, followed by a dedicated section is presented with the performance of the pump method with the aim of achieving the required parameters for the safety and operation of the CO_2 pump. In order to evaluate the ejector performance, entrainment ratio, w, and ejector efficiency, $\eta_{ejector}$, are utilized, as defined in Equations (5.3) and (5.4), respectively from Kohler et al. [88].

$$w = \frac{\dot{m}_{suction}}{\dot{m}_{motive}} \tag{5.3}$$

where *suction* refers to the suction nozzle flow and *motive* refers to the motive nozzle flow.

$$\eta_{ejector} = w\frac{h(s_{si}, p_d) - h_{si}}{h_{mi} - h(p_d, s_{mi})} \tag{5.4}$$

where h is specific enthalpy, p is pressure, s is specific entropy, si denotes the suction nozzle inlet, mi denotes the motive nozzle inlet, and d denotes the ejector diffuser outlet. The pressure lift achieved by the ejector is defined as the difference in pressure between the ejector diffuser outlet and the evaporator outlet.

5.3.1 Variable diameter motive nozzle

The motive nozzle diameter variation was used to search for the gas cooling pressure corresponding to the maximum COP, as shown in Figure 5.12, validating motive nozzle diameter modulation as an effective means of gas cooling pressure variation. Entrainment ratio, ejector pressure lift and efficiency trends with motive nozzle modulation (i.e., gas cooler pressure) at various ambient temperature are presented in Figures 5.13, 5.14 and 5.15, respectively. In nearly all points presented in Figure 5.13, the entrainment ratio is directly proportional to the pressure in the gas cooler pressure. This is because the motive pressure is the driving force of the ejector, which increases the entrained flow rate from the evaporator and thus, the cooling capacity. As the gas cooler pressure increases, the motive mass flow rate typically decreases due to the inverse relationship of compressor mass flow rate to pressure ratio. Furthermore, with increasing gas cooler pressure for a given ambient condition, the motive nozzle inlet specific enthalpy

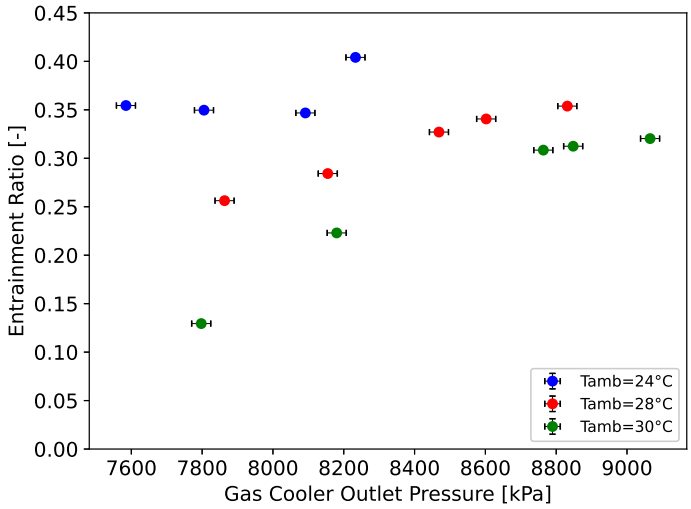

FIGURE 5.13: Entrainment ratio with varying gas cooler pressure via motive nozzle modulation

decreases, thus leading to a lower motive nozzle outlet quality for scenarios where the expansion process enters the vapor dome. Thus, the fraction of the total mass flow passing through the evaporators further increases. The combination of these trends explains the observation of the direct relation of entrainment ratio and motive nozzle inlet pressure.

Regarding the pressure lift shown in Figure 5.14, the experimental results show the expected result of a direct relationship between ambient temperature and ejector pressure lift due to the larger amount of available expansion work to be recovered at higher gas cooler pressures. Looking more closely, higher pressure lift values at lower gas cooling pressures were observed, which then stabilized for ambient temperatures of 28 °C and 30 °C, while remaining nearly constant at 24 °C ambient. The main explanation regarding this difference in behavior between higher ambient temperature (28 °C and 30 °C) and 24 °C ambient temperature is the strong dependence of ejector diffuser outlet pressure with nozzle diameter. While at a temperature of 24 °C, only slight changes in ejector geometry are required to achieve conditions that maximize COP, higher ambient temperatures require more

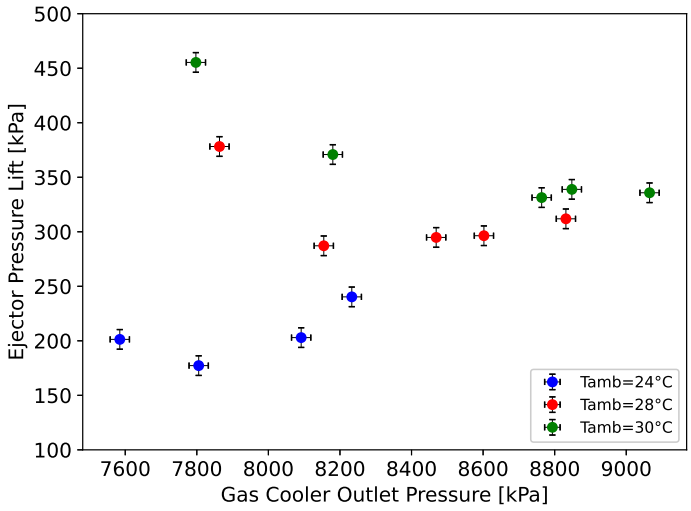

FIGURE 5.14: Ejector pressure lift with varying gas cooler pressure via motive nozzle modulation

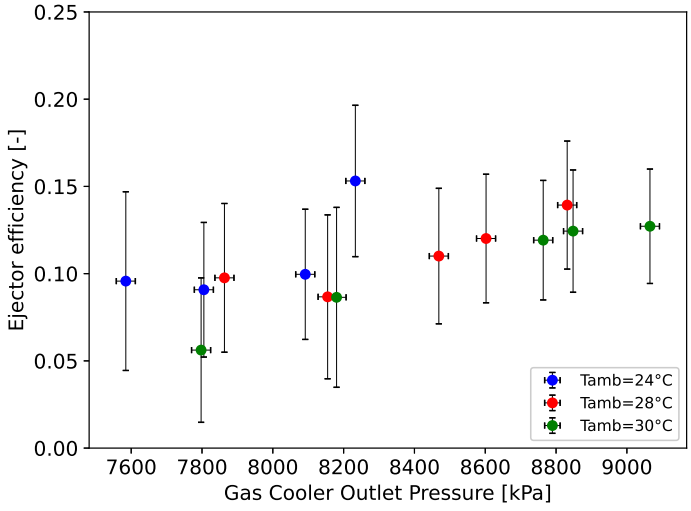

FIGURE 5.15: Ejector efficiency with varying gas cooler pressure via motive nozzle modulation

major changes in ejector geometry and thus, higher diffuser outlet pressure changes. This explains why pressure lift changes are more pronounced when the ejector is further from the conditions that maximize system performance. The combination of these two parameters explains the ejector efficiency behavior shown in Figure 5.15.

Considering that the outlet evaporator superheat was fixed at 15 K, the general trend shows an increase in ejector efficiency as the pressure at the gas cooler increases, with the sole exception of the test at 78.63 bar and an ambient temperature of 28 °C. This result is likely due to the high ejector pressure lift at that point that affects the efficiency calculation. It is worth mentioning that an increase in the efficiency of a single component does not always increase overall efficiency. To support this statement, it can be seen that the points with the highest ejector efficiency do not necessarily correspond to the points where system COP is highest. Moreover, contrary to many expansion work recovery device control methods, this variation in diameter did not significantly impact the ejector efficiency.

5.3.2 Variable speed CO_2 pump

Applying a pump to compress the subcooled liquid, where the temperature and pressure of the refrigerant are below their respective critical values, or supercritical liquid, where the fluid pressure is above the critical pressure but the temperature is below the critical temperature, resulted in consistent trends and reliable operation. As mentioned above, in order to respect the safety constraints of the pump (avoid cavitation, a maximum temperature inlet of 25 °C and a maximum discharge pressure of 100 bar) a dedicated test condition is presented. The manufacturer-recommended subcooling at the pump inlet is 5 K, which necessitated the use of an IHX. Additionally, by varying the CO_2 pump speed to control the motive inlet pressure and the ejector performance, the suction pressure of the pump, which is also the pressure at the gas cooler outlet as shown in Figure 5.1, also varies with the pump speed as a secondary effect. This implies that, by increasing the pump speed, the pressure in the gas-cooler can decrease, reducing the degree of subcooling, and thus, increasing the risk of cavitation. Additionally, even the pump suction temperature can increase as the rotational speed of the

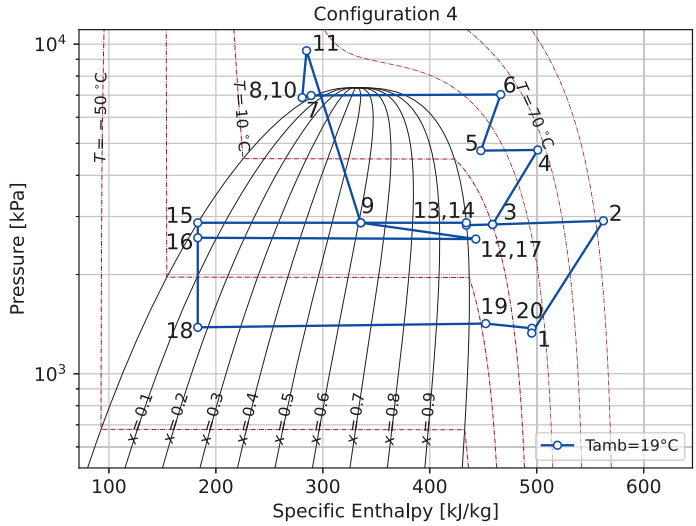

FIGURE 5.16: p-h cycle in Configuration 4, which utilized the CO_2 pump

pump increases, making it difficult to remain below the manufacturer limit of 25 °C . The maximum speed the pump was operated at was limited to a speed that would keep the pump discharge pressure below the maximum design discharge pressure of 100 bar. For all the reasons explained above, the ambient temperature for this specific evaluation is fixed at 19 °C. With the aim of making the comparison as fair as possible, and to isolate as much as possible the effect of the pump alone, the pump testing (Configuration 4) is compared to the test stand with both the ejector and the IHX (Configuration 2+IHX), the comparison is evaluated with all the other parameters fixed as shown in Table 5.6, working in subcritical conditions with an initially-fixed gas cooler pressure of 70 bar.

To operate the CO_2 pump, starting from the baseline conditions with a fixed gas cooler pressure of 70 bar and an ambient temperature of 19 °C, the IHX bypass valves were opened, and the CO_2 pump was engaged with a speed corresponding to the volumetric flow at the gas cooler outlet. An example of Configuration 4 cycle on a p-h diagram is presented in Figure 5.16.

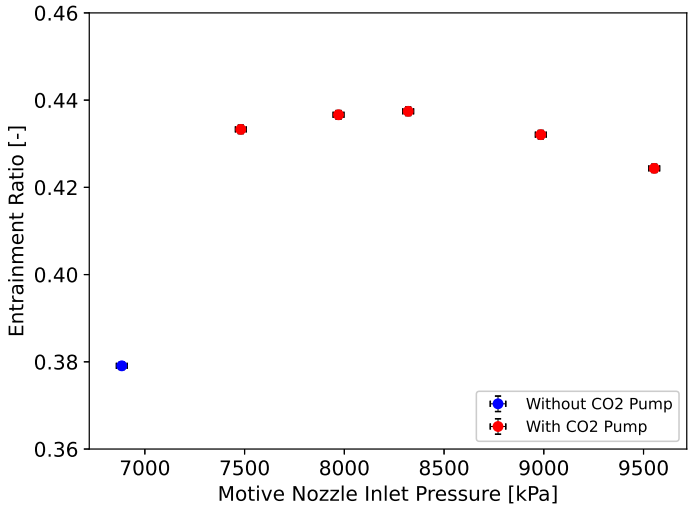

FIGURE 5.17: Entrainment ratio with motive nozzle inlet pressure

Once the CO_2 pump is correctly engaged, the pump speed is increased to control ejector performance. A comparison between Configurations 4 and Configuration 2 with the IHX, with increasing pump speed and thus, motive nozzle inlet pressures up to 100 bar, was conducted. Ejector entrainment ratio, pressure lift and efficiency are presented in Figures 5.17, 5.18, and 5.19, respectively.

Figures 5.18 and 5.19 show nearly linear trends as pump speed increases, while the entrainment ratio illustrated in Figure 5.17 increases rapidly around 75 bar and then is somewhat stable as the motive nozzle inlet pressure increases. This regulation allows an increase in cooling capacity through the use of the pump due to its direct relation to the entrainment ratio. Despite a somewhat insignificant decrease in compressor power consumption, the overall system COP increases through use of the pump. The overall pump efficiency varied from 22% to 38% during the tests. This low efficiency was due to the maximum pump operating speed being approximately 40% of the design speed for the pump. The pump was intentionally oversized due to difficulty in finding the correct pumps designed for these

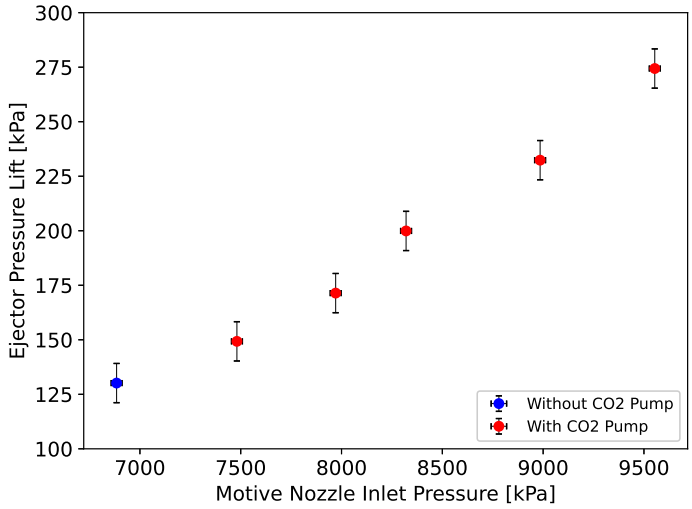

FIGURE 5.18: Pressure lift with motive nozzle inlet pressure

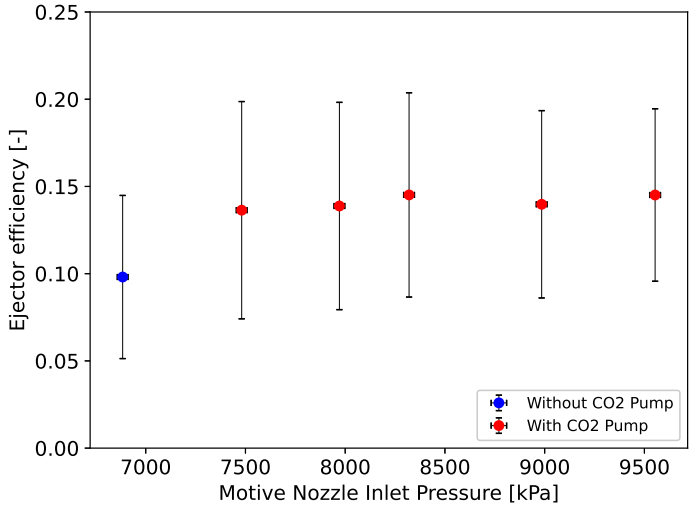

FIGURE 5.19: Ejector efficiency with motive nozzle inlet pressure

purposes and the desire to also be able to accommodate evaporation conditions associated with air conditioning operations. Such a strong sensitivity to rotational speed was not expected, and therefore it is recommended that, in future investigations, different pumps are utilized for air conditioning and refrigeration applications, highlighting a challenge of developing flexible tests stands for laboratory work instead of single-application machines. Increased pump efficiency would further increase the COP benefit of the combined use of the ejector and pump. With the aim of reducing the impact of the oversized pump efficiency on the system COP, an alternative COP, COP_{mec}, is presented in equation (5.5) top offer a more general performance trend.

$$COP_{mec} = \frac{\dot{Q}_{cool,LT} + \dot{Q}_{cool,MT}}{P_{comp,LT} + P_{comp,MT} + \dot{m}\Delta h_{pump} + P_{fans}} \tag{5.5}$$

Where $\dot{m}\Delta h_{pump}$ is the product of the mass flow and the specific enthalpy difference across the CO_2 pump. This COP has the meaning of a "mechanical coefficient of performance", where the mechanical and electrical efficiency are therefore equal to 1, this parameter represents the maximum COP that could be achieved with a perfectly sized pump without mechanical losses. Additionally, in order to evaluate the impact of the assumed pump efficiency, two additional parameters are presented in equation (5.6) and equation (5.7).

$$\Delta COP_{\%(mec)} = \frac{COP_{conf.4(mec)} - COP_{conf.2+IHX}}{COP_{conf.2+IHX}} 100 \tag{5.6}$$

$$\Delta \dot{Q}_{\%} = \frac{\dot{Q}_{conf.4} - \dot{Q}_{conf.2+IHX}}{\dot{Q}_{conf.2+IHX}} 100 \tag{5.7}$$

With $\dot{Q}$ being the overall cooling capacity and COP as presented in equation (5.2).

The percentage difference in COP with ejector inlet pressure are presented in Fig. 5.20. In this configuration, using the CO_2 pump leads to an increase in overall cooling capacity up to 6% when the pump was at maximum tested speed, while the COP gradually decreased with the motive nozzle inlet pressure. This trend is justified by the fact that increasing the inlet pressure of the ejector means increasing the rotational speed of the

pump and thus the consumed electrical power. Under these test conditions, the improving effect of cooling capacity is not sufficient to compensate for the increase in power consumption leads to a decreasing COP. Looking at the $\Delta COP_{\%(mec)}$, the absolute values are higher due to the lower power consumption of the pump. However, the trend is not clear as the ejector inlet pressure varies. One of the major explanations is the calculation of the $\dot{m}\Delta h_{pump}$. The change in specific enthalpy does not necessarily increase with increasing pump speed as one might expect. As pressure lift in creases with rpm, the mass flow through the gas cooler increases, and this leads to an increase in the inlet temperature of the CO_2 pump of nearly 3 K. This effect influences the calculation of the specific enthalpy difference, which helps justify an unclear trend in the figure, due to the fact that not only the pump performance is behind it, but also the operation of the gas cooler and the IHX. Nevertheless, comparing the mechanical COP is of fundamental importance in understanding the impact of pump efficiency and the room for improvement. The trend of $\Delta COP_{\%(mec)}$, suggesting that with a perfectly sized pump, the use of a CO_2 pump to regulate ejector performance could provide appreciable benefits in terms of overall COP of maximum 3.8% in subcritical conditions. A summary of measured COP, gas cooler outlet pressure, motive nozzle inlet pressure, cooling capacities, speed of the pump, compressor and pump power consumption for all points shown in Figure 5.20 is provided in Table 5.6.

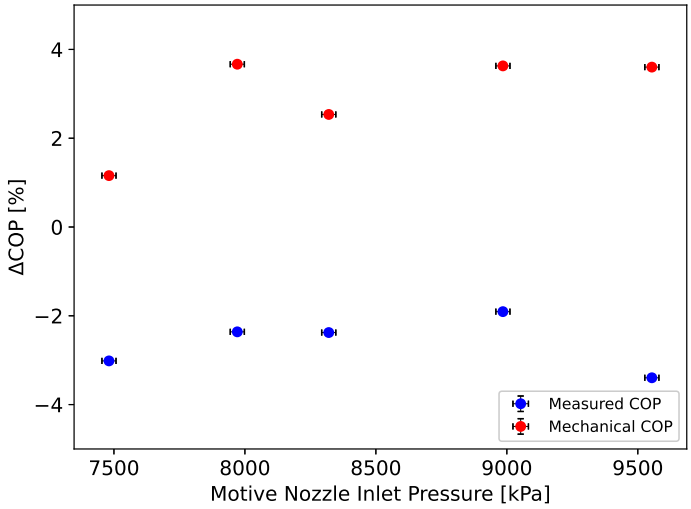

FIGURE 5.20: Summary of data with and without CO_2 pump

TABLE 5.6: Summary of data with and without CO_2 pump.

t_{amb} [°C]	Configuration [-]	$p_{gc,out}$ [kPa]	$p_{pump,out}$ [kPa]	rpm [r/min]	COP [-]	$\dot{Q}_{cool,LT}$ [kW]	$\dot{Q}_{cool,MT}$ [kW]	$P_{comp,LT}$ [kW]	$P_{comp,MT}$ [kW]	P_{pump} [kW]
19	Ejector+IHX	6987 ± 26.9	-	-	1.51 ± 0.016	2.76 ± 0.008	4.70 ± 0.012	0.98 ± 0.032	3.39 ± 0.032	-
	Ejector+CO_2 pump	7085 ± 26.9	7481 ± 26.9	125	1.46 ± 0.014	2.63 ± 0.014	5.17 ± 0.012	0.96 ± 0.032	3.43 ± 0.032	0.38 ± 0.032
	Ejector+CO_2 pump	7047 ± 26.9	7971 ± 26.9	130	1.47 ± 0.014	2.58 ± 0.014	5.35 ± 0.012	0.97 ± 0.032	3.41 ± 0.032	0.43 ± 0.032
	Ejector+CO_2 pump	7015 ± 26.9	8320 ± 26.9	140	1.47 ± 0.014	2.50 ± 0.014	5.48 ± 0.013	0.99 ± 0.032	3.41 ± 0.032	0.47 ± 0.032
	Ejector+CO_2 pump	7005 ± 26.9	8985 ± 26.9	155	1.48 ± 0.014	2.58 ± 0.014	5.61 ± 0.013	1.01 ± 0.032	3.41 ± 0.032	0.56 ± 0.032
	Ejector+CO_2 pump	6987 ± 26.9	9554 ± 26.9	170	1.46 ± 0.014	2.56 ± 0.014	5.65 ± 0.013	1.02 ± 0.032	3.41 ± 0.032	0.64 ± 0.032

5.4 Chapter conclusions

This chapter presented an experimental analysis comparing two ejector control methods and four cycle architectures applied in a two-evaporator transcritical CO_2 refrigeration cycle with an approximate cooling capacity of 8 kW. The different configurations tested are focused in the same experimental facility. In particular, the two ejector control methods assessed were motive nozzle diameter variation via a manually-adjustable needle located in the motive nozzle throat and motive nozzle inlet pressure modulation through a variable-speed pump placed between the condenser/gas cooler outlet and the ejector motive nozzle inlet. The assessed cycles were flash tank economization applied upstream of the MT evaporator (Baseline, Configuration 1), ejector (Configuration 2), flash tank with an IHX (Configuration 3) and an IHX with an ejector and a pump upstream of the ejector motive nozzle inlet (Configuration 4). The comparisons were conducted at 24 °C, 28 °C and 30 °C ambient temperatures, and at 19 °C only for Configuration 4. The gas cooler outlet pressure was varied at each ambient condition for each cycle in an effort to identify the gas cooling pressure that resulted in the maximum COP. Ejector parameters such as entrainment ratio, efficiency, and pressure lift were also assessed.

The gas cooling pressure where the maximum COP occurred for each cycle decreased as ambient temperature decreased. Maximum COP benefits of 2.3%, 4.6% and 3.7% at 24 °C, 28 °C and 30°C ambient conditions, respectively, were achieved with the ejector alone is used and a COP increase of 5.6%, 9.5%, and 8.9% at 24 °C, 28 °C and 30 °C, respectively, were achieved using the IHX compared to baseline.

With respect to ejector control, it was found that modulation of the motive nozzle diameter led to a maximum ejector efficiency variation of approximately 6%. The configuration utilizing the CO_2 pump was tested at only 19 °C ambient and was found to be able to increase ejector efficiency by approximately 11% relative compared to the ejector configuration at the same conditions. Furthermore, correlations between nozzle position or pump speed and ejector entrainment ratio, pressure lift, and efficiency were clearly identifiable. Therefore, both methods of ejector control were validated in their ability to control the ejector. All tests utilizing the pump

resulted in a lower COP with a maximum decrease of 6.1% and a higher cooling capacity with a maximum increase of 6.2% compared to the ejector cycle without the pump. A theoretical analysis with the definition of a mechanical coefficient of performance (COP_{mec}), corresponding to a theoretical value of a perfectly sized pump, was conducted, showing a potential theoretical increase of 3.68% compared to the ejector cycle without the pump. However, the pump was only tested with the system in subcritical mode. Conducting the test under subcritical conditions eliminates the possibility of comparing this configuration in areas where the ejector is most commonly used, i.e. under transcritical conditions. Safety and inefficiency limitations resulting from oversizing, preclude the appropriateness of this configuration in a real plant. At this stage of experimentation, the conclusions regarding this configuration do not definitively support the idea that a CO_2 pump can increase the efficiency of a commercial CO_2 refrigeration cycle. Concluding, raising the evaporation temperature, is a way to increase the mass flow rate, and thus the speed of the pump required, theoretically working under more optimal conditions for the pump, opening up possible development in air conditioning systems.

Chapter 6

CO_2 supermarket with HVAC supply through ice thermal energy storage

The usual supply water temperature for air handling units in cooling operation is around 7 °C, which is a limiting factor for the water temperature range in the heat storage, in the view of avoiding any risk of freezing. For this reason, the maximum heat storage in water is around 20 MJ/m^3, provided that no heat exchanger is inserted between the storage and the AC water loop. The volumetric storage capacity can be significantly increased by Ice Thermal Energy Storage (ITES) systems, where values around 170 MJ/m^3 can be easily reached even considering heat loss and the need to guarantee water flow within ice coils.

In this chapter, a supermarket with HVAC supply thanks to an ice thermal energy storage is considered. The two operating modes, wintertime and summertime, are considered. In summertime, where the air conditioning load is faced by a typical water chiller designed for 12 – 7 °C water temperature, the ITES is used as thermal storage taking advantage of the availability of low temperature cooling power from the commercial refrigeration unit. In wintertime, the ITES is used as storage to provide hot water (45 °C) for space heating, reclaiming heat from the commercial refrigeration unit. The purpose of these configurations resides mainly in shaving the peaks of electrical power, either by replacing the heat pump (HP) operation during some peak hours, or by operating the ITES in parallel with the HP. The system is modelled through in-house routines which are linked to a

more comprehensive tool of simulation of the thermal behavior of buildings and of the commercial refrigeration plant.

6.1 Methods and case study

The case study supermarket is located close to Rome, seaside and is supplied with a typical CO_2 Commercial Refrigeration Unit (CRU), for the display and storage of chilled and frozen food. There are two reversible heat pumps operating on R-410A: one for the Domestic Hot Water DHW supply (Heat Pump 1) and one for the HVAC system (Heat Pump 2) of the sales area and of the back of the store (warehouse, food processing, offices ecc.). The supermarket has a bakery and a deli shop, whose ovens and heaters are used to cook ready-made meals, especially early in the morning, when the air conditioning systems is also running at full power to restore indoor temperature conditions after the night pause. This results in a huge peak in electrical energy use, when fares are at the highest level. In the search for a reduction in the peak of electrical energy use, an Ice Thermal Energy Storage (ITES) has been introduced to provide a significant energy storage in favour of air conditioning. Ice is produced by means of the CRU during night-time, when it is operating at favourable climatic conditions and at partial load. The nominal refrigerating capacity for the CRU is 22 kW at -35 °C (LT), and 118 kW at -10 °C (MT) including two 35 kW evaporators at -10 °C for the ITES. The summertime configuration sketched in Figure 6.1 is first considered. The ITES consists of a water tank with two submerged ice-making evaporators (one in the figure for ease of schematic), connected in parallel to the medium temperature (MT) refrigerated cabinets. The ITES is connected via a heat exchanger for heat recovey (HR_3) to a water tank (HVAC Tank) which supplies the Air Handling Units (AHU). The HVAC tank is modelled via the Trnsys Type 4, which allows a fixed number of internal nodes to take into account the stratification. The heat exchanger is needed to decouple the two mass flow rates, and allows the use of differently treated water in the two circuits. The reversible heat pump (Heat Pump 2), which operates as a chiller in the summer, is also connected to the same water tank, in parallel with the ITES, in order to cover the whole AC demand. The ITES consists of a 12 m^3 water tank, thermally insulated (with a 4 cm thick panel of XPS) to reduce heat loss, supplied with two submerged packages of 12 coils each, with an external diameter of 21.3 mm for a total

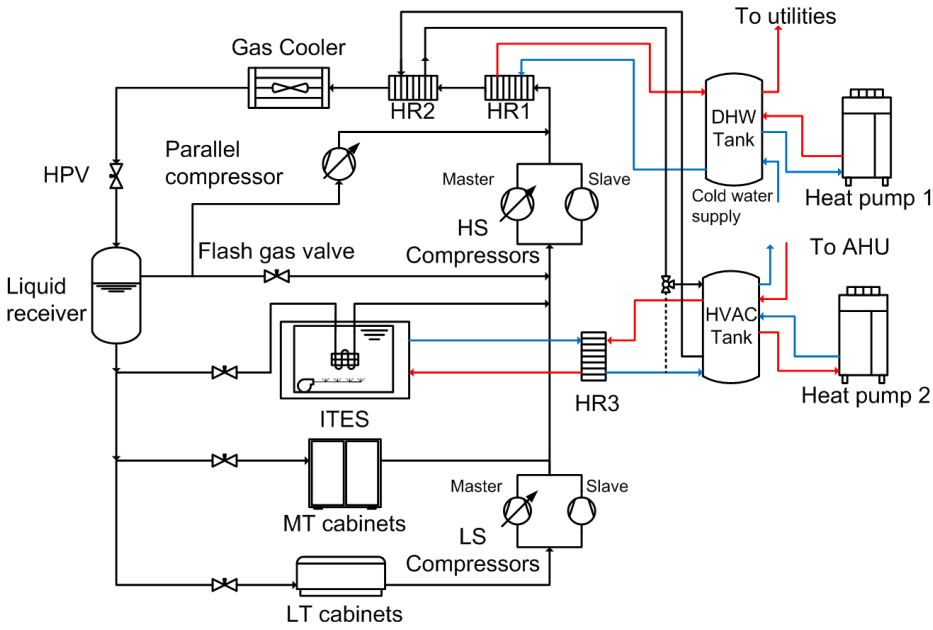

FIGURE 6.1: Schematic drawing of the supermarket plant in summertime

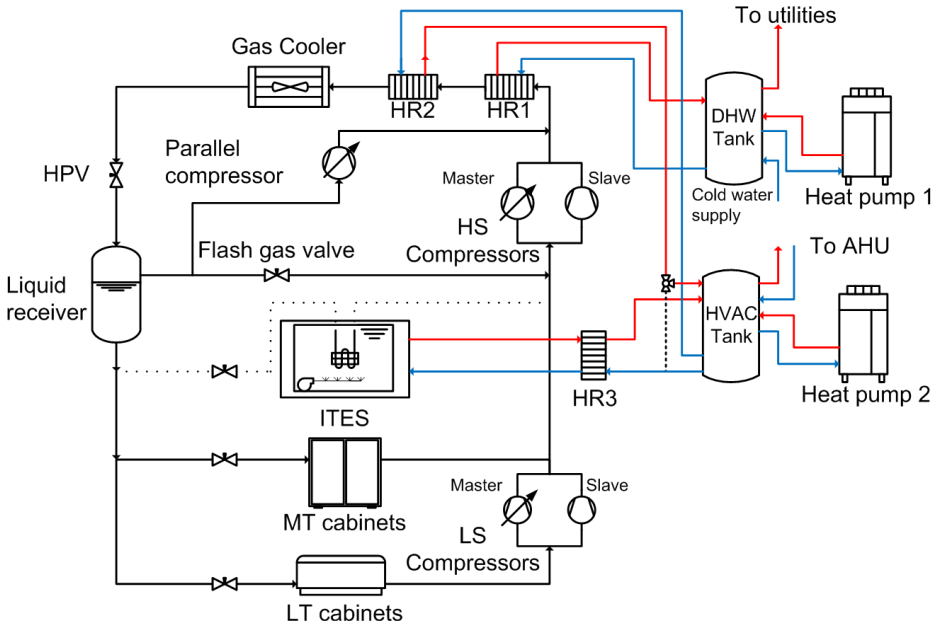

FIGURE 6.2: Schematic drawing of the supermarket plant in wintertime

length of 720 m. They represent two separate evaporators for the CRU at -10 °C, each controlled by an electronic expansion valve. About 6000 kg of ice can be formed, providing a global latent storage of 2000 MJ. An air blower supplying approximatively 100 m^3/h of air at ambient temperature distributes air at the bottom of the water tank to improve convection on the water side during ice melting for the discharge phase. In this phase, the thermal storage is used until the water temperature raises up to 5 °C, which is the limit temperature for obtaining, at the HR_3, chilled water at 7 °C to be delivered at the Air Handling Units (AHU). The water is then supposed to return from the AHU at 12 °C, resulting in a return water temperature to the ITES of around 10 °C. In wintertime (Figure 6.2) the ITES is used as a hot water storage tank for heat recovery from the CRU, using in this case the ITES in parallel to the water tank (HVAC Tank) to allow some sensible heat storage. In this case the ITES evaporator is not used. In this case the storage is heated during the night reclaiming heat from the CRU (HR_2), in order to provide heat for the space heating. The

commercial refrigeration unit is forced to work in transcritical condition with a fixed gas cooler pressure of 78 bar, which is close to the lower limit of transcritical operation. Nevertheless, the thermal storage is designed for summer conditions and only secondarily an analysis of possible feasibility of winter operation is also investigated with the following control rules:

- During the night, the CRU provides heat up to an ITES limit temperature of 50 °C; during its charge, water flows through HR_2 and then through the three-way valve along the dotted line as shown in Figure 6.2.
- During the day, the storage provides heat for space heating until the ITES temperature is below 35 °C, or the ITES supply temperature is below the HVAC tank temperature; then the heat supplied comes straight from the CRU.

The heat pump only provides heat when the tank temperature drops below 40 degrees, i.e. when the CRU and ITES do not meet the required heat load.

6.2 System modelling

6.2.1 Refrigeration unit and HP

To investigate the effectiveness of the ITES in terms of daily energy use or peak shifting, a comprehensive model is used. The cooling/heating load for the building is estimated hourly through the TRNSYS Type 56 dedicated to building dynamic simulation. A prediction of the annual refrigerating capacity profile with an hourly time step of display cabinets and cold rooms is then carried out as a function of the indoor climate conditions and operating conditions (defrosting, night blinds etc). The commercial refrigerating unit is modelled with in-house Types. The model can simulate refrigerating units equipped with the most widespread solutions to improve the efficiency of transcritical cycles, including subcooling via a dedicated mechanical system, parallel compression and also with heat recovery facilities to allow the production of domestic hot water (DHW) and space heating and cooling also in the view of a Demand Side Management for the electrical grid. The commercial refrigeration unit considered in this paper is a CO_2 transcritical refrigeration plant with parallel compressor, with two

temperature levels, for the frozen (-35 °C) and chilled (-10 °C) food. The reversible heat pump is a commercial product whose performance is predicted from the manufacturer data as a function of the source/supply heat exchanger temperature, and load. This model, implemented in the TRNSYS [89] simulation environment, is linked to a code in Matlab dedicated to the simulation of the ITES, as described below.

6.2.2 Ice Thermal Energy Storage (ITES)

In the ITES considered, ice forms on the outside of the coils immersed in the tank (ice-on coil external melt). The charging and discharging phases of the Ice Thermal Energy Storage have been simulated through heat and mass balances with a thorough heat transfer analysis, specifically adapted to the operating conditions in the water tank.

Charging phase

In the charging phase, water in the tank is first cooled down to 0 °C, and then ice forms externally on the cooling coils. These are fed by a mixture of liquid and vapour CO_2 in equilibrium at the evaporating temperature of -10 °C. In the simulation reported in this chapter, the initial water temperature is assumed to be 10 °C. The estimation of the time needed to reduce the water temperature down to the freezing point is based on a simple energy balance once the cooling capacity is known, which is 70 kW in this case. In fact, measured data on the refrigerant side show that the evaporator is able to exchange the full capacity during the cooling phase. Ice formation over the coils is predicted through the well-known analytical model by London and Seban [90]. Water is assumed to be at its freezing point, and the heat flow rate per unit length, flowing in series through the ice conductive resistance and the internal convection one, is:

$$q' = \Delta t_o / (R'_{ice} + R'_o) \tag{6.1}$$

where Δt_o is the temperature difference between the temperature of water at the freezing point (0 °C) and the evaporating temperature of the refrigerant, R'_{ice} is the conductive resistance of ice and R'_o is the internal convective resistance per unit length, on the refrigerant side, assumed to be constant along the evaporator length and equal to its average value. In this model

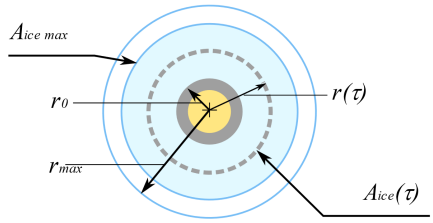

FIGURE 6.3: Schematisation of ice formation on the coil

the external convective resistance (water side) is neglected because of the assumption on the initial temperature of water at the freezing point, and the conductive resistance of the evaporator tube is negligible. The heat flow rate per unit length, neglecting the ice subcooling, provides the extraction of the latent heat of freezing at the surface $A_{ice}(\tau)$:

$$q' = \frac{dM_{ice}}{d\tau}\lambda_{ice} = -2\pi\rho_{ice}\lambda_{ice}r\frac{dr}{d\tau} \tag{6.2}$$

where M_{ice} is the mass of ice and λ_{ice} the latent heat of fusion. Combining the two equations above to simplify the heat flow rate and introducing the heat losses, provides the following differential equation expressing the radius of ice formation as a function of time:

$$-2\pi\rho_{ice}\lambda_{ice}r\frac{dr}{d\tau} = \frac{\Delta t}{\left(\frac{\log(\frac{r}{r_o})}{2\pi k_{ice}} + \frac{1}{2\pi r_o h_o}\right)} - UA_{env}(t_{env} - t_w) \tag{6.3}$$

where k_{ice} is the ice thermal conductivity, h is the heat transfer coefficient inside the pipe, ρ_{ice} is the density of ice. r is the radial position of the growing ice and r_o is the initial radius (corresponding to the outer radius of the cooling coil as shown in Figure 6.3), t_w is the temperature of the water in the tank (assumed to be uniform) and UA_{env} the overall thermal conductance between the ice tank and the surrounding with an U-value equal to 0.83 W/m^{2}K. Since the radius increases with time, the thermal resistance increases with time, and consequently both the heat flow rate and the cooling capacity decrease. The analytical model is able to predict the amount of ice formed as a function of time during the charge of the ITES, and as a consequence the cooling power required. A 12 m^3 ITES is

considered, with water at an initial temperature of 10 °C;

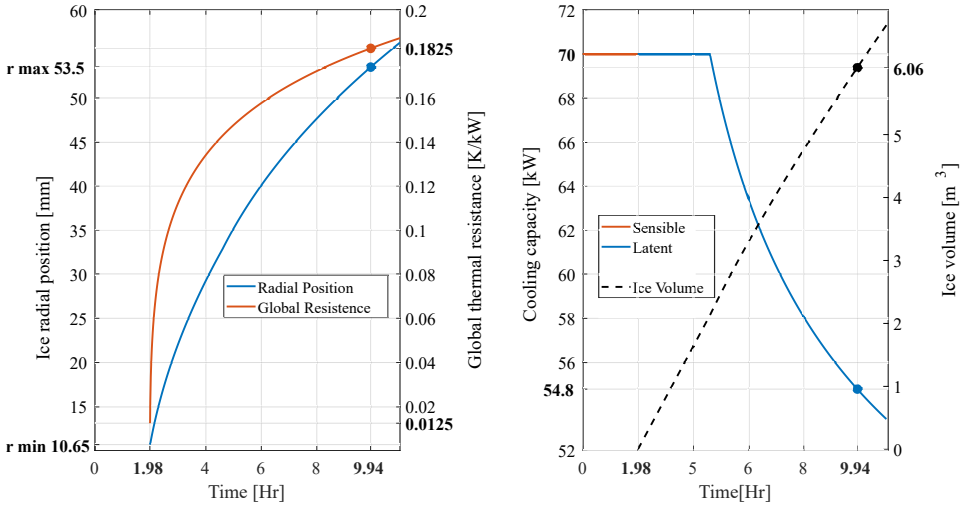

FIGURE 6.4: (left) Ice radius and global thermal resistance trend during the charging phase
(right) Ice volume and cooling capacity trend during the charging phase

Figure 6.4 left, shows the trends of the global thermal resistance and the ice front radial position over time during charging; the global resistance increases as the ice grows, since in this configuration the ice is not removed during charging. The initial radius corresponds to the pipe radius used in the tank (r_{min}=10.65 mm), and the final radius is given by the manufacturer (r_{max}=53.5 mm). Figure 6.4 right, shows the cooling capacity trend, divided into sensible and latent, and ice formation. At the start of the process, the cooling demand is intentionally limited to 70 kW by the size of the expansion valves of the refrigerating unit (Figure 6.4 right), given that the coils could transfer a higher flow rate to liquid water. Once water is chilled to the freezing point (1.98 hours) and ice builds up, its thermal resistance increases ((Figure 6.4 left), and when it becomes the bottleneck of the heat transfer, the cooling demand decreases below the design value. The charge has to be stopped when it reaches the maximum outer radius of ice set by the manufacturer at 53.5 mm, to prevent the ice coils from getting in touch each other. This process takes approximately 10 hours, 6.06 m^3 of ice is produced

and the cooling demand at the end of the process is reduced to 54.8 kW. The total amount of energy made available in the ITES is therefore around 2100 MJ, considering latent heat, the sensible heat up to 5 °C (maximum useful temperature for the purpose of the application) while neglecting the thermal capacity of the cooling coils. This corresponds to a volumetric storage capacity of 175 MJ/m^3.

Discharging phase

For the discharge model, an analytical solution was used to predict the ice-melting performance of the ITES. The ice cylinders were melted externally by water flowing across them, and with the aim of increasing heat exchange at the water-ice interface, a blower is used to increase the turbulence of water in the tank during discharge. The water exiting the ITES is useful for AC purposes up to 5° C, and this parameter determines the maximum duration of the discharging phase. A global energy balance approach is applied to the water in the liquid phase and melting, thus the boundaries of the control volume are the water-ice interface and the tank walls. The system is sketched in Figure 6.5, with the heat rates through the boundaries, that are plotted in the dashed lines. The energy balance gives the following expression:

$$\frac{dU}{d\tau} = \dot{Q}_{AC,load} + \dot{Q}_{losses} + \dot{Q}_{ice} + \dot{Q}_{blower} \tag{6.4}$$

where the first term on the left is the rate of change of internal energy in the water and, in order, the terms on the right correspond to: the heat flux from the heat exchanger HR_3 (i.e. the cooling demand), the heat loss to the surrounding at t_{env}, the heat exchanged by ice on water and the heat contribution due to the blowing of air at ambient temperature into the tank. The blower creates a mixing effect that allows the tank to be considered as an unstratified tank. By making explicit the terms, we obtain the following equation, similar to the equation from the model proposed by Lee and Jones [91]:

$$\begin{aligned} c_w M_w \frac{dt_w}{d\tau} = \dot{m}_w c_w (t_r - t_w) + UA_{env}(t_{env} - t_w) - h_e A_{ice}(t_w - t_{ice}) \\ - \frac{dM_w}{d\tau} c_w (t_w - t_{ice}) + \dot{m}_{air} c_{air} (t_{air} - t_w) \end{aligned} \tag{6.5}$$

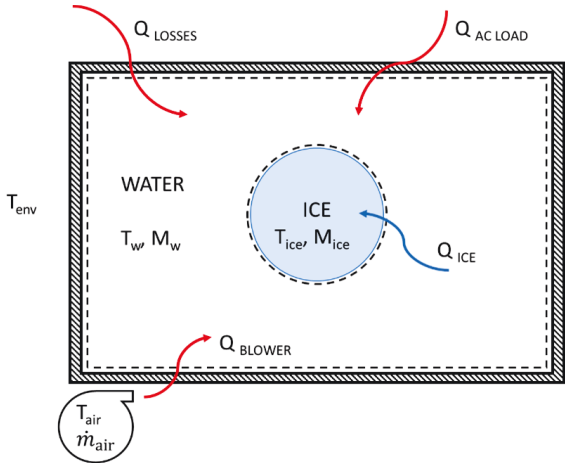

FIGURE 6.5: Energy balance scheme during the discharging phase

where $\dot{m}_w$ and t_r are the mass flow rate of water and the return water temperature from HR_3 to the tank while t_w and M_w are the water tank temperature and the water mass respectively; regarding the heat transfer, the value of the thermal external convective coefficient h_e in the heat transfer between the water and the ice is estimated from manufacturer tests as 930 W/m^2K. It is approximatively constant despite the variation of the ice radius during melting thanks to the forced convection introduced by the blower. The ice surface (A_{ice}) is considered at $t_{ice} = 0$ °C; the fourth right term is the sensible heat for the melted water which is heated from the freezing-point $t_o = t_{ice}$ to t_w and the last term corresponds to the heat contribution due to blowing of air into the tank, where t_{air} is the blower outlet temperature and m_{air} is the mass flow rate. Similarly to the case of charging, the subcooling of ice is also considered negligible [90]. Additionally, the mass conservation at the ice-water interface gives:

$$\frac{dM_w}{d\tau} = -\frac{dM_{ice}}{d\tau} = \frac{q_{ice}}{\lambda_{ice}} = \frac{h_e A_{ice}(t_w - t_{ice})}{\lambda_{ice}} \tag{6.6}$$

Where λ_{ice} is the latent heat of freezing for water. The final equation is obtained from Eq. (6.4) and Eq. (6.5) and discretized in time, where for the

reasons described above, $t_{w,target}$ is assumed to be at 5 °C:

$$\frac{t_w(n+1)-t_w(n)}{\Delta\tau} = -\frac{h_e A_{ice}(n)}{c_w M_w(n)}(t_w(n)-t_{ice})\left(\frac{c_w(t_w(n)-t_{ice})}{\lambda_{ice}}+1\right) + \frac{\dot{m}_w(n)(t_r-t_{w,target})}{M_w(n)} + \frac{U_{env}A_{env}(t_{env}-t_w(n))}{c_w M_w(n)} + \frac{\dot{m}_{air}c_{air}(t_{air}-t_w(n))}{c_w M_w(n)} \tag{6.7}$$

From the Eq. (6.7), water temperature is calculated at each time step, and then the quantity of ice is determined by mass conservation. Once the quantity of ice available is known from the cooling charge model, for a given load profile required by AC, the model gives the trend of water tank temperature, the trend of ice quantity and thus the maximum duration of the tank.

In summary, this is a simplified model that is intended to provide a useful tool for predicting the energy accumulated during charging phase, and predicting how this energy is used during the discharging phase.

6.3 Energy performance evaluation

From the above equation, water temperature is calculated at each time step, and then the quantity of ice is determined by mass conservation. Once the quantity of ice available is known from the cooling charge model, for a given load profile required by AC, the model gives the trend of water tank temperature, the trend of ice quantity and thus the maximum duration of the tank.

6.3.1 Option for use

In the following section, the energy and electrical power consumption performance in the summer and winter case are analysed.

Summer

The system shown in Figure 6.1 allows various conditions of use and can supply the required AC load. The main objective in the actual plant is to shave the peak in electrical energy use. The most critical condition in

terms of electricity use for the supermarket considered in this paper is in the morning when, in addition to all the supermarket's appliances, both ovens and heaters for the deli shop and the air conditioning are switched on. Reducing the peak electric power use allows a significant reduction in the investment cost for the connection to the electrical grid. Nonetheless, there may be also other uses for the storage: since the reduction in the early morning peak may be necessary only some days a year, the storage could be used with other strategies. The feasibility of peak shaving is being explored, to decrease the size of the reversible heat pump and to reduce electricity power request during peak periods, thus taking advantage of the hourly tariff. An AC cooling demand has been identified (daily summer profile in Figure 6.6), and the two modes of use were analysed:

- Case 1: Supply the ITES available energy in the early morning, when the supermarket's electrical demand is at its peak (blue).
- Case 2: Supply the ITES available energy to cover the AC demand peak that occurs in the central hours (orange).

Through the model above described, and with the support of experimental data from the field, the water temperature in the storage and the mass of ice for both cases are calculated and shown in Figure 6.6, The initial amount of ice (1607 kg) is that built in 4 hours, according to the charge model. In both cases, the water temperature trend (solid line) shows a behaviour consistent with ice melting curves (dashed line). After an initial linear increase until low water temperature prevents effective heat transfer with ice, ice melting occurs and a sudden increase in water temperature coincides with the complete melting of ice. In Case 1 the ITES is able to supply the AC load for 5 hours 41 minutes (until 11:40 AM) while in Case 2 the ITES is used from 9:34 to 20:09 AM (10 hours 35 minutes) reducing the maximum load on HP_2 from 74.19 kW down to 45.9 kW, allowing a reduction in the required capacity of the reversible heat pump. The cooling power supplied by the ITES is always lower than the maximum value as estimated by the manufacturer for such operating conditions. The two colored areas represent the net available energy provided by the tank; they are slightly different because in Case 2 the storage is used later in the day and it is subject to higher heat loss; this can also be seen in Figure 6.6 where the ice trend gradually drops at the beginning of the day, when the storage is not yet used. Finally, the discharge and charge models, interfaced

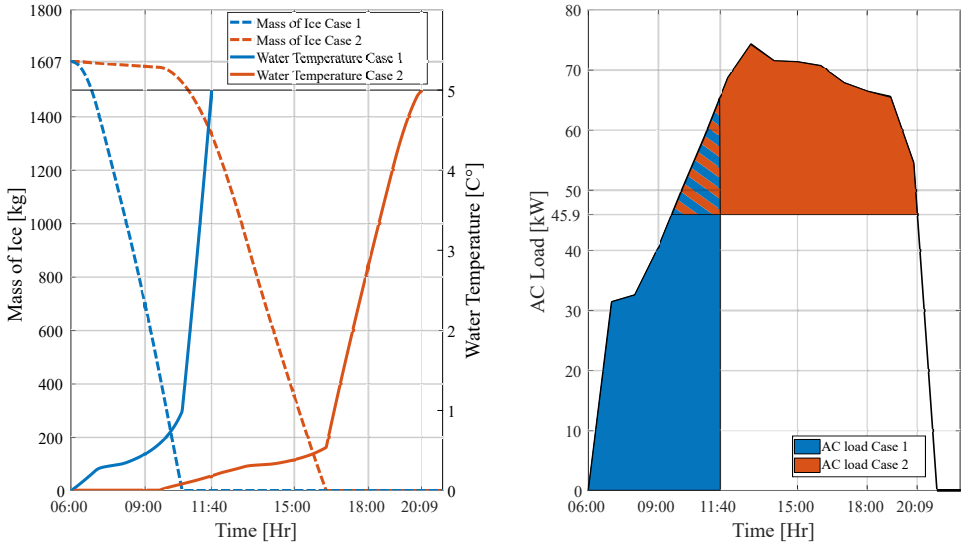

FIGURE 6.6: Mass of Ice and Water temperature trend during discharging phase (left) AC cooling load and different control strategies (right)

with the TRNSYS model previously mentioned for the prediction of the performance of the CRU, allow the two cases to be compared in terms of cooling and electrical energy use. The cooling energy used in the two cases is summarised in Table 6.2. The ITES charge energy is the energy supplied by the CRU through the evaporators during charging time, the ITES available energy is the energy usable for AC purposes (until 5 °C), followed by the ITES net available energy which is net of heat loss. An ITES efficiency is defined based on the cooling energy values as:

$$\eta_{ITES} = \frac{ITES_{net\ available\ energy}}{ITES_{charge\ energy}} \tag{6.8}$$

Case 2 shows a lower efficiency since the ITES is used later in the day, resulting in higher heat loss. In Table 2 are listed the electrical energy used by the HP_2 (water chiller operation) to face alone the whole daily cooling demand for HVAC; the total electrical energy needed if the ITES is used; the electrical energy needed during the night by the CRU for the ITES

TABLE 6.1: Cooling energy values comparison in both cases

Cooling energy [kWh/day]	Case 1	Case 2
ITES charge energy	280.0	280.0
ITES available energy	242.8	242.8
ITES net available energy	226.1	209.8
ITES efficiency	80.7%	74.9%

TABLE 6.2: Electrical energy values and COP comparison in both cases

Electrical energy [kWh/day]	Case 1	Case 2
Heat Pump 2 alone	292.3	292.3
ITES + Heat Pump	373.8	356.9
ITES charge	145.2	145.2
Extra electrical energy	81.5	64.6
COP of CRU for ITES charge	1.93	1.93
EER of heat pump	3.55	2.60

charging process and finally the extra energy to be supplied when the ITES is used, compared to an operation with the heat pump alone. The first and third rows have the same values since the same heat pump is used and the storage is charged at the same time (night-time) in both cases. The COP for ITES charge is calculated for the production of the "ITES charge energy" by the CRU. The EER of the heat pump is the average value of the EER of the heat pump during operation in the periods otherwise served by the ITES. The use of ITES is never energy profitable, due to the low COP of the commercial refrigeration unit even if working at favourable temperature conditions during night-time, and to the efficiency of the storage process itself, estimated by Eq. (6.8). In fact, the ITES is charged at the evaporating temperature of -10 °C, while the reversible heat pump is operated at an evaporating temperature of around 3 °C. Case 2 shows less electrical energy usage than Case 1 when the ITES is operated, because the storage is used when the heat pump would have had lower EER values.

Winter

Similarly to the summer operation mode, an analysis of a winter day is presented. It is important to emphasise that, as mentioned before, the system was designed for reducing peaks in electrical power use in summer. The daily heat load profile for space heating (SH load), shown as black solid line in Figure 6.7, has its peak in the early morning, when supermarket's electricity is also at its highest. Thus, the question is whether it is profitable to use the ITES or not, since in this case, unlike in summer, the only logic solution is to exploit the stored energy in the morning. The comparison of daily energy fluxes and temperatures with and without ITES is shown in Figure 6.7. The SH load (black solid line) remains the same in the two operating modes. In the case with ITES, the heat recovery from the CRU through HR_2, shown in blue line, is used to charge the ITES exclusively during the night (from 8 p.m to 4 a.m.) and the temperature in the ITES (red dashed line) increases up to upper limit of 50 °C. The storage tank supplies heat (red solid line) from 6 a.m. until 11:00 AM, then the CRU is used directly in heat recovery mode to meet the heat demand. The two systems (CRU and ITES) do not work simultaneously: the operation control logic uses the ITES first and then the CRU. The HP goes into operation when the temperature in the HVAC tank (red dashed line) drops below 40 °C. In the case with ITES, the energy demand from the heat pump (green line) is required between 11 a.m. and 1 p.m. up to 27.8 kW. In the case without the ITES, the demand from the heat pump is more marked and has a peak, up to 66.5 kW, at the early morning. Similarly to the summer case, the use of ITES allows a lower capacity of the heat pump. Figures 6.8 and 6.9 show a quantitative energy analysis, comparing the use of the storage in terms of electrical energy and thermal energy absorbed. The values shown are calculated from the energy balance on the HVAC tank, the two cases do not match perfectly due to the differences in heat losses in the two cases, the stratification of the tank and the fact that the storage is not at exactly the same temperature at the end of the day in the case with or without ITES. As expected, in the case without ITES, the energy use for the heat pump is higher (+91%), as is the heat supplied by the CRU (+32%). It is important to mention that "heating energy HR_2" only considers the heat recovered directly from the HR_2, thus excluding heat from the ITES. Approximately, in this specific supermarket, the storage tank provides up to about 30% of the heat produced. In the case of the ITES, electricity consumption from the

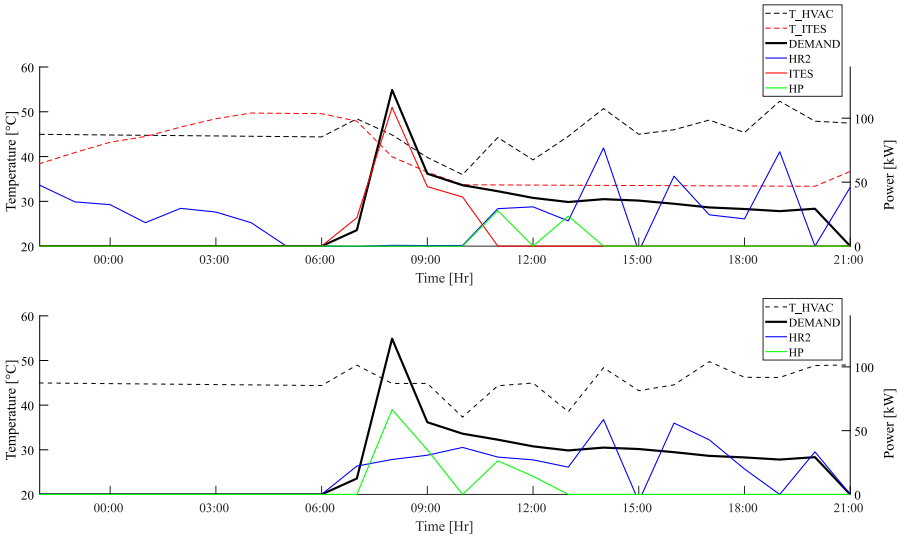

FIGURE 6.7: Comparison of daily energy flows in the winter case with storage (above) and without storage (below)

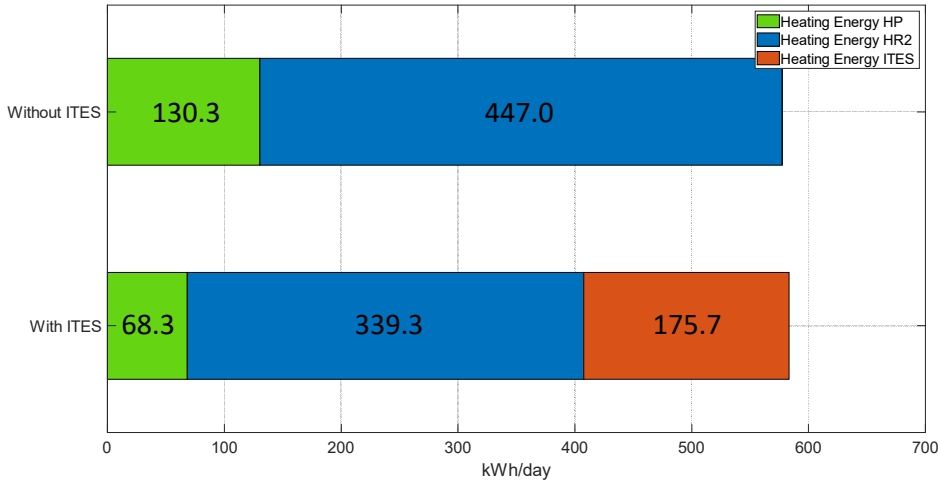

FIGURE 6.8: Comparison between daily heating energy values in both cases

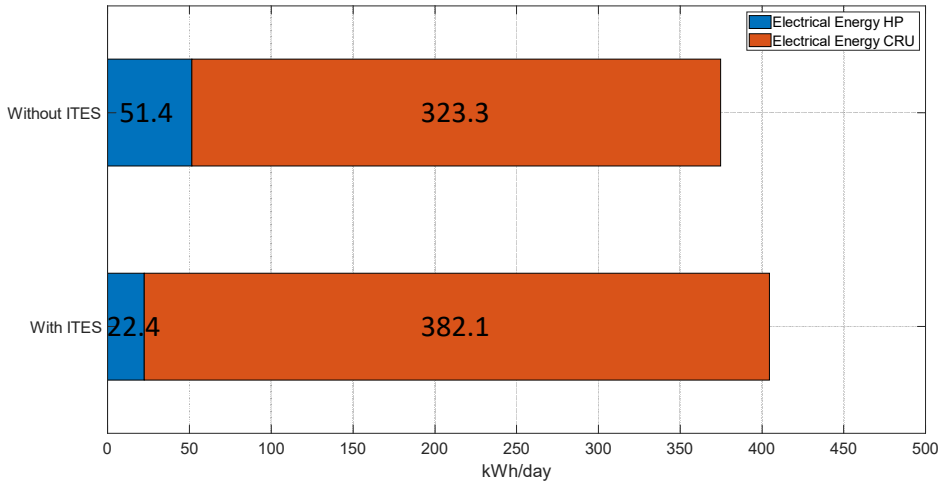

FIGURE 6.9: Comparison between daily electrical energy values in both cases

heat pump is reduced by 56%, while electricity consumption from the CRU is increased by 18%. The main reason for the non-energy-efficiency, even in the winter case, is due to the fact that the CRU is forced into transcritical operation to provide heat in winter, and the efficiencies of the commercial refrigeration unit are still lower (although less pronounced than in the summer case) than those of the heat pump. The real convenience may therefore once again be in the reduction of peak electricity demand in the morning; A trend of electrical power use (only for refrigeration and heating) is shown in Figure 6.10, where a reduction in the morning (at 08:00 AM) is shown, from 35.4 to 13.4 kW. Furthermore, the use of ITES could allow a lower size of the heat pump from 66.5 to 27.8 kW of heating capacity, but the summer operation forces to cover 45.9 kW of cooling capacity.

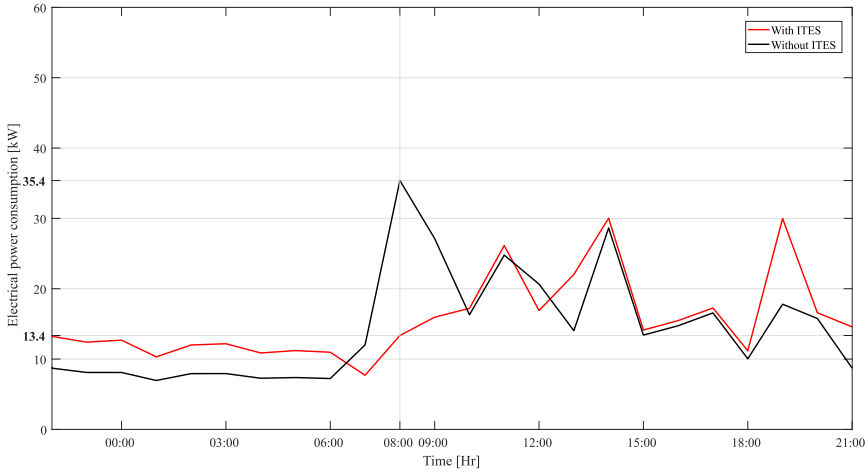

FIGURE 6.10: Comparison of the daily trend in electrical power absorption for refrigeration and heating

6.3.2 Yearly energy evaluation

A comparison of monthly electrical energy use between ITES (right columns) and non-ITES (left columns) systems is shown in Figure 6.11. As expected from the daily comparison, the solution with ITES requires more energy, with the exceptions of April, May and October, when storage is not used. The months with the highest energy requirement are the summer months when the cooling load is higher. Respect to the figure from July to September the storage is used in summertime operating mode, and from November to March in wintertime operating mode.

6.3.3 Cost Analysis

Since in this specific analysis storage is used to contain costs, an economic analysis over the years of supermarket operation is conducted. The difference between the two scenarios (with and without a storage) in terms of cost is defined as:

$$\Delta_{cost} = (CC + RC) - (CC_{ITES} + RC_{ITES}) \tag{6.9}$$

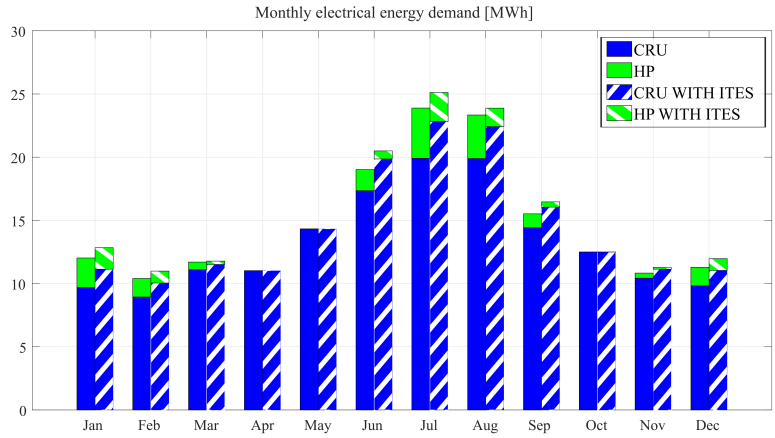

FIGURE 6.11: Monthly electrical energy used in one year in both cases

Where CC are the capital costs and RC the running costs defined as follows:

$$RC = AEC\frac{(1+r)^n - 1}{(1+r)^n r} \tag{6.10}$$

Where n is the lifetime of the investment in years, r is the discount rate assumed to be 6.5% (Giunta et al. [92]), and AEC are the annual energy costs calculated as:

$$AEC = \sum_{h=1}^{n} E_h e_h \tag{6.11}$$

where E_h represents the hourly absorption of electricity during the year, and e_h represents the hourly cost of electricity; an Italian 3- band electricity tariff is assumed (see Fig. 6.12). The first slot is called F1: active from Monday to Friday, from 8.00 am to 7.00 pm, excluding national holidays. The second slot is called F2: active from Monday to Friday, from 7:00 am to 8:00 am and from 7:00 pm to 11:00 pm, and on Saturday from 7:00 am to 11:00 pm, except on Saturdays which are national holidays. Finally, there is the third slot called F3: active from Monday to Saturday from 11:00 pm to 7.00 am and all day on Sundays and public holidays. The prices for the three slots are 0.501 €/kWh for F1, 0.521 €/kWh for F2 and 0.491 €/kWh for F3. These values are

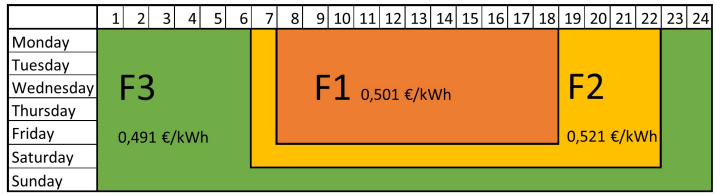

FIGURE 6.12: Hourly tariff scheme

taken from the section "prices and tariffs" in the *Italian Regulatory Authority for Energy, Networks and Environment (ARERA)* [93]. Regarding capital costs, in the case without storage the installation of a transformer room to supply the supermarket with medium-voltage electricity is required, due to the high absorption peak. The cost of this operation is estimated at around 100 k€, while the cost of the air-to-water heat pump for air conditioning and space heating is 26 k€ (70 kW cooling) with a total initial cost of 126 k€. With the ITES, the total cost of the tank + installation equals 10 k€, while the heat pump can be under-sized from 70 to 50 kW reducing its cost to 17.2 k€, giving a total amount of 27.2 k€. Since the objective of this analysis is the absolute value of the cost difference, other costs are not considered in this analysis. A comparison over 10 and 15 years of operation between the two solutions is proposed in Fig. 6.13. The solution with storage is the most economical over time, going from 764.29 k€ to 705.29 k€ in 10 years (8% saving) and from 960.86 k€ to 912.97 k€ in 15 years (5% saving). This analysis is done with a fixed energy price over the years, the greater the price variation the greater the potential profit due to the use of ITES could be.

6.4 Chapter conclusions

A real case of a supermarket where the refrigerating unit provides also cooling and heating in favour of the building is investigated in this chapter. Ice thermal energy storage (ITES) is used, when many other electrical appliances (ovens etc) are in use and is therefore recommended for its ability in regard to reduce electrical power peaks in the morning, and a better exploitation of tariffs. Nevertheless the individual case must be evaluated since the use of heat storage in the case under consideration shows to be

TABLE 6.3: Summary values of costs for the duration of 10 and 15 years

10 Years

	Whitout ITES		With ITES	
Capital cost				
	Power supply	100.000 €	ITES storage	15.000 €
	Heat Pump	26.000 €	Heat Pump	17.200 €
Running cost				
		638.292 €		673.393 €
TOTAL				
		764.292 €		705.593 €
Δ_{Cost}		-		**-58.699 €**

15 Years

Capital cost				
	Power supply	100.000 €	ITES storage	15.000 €
	Heat Pump	26.000 €	Heat Pump	17.200 €
Running cost				
		834.857 €		880.769 €
TOTAL				
		960.857 €		912.969 €
Δ_{Cost}		-		**-47.888 €**

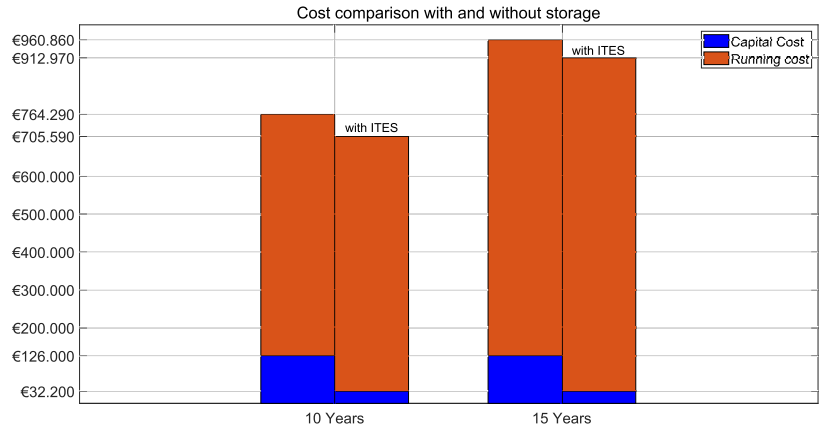

FIGURE 6.13: Cost comparison for the lifetime of the supermarket with and without storage

detrimental for the energy efficiency, as expected, but allows to shave electric power peaks. An estimation of the daily energy use is conducted for both winter and summer typical operation.

In summer two cases are evaluated: Case 1, supplying the whole AC demand early in the morning, and Case 2, to assist the water chiller in covering the air conditioning peak demand, thus allowing a reduction in its design size. With Case 1 the ITES is better exploited, showing an higher efficiency (80.7%) compared to Case 2 (74.9%). However, because the storage is used when the heat pump would have had lower EER values, Case 2 shows lower electrical energy usage than Case 1.

In the winter operation, an higher energy use is experienced as well. Then, an analysis on an annual basis is conducted, confirming an increase in energy need when ITES is used, for almost every month of the year.

However, the cost analysis shows that the reduction in size of the reversible heat pump, and the chance to avoid the installation of an electrical transformer in a dedicated room allows saving 58699 € in 10 years or 47888 € in 15 years, thus making the choice of ITES profitable in the usual lifetime

for these plants.

Chapter 7

Conclusions and future research

The thesis deals with different solutions for improving the performance of CO_2 systems. In particular the improvement methods are divided into two main parts. The first part with the focus on the possibility of using zeotropic mixtures: directly within well-known transcritical CO_2 plant configurations with CO_2-based blends and inside a dedicated mechanical subcooling system. The second part focuses on commercial refrigeration, starting analysing and comparing different cycle architectures and then an energy and economic analysis of the overall system and its interaction with the supermarket building, using a thermal energy storage. The conclusions concerning the two parts are presented in this chapter as an answer to the questions raised in the introduction (Sec. 1.3), to motivate the work carried out.

7.1 Answer to specific research questions

1. *The existing works regarding the possible utilization of the CO_2-based blends are focused on air-conditioning systems or small stand-alone refrigeration systems and no works have been found in relation to condensing unit applicable to small-sized refrigeration applications.*

   The use of CO_2-doped blends as a possible improvement of two classical CO_2 cycles, the internal heat exchanger and parallel compression ones have been analysed from a theoretical approach. R-152a, R-1234yf, R-1234ze(E) and R-1233zd(E) have been considered as doping agents to modify the performance of the selected architectures. Results

have been based on the use of a comprehensive model using REFPROP v10.0 and its mixing rules as reference. It has been predicted that 5-10% CO_2 doping tends to enhance the COP of the architectures, but this is accompanied by a reduction of the volumetric cooling capacity. The optimum mass proportion of additive is independent on the evaporating level, being only dependent and positive for environment temperature above 20 ºC. CO_2 doping with pure fluids which have higher critical temperature than CO_2 allows the optimum condition of the cycle to go to subcritical operation, causing a reduction of the operating pressures in all the cycles.

Considering the IHX architecture, COP improvements are predicted in environment temperature higher than 25 ºC, reaching maximum improvement around 30 ºC and being attenuated at 40 ºC. Enhancements up to 7.70% were predicted with the mixture CO_2/R-1233ze(E) [90/10%]

In relation to the PC layout, the use of refrigerant blends deals with the fractionation of the refrigerant in the phase-separation vessel, where two flows with different compositions are generated. The saturated vapour contains a higher proportion of the most volatile component (CO_2 in this work), and the saturated liquid is enriched with the least volatile component. This fractionation introduces modifications to the cycle, which can be considered as another mechanism to enhance the performance. For the PC cycle, CO_2-doped has wider range of benefit. Enhancements up to 11.98% were predicted with the mixture CO_2/R-1233zd(E) [95/5%].

Future Work

Models developed to predict these mixtures are often inaccurate due to a lack of experimental data. As part of future work, the theoretical model can be refined by incorporating additional experimental data tested in this thesis. A more accurate model, aimed at predicting the performance of a plant with sufficient accuracy, is a valuable tool for

large-scale studies. This model can be tested under various climatic conditions and subsequently optimized for specific purposes.

2. *There is a lack of experimental data for the evaluation of different CO_2 refrigeration cycles with doping agents.*

   An experimental comparison of a CO_2 base refrigeration cycle with and without internal heat exchanger (IHX) working with CO_2/R-152a mixtures at 5% and 10% mass composition of R-152a as refrigerants has been conducted. The experimental campaign has allowed to demonstrate the enhancement of COP in typical CO_2 cycles with the use of mixtures replacing pure CO_2. Using CO_2/R-152a blends instead of pure CO_2 as refrigerants in a base cycle improved the COP at high heat rejection temperatures. The use of CO_2/R-152a [90/10%] mixture provided COP improvements up to 10.2%. Using CO_2/R-152a [95/5%] gave maximum COP improvement of 11.2%. On the other hand, for a cycle with IHX, using the evaluated mixtures as working fluids instead of pure CO_2 was almost always detrimental for the energy efficiency.

   The COP of the cycle is the main parameter studied, however, other parameters such as cooling capacity, heat rejection pressure or discharge temperature of the compressor have been considered as well. As a consequence of the use of blends, some disadvantages were found: cooling capacity is reduced and the discharge temperature of the compressor is increased. However, the optimum heat rejection pressure is reduced, which is an advantage of using mixtures because it allows the cycle to work in subcritical conditions, where the control is easier, and it can allow to avoid using the liquid receiver. The importance of this experimental results relies on the COP enhancement of typical CO_2 cycles by using CO_2 based mixtures instead of pure CO_2 as working fluids. It is noted that COP improvements take place particularly at high heat rejection temperatures. Selection of the cycle configuration is also important as base cycle has significant improvements at high temperatures while cycle with IHX do not. COP obtained with base cycle with mixtures is almost equal to that of IHX cycle with pure CO_2 for high heat rejection temperatures which implies a reduction

of the compressor discharge temperature and the non-existence of the additional heat exchanger (IHX), two mentionable feats due to CO_2/R-152a blends utilization.

Future Work

Regarding the use of CO_2-doped blends, some future research can be developed as for example determining experimentally the optimum composition of the mixture or testing other additives. Studying the mixture impact on more complex cycles such as the integrated mechanical subcooling can also be beneficial for the overall cycle behaviour.

Moreover, an interesting part is the study of these mixtures within heat pumps: identifying blends of natural substances that could be effectively used in the next generation high-temperature heat pumps. The choice of using natural substances as blend components arises from the need of developing an environmentally friendly refrigerant, that could effectively fulfil the current regulations on the use of greenhouse gases. Additionally, these blends typically exhibit a high temperature glide that would be exploited to match the secondary fluid temperature profile in the specific applications to maximise the system performance.

3. *Dai et al. launched a hypothesis about the use of zeotropic refrigerant mixtures with matching temperature glide in the DMS cycle, to reduce the temperature difference in the subcooler and thus to improve the performance of the combination. However, Dai's hypothesis has not been verified experimentally for the moment.*

The possibility to enhance the performance of a transcritical CO_2 refrigeration plant using a dedicated mechanical subcooling system with zeotropic refrigerant mixtures has been addressed theoretically and experimentally. Using Dai et al. model adapted to an existing test plant, the performance of three blends composed of R-32, R-600

or CO_2 with the base fluid R-152a has been evaluated. It has been observed that, theoretically, it is possible to obtain higher COP values in relation to the use of pure fluids. However, trends presented by Dai et al. have not been reproduced in the simulations. The difference, whose cause cannot be defined, could be associated to the different used overall compressor efficiencies and with updated tool for refrigerant properties prediction, which differ from the previous works. Theoretical simulation has identified the blend R-600/R-152a [60/40%] as the best performing one, with theoretical COP improvements up to 0.46%.

Three refrigerant blends, R-152a/R-32 [60/40%], R-600/R-152a [60/40%] and R-152a/CO_2 [90/10%] have been tested experimentally against the operation with R-152a as refrigerant in the dedicated subcooling system. It has been verified that the mixture R-600/R-152a [60/40%] is able to enhance the COP of the plant up to 1.4%. In addition, the mixture R-152a/CO_2 [90/10%], which has good matching temperature profiles in the subcooler, could also improve the performance of the plant if the subcooler was resized. However, the other mixtures did not show good performance. The experimental results indicated that the improvements are higher for blends with low volumetric cooling capacity and that these mixtures work with a moderate subcooling degree and have low power consumption in the auxiliary compressor. Furthermore, as suggested by Dai et al. [63], the mixtures which effective temperature glide matches with the CO_2 temperature evolution in the subcooler, enhance the thermal performance of the subcooler. Consequently, the evaporating level in the subcooler with the mixture can be higher than with the pure fluid and enhance the performance of the auxiliary cycle and thus of the cycle combination. Finally, it needs to be mentioned that the use of zeotropic blends in the subcooler allows to reduce the irreversibilities in this heat exchanger.

4. *Despite the significant amount of research that has been conducted on the topic of performance enhancing measures to transcritical CO_2 refrigeration cycles, there are very few publications that cover so many cycles compared on the same refrigeration plant, nor are there any papers which conduct an*

experimental comparison of the use of a CO_2 pump as a method of ejector control.

An experimental analysis comparing two ejector control methods and five cycle architectures applied in a two-evaporator transcritical CO_2 refrigeration cycle is carried out. In particular, the two ejector control methods assessed were motive nozzle diameter variation via a manually-adjustable needle located in the motive nozzle throat and motive nozzle inlet pressure modulation through a variable-speed pump placed between the condenser/gas cooler outlet and the ejector motive nozzle inlet. The assessed cycles were flash tank economization applied upstream of the MT evaporator, ejector, flash tank with an IHX, an IHX with an ejector and a pump upstream of the ejector motive nozzle inlet. Ejector parameters such as entrainment ratio, efficiency, and pressure lift were also assessed.

The gas cooler outlet pressure was varied at each ambient condition for each cycle in an effort to identify the gas cooling pressure that resulted in the maximum COP. Ejector parameters such as entrainment ratio, efficiency, and pressure lift were also assessed. Ejector and IHX cycles increased COP by 4.64% and 9.47%, respectively.

With respect to ejector control, it was found that modulation of the motive nozzle diameter led to a maximum ejector efficiency variation of approximately 6%. The configuration utilizing the CO_2 pump was found to be able to increase ejector efficiency by approximately 11% relative compared to the ejector configuration at the same conditions. Furthermore, correlations between nozzle position or pump speed and ejector entrainment ratio, pressure lift, and efficiency were clearly identifiable. Therefore, both methods of ejector control were validated in their ability to control the ejector. All tests utilizing the pump resulted in a lower COP with a maximum decrease of 6.1% and a higher cooling capacity with a maximum increase of 6.2% compared to the ejector cycle without the pump. However, the pump was only tested with the system in subcritical mode.

Future work

Focusing on different cycle configurations, future work is to optimize both ejector and pump designs for the operating conditions and capacity of this test stand to increase the COP benefit of both cycles and to analyze results with the pump in transcritical conditions. As the safety constraints for pump operation were found to be more restrictive than anticipated, future work will aim to allow the CO_2 pump to be used at higher ambient temperatures safely for the system. Finally, the position of the IHX low-temperature flow should re-evaluated.

5. *Clearly defining the potential improvements of a thermal energy storage in a complex system such as a real supermarket is not straightforward, energy and cost parameters over the lifetime of the system must be taken into account and there is a lack of analysis based on real data from the field.*

A real case of a supermarket where the refrigerating unit provides also cooling and heating in favour of the building is investigated in this chapter. Ice thermal energy storage (ITES) is used, to reduce electrical power peaks in the morning, when many other electrical appliances (ovens etc) are in use. The use of heat storage in such a case shows to be detrimental for the energy efficiency, as expected, but allows to shave electric power peaks. An estimation of the daily energy use is conducted for both winter and summer typical operation.

In summer two cases are evaluated: Case 1, supplying the whole AC demand early in the morning, and Case 2, to assist the water chiller in covering the air conditioning peak demand, thus allowing a reduction in its design size. With Case 1 the ITES is better exploited, showing an higher efficiency (80.7%) compared to Case 2 (74.9%). However, because the storage is used when the heat pump would have had lower EER values, Case 2 shows lower electrical energy usage than Case 1.

In the winter operation, an higher energy use is experienced as well. Then, an analysis on an annual basis is conducted, confirming an

increase in energy need when ITES is used, for almost every month of the year.

However, the cost analysis shows that the reduction in size of the reversible heat pump, and the chance to avoid the installation of an electrical transformer in a dedicated room allows saving 58699 € in 10 years or 47888 € in 15 years, thus making the choice of ITES profitable in the usual lifetime for these plants.

Future work

When an ITES is used in a commercial refrigeration systems the management of the system plays an important role: there is still room for improving the performance by acting mainly on the control of the plant; in this specific case analyzed, charging phase need to me optimize having a significant impact on overall energy consumption. Moreover, the study of systems with heat storage is crucial in both heat pumps and refrigeration to exploit electrical energy when it is available, or to provide energy to a user by decoupling supply and demand load.

Appendix A

Uncertainties calculation

To evaluate the measurement uncertainties of $\dot{Q}_o$ and COP, the method proposed by Moffat [84] and extended by Aprea et al. [94] was used. The previous mentioned method was broadened in this work to include the uncertainty of the refrigerant composition.

A.1 Mass composition error

The mass composition of the components of a mixture [Z_1,Z_2] are expressed by:

$$Z_1 = \frac{M_1}{M_1 + M_2} \tag{A.1}$$

$$Z_2 = \frac{M_2}{M_1 + M_2} \tag{A.2}$$

The uncertainty of the mass composition of the first component is:

$$\begin{aligned} I_{Z_1} =& \sqrt{\left(\frac{\delta Z_1}{\delta M_1}\epsilon_M\right)^2 + \left(\frac{\delta Z_1}{\delta M_2}\epsilon_M\right)^2} \\ =& \sqrt{\left(\frac{M_2}{(M_1+M_2)^2}\epsilon_M\right)^2 + \left(\frac{M_1}{(M_1+M_2)^2}\epsilon_M\right)^2} \end{aligned} \tag{A.3}$$

Thus, the value of the mass composition of the refrigerant mixture is:

$$\begin{aligned} Z + I_Z =& [Z_1 + I_{Z_1}, 1 - Z_1 - I_{Z_1}] \\ Z - I_Z =& [Z_1 - I_{Z_1}, 1 - Z_1 + I_{Z_1}] \end{aligned} \tag{A.4}$$

A.2 Enthalpy measurement error

From the experimental measurements (p and t) and using Refprop v.10 the specific enthalpy values are calculated. These values are subjected to an uncertainty derived by the accuracies (ϵ) of temperature and pressure measurement devices, as well as, (if needed) to the uncertainty of the refrigerant composition (Z). The uncertainty of the specific enthalpy is calculated as:

- For enthalpies calculated through p measurement (for saturated vapour x_v=1):

$$h_o = f(p, x_v, Z) \tag{A.5}$$

$$I_h = \sqrt{I_p + I_Z} \tag{A.6}$$

$$\begin{aligned} I_p =& \frac{|h_{p+} - h_o| + |h_{p-} - h_o|}{2} \\ =& \frac{|h(p+\epsilon_p, x_v, Z) - h_o| + |h(p-\epsilon_p, x_v, Z) - h_o|}{2} \end{aligned} \tag{A.7}$$

$$\begin{aligned} I_Z =& \frac{|h_{Z+} - h_o| + |h_{Z-} - h_o|}{2} \\ =& \frac{|h(p, x_v, Z+I_Z) - h_o| + |h(p, x_v, Z-I_Z) - h_o|}{2} \end{aligned} \tag{A.8}$$

  Thus, the value of the enthalpy is expressed by:

$$h = h_o \pm I_h \tag{A.9}$$

- For enthalpies calculated through p and t measurements:

$$h_o = f(p, t, Z) \tag{A.10}$$

$$I_h = \sqrt{{I_p}^2 + {I_t}^2 + {I_Z}^2} \tag{A.11}$$

$$
\begin{aligned}
I_p &= \frac{|h_{p+} - h_o| + |h_{p-} - h_o|}{2} \\
&= \frac{|h(p+\epsilon_p, t, Z) - h_o| + |h(p-\epsilon_p, t, Z) - h_o|}{2}
\end{aligned} \tag{A.12}
$$

$$
\begin{aligned}
I_t &= \frac{|h_{t+} - h_o| + |h_{t-} - h_o|}{2} \\
&= \frac{|h(p, t+\epsilon_t, Z) - h_o| + |h(p, t-\epsilon_t, Z) - h_o|}{2}
\end{aligned} \tag{A.13}
$$

$$
\begin{aligned}
I_Z &= \frac{|h_{Z+} - h_o| + |h_{Z-} - h_o|}{2} \\
&= \frac{|h(p, t, Z+I_Z) - h_o| + |h(p, t, Z-I_Z) - h_o|}{2}
\end{aligned} \tag{A.14}
$$

Thus, the value of the enthalpy is expressed by:

$$
h = h_o \pm I_h \tag{A.15}
$$

A.3 Cooling capacity uncertainty

Cooling capacity is computed as product of the refrigerant mass flow rate and the enthalpy difference in the evaporator.

$$
\dot{Q} = \dot{m}_{ref}(h_{o,out} - h_{o,in}) \tag{A.16}
$$

Its uncertainty is evaluated with:

$$
\begin{aligned}
I_{\dot{Q}_o} =& \sqrt{\left(\frac{\delta \dot{Q}_o}{\delta \dot{m}_{ref}}\epsilon_{\dot{m}}\right)^2 + \left(\frac{\delta \dot{Q}_o}{\delta h_{o,out}} I_{h_{o,out}}\right)^2 + \left(\frac{\delta \dot{Q}_o}{\delta h_{o,in}} I_{h_{o,in}}\right)^2} \\
=& \sqrt{((h_{o,out} - h_{o,in})\epsilon_{\dot{m}})^2 + (\dot{m}_{ref} I_{h_{o,out}})^2 + (\dot{m}_{ref} I_{h_{o,in}})^2}
\end{aligned} \tag{A.17}
$$

A.4 COP uncertainty

COP is calculated as quotient of the overall cooling capacities and the measurement of the overall compressors power consumption:

$$COP = \frac{\dot{Q}_o}{P_C} \tag{A.18}$$

Its uncertainty is evaluated with:

$$\begin{aligned} I_{COP} =& \sqrt{\left(\frac{\delta COP}{\delta \dot{Q}_o} I_{\dot{Q}_o}\right)^2 + \left(\frac{\delta COP}{\delta P_C} \epsilon_{P_C}\right)^2} \\ =& \sqrt{\left(\frac{1}{P_C} I_{\dot{Q}_o}\right)^2 + \left(\frac{-\dot{Q}_o}{{P_C}^2} \epsilon_{P_C}\right)^2} \end{aligned} \tag{A.19}$$

The COP value is expressed as:

$$COP = COP \pm I_{COP} \tag{A.20}$$

When the cooling capacity is calculated as the sum of several cooling capacities such as the power consumption (as in booster system) the procedure remains identical, with only the extension of the additional parameters keeping the form as in the following equation [84]:

$$I_y = \sqrt{\sum \left(\frac{\partial Y}{\partial X_i} I_{x_i}\right)^2} \tag{A.21}$$

Bibliography

[1] International Institute of Refrigeration, 2017. 35th Informatory note on Refrigeration Technologies. The impact of the refrigeration sector on climate change. IIR, France.

[2] Dupont J. L. DP, Lebrun P., Ziegler F. The Role of Refrigeration in the Global Economy (2019), 38th Note on Refrigeration Technologies. 2019. p. 12.

[3] 1987 Montreal Protocol on Substances that Deplete the Ozone Layer - 1522 UNTS 3, 26 ILM 1541, 1550 (1987).

[4] Nations U. Amendment to the Montreal Protocol on Substances that Deplete the Ozone Layer. Kigali 2016.

[5] European Commission. Regulation (EU) No 517/2014 of the European Parliament and of the Council of 16 April 2014 on fluorinated greenhouse gases and repealing Regulation (EC) No 842/2006. 2014.

[6] Proposal for a REGULATION OF THE EUROPEAN PARLIAMENT AND OF THE COUNCIL on fluorinated greenhouse gases, amending Directive (EU) 2019/1937 and repealing Regulation (EU) No 517/2014.

[7] Publications S. World Guide to Transcritical CO2 Refrigeration - Part I. 2020:182.

[8] Calleja-Anta, D., Nebot-Andrés, L., Cabello, R., Sánchez, D., Llopis, R., 2021. A3 and A2 refrigerants: Border determination and hunt for A2 low-GWP blends. International Journal of Refrigeration.

[9] International Electrotechnical Commission, 2019. Voting Result 61C/792/FDIS, SC 61C Safety of refrigeration appliances for household and commercial use.

[10] EN 378-1:2016(MAIN) Refrigerating systems and heat pumps - Safety and environmental requirements - Part 1: Basic requirements, definitions, classification and selection criteria.

[11] ANSI/ASHRAE 34-2022, Designation and Safety Classification of Refrigerants.

[12] Gay, N.H., 1931. Refrigerating System. US Patent 1,836,318.

[13] Fang Liu, Yong Li, and Eckhard A. Groll. "Performance enhancement of CO2 air conditioner with a controllable ejector". In: *International Journal of Refrigeration* 35 (6 Sept. 2012), pp. 1604–1616. ISSN: 0140-7007. DOI: 10.1016/J.IJREFRIG.2012.05.005.

[14] Lucas, C., Koehler, J., 2012. Experimental investigation of the COP improvement of a refrigeration cycle by use of an ejector. International Journal of Refrigeration 35, 1595–1603.

[15] Stefan Elbel and Pega Hrnjak. "Experimental validation of a prototype ejector designed to reduce throttling losses encountered in transcritical R744 system operation". In: *International Journal of Refrigeration* 31 (3 May 2008), pp. 411–422. ISSN: 0140-7007. DOI: 10.1016/J.IJREFRIG.2007.07.013.

[16] Hafner, A., Försterling, S., Banasiak, K., 2014. Multi-ejector concept for R-744 supermarket refrigeration. International Journal of Refrigeration 43, 1–13.

[17] Haida, M., Banasiak, K., Smolka, J., Hafner, A., Eikevik, T.M., 2016. Experimental analysis of the R744 vapour compression rack equipped with the multi-ejector expansion work recovery module. international journal of refrigeration 64, 93–107.

[18] Zhu, J., Elbel, S., 2018. Experimental investigation of a novel expansion device control mechanism: Vortex control of initially subcooled flashing R134a flow expanded through convergent-divergent nozzles. International Journal of Refrigeration 85, 167–183.

[19] S.M. Hojjat Mohammadi. "Theoretical investigation on performance improvement of a low-temperature transcritical carbon dioxide compression refrigeration system by means of an absorption chiller aftercooler". In: *Applied Thermal Engineering* 138 (2018), pp. 264–279. ISSN: 1359-4311. DOI: https://doi.org/10.1016/j.applthermaleng.

2018.04.006. URL: https://www.sciencedirect.com/science/article/pii/S1359431117379784.

[20] Park, C., Lee, H., Hwang, Y., Radermacher, R., 2015. Recent advances in vapor compression cycle technologies. International Journal of Refrigeration 60, 118-134.

[21] Llopis, R., Nebot-Andrés, L., Sánchez, D., Catalán-Gil, J., Cabello, R., 2018. Subcooling methods for CO2 refrigeration cycles: A review. International Journal of Refrigeration 93, 85-107.

[22] E. Torrella et al. "Energetic evaluation of an internal heat exchanger in a CO2 transcritical refrigeration plant using experimental data". In: *International Journal of Refrigeration* 34 (1 Jan. 2011), pp. 40–49. ISSN: 0140-7007. DOI: 10.1016/J.IJREFRIG.2010.07.006.

[23] Cavallini, A., Cecchinato, L., Corradi, M., Fornasieri, E., Zilio, C., 2005. Two-stage transcritical carbon dioxide cycle optimisation: A theoretical and experimental analysis. International Journal of Refrigeration 28, 1274-1283.

[24] Sánchez D., Calleja-Anta, D., Nebot-Andrés, L., Catalán-Gil, J., Llopis. R., Cabello, R., 2020. Experimental analysis of alternative blends of refrigerants for CO2 transcritical refrigeration., VIII Ibero-american congress on refrigeration sciences and technology, CYTEF 2020, Public Universtity of Navarra, Spain.

[25] Bertelsen, S.K., Haugsdal, S.B., 2015. Design and measurement of a CO2 refrigeration system with integrated propane subcooler at high air temperature operations, Department of Energy and Process Engineering. Norwegian University of Science and Technology, Trondheim, Norway.

[26] Llopis, R., Cabello, R., Sánchez, D., Torrella, E., 2015. Energy improvements of CO2 transcritical refrigeration cycles using dedicated mechanical subcooling. International Journal of Refrigeration 55, 129-141.

[27] Rodrigo Llopis et al. "Experimental evaluation of a CO2 transcritical refrigeration plant with dedicated mechanical subcooling". In: *International Journal of Refrigeration* 69 (Sept. 2016), pp. 361–368. ISSN: 0140-7007. DOI: 10.1016/J.IJREFRIG.2016.06.009.

[28] Nebot-Andrés, L., Sánchez, D., Calleja-Anta, D., Cabello, R., Llopis, R., 2021. Experimental determination of the optimum working conditions of a commercial transcritical CO2 refrigeration plant with a R-152a dedicated mechanical subcooling. International Journal of Refrigeration 121, 258-268.

[29] Dai, B., Qi, H., Liu, S., Ma, M., Zhong, Z., Li, H., Song, M., Sun, Z., 2019. Evaluation of transcritical CO2 heat pump system integrated with mechanical subcooling by utilizing energy, exergy and economic methodologies for residential heating. Energy Conversion and Management 192, 202-220.

[30] Dai, B., Zhao, X., Liu, S., Yang, Q., Zhong, D., Hao, Y., Hao, Y., 2020. Energetic, exergetic and exergoeconomic assessment of transcritical CO2 reversible system combined with dedicated mechanical subcooling (DMS) for residential heating and cooling. Energy Conversion and Management 209, 112594.

[31] Lawrence, N., Elbel, S., Hrnjak, P.S., 2018. Design and validation of a transcritical CO2 mobile refrigerated container system for military applications, in: 13th IIR Gustav Lorentzen Conference on Natural Refrigerants. pp. 882–890.

[32] Barta, R.B., Hugenroth, J.J., Groll, E.A., 2018. Modeling of S-RAM energy recovery compressor integration in a transcritical carbon dioxide cycle for application in multi-temperature refrigerated container systems, in: 13th IIR Gustav Lorentzen Conference. https://doi.org/10.18462/iir.gl.2018.1117.

[33] Mazyar Karampour and Samer Sawalha. "State-of-the-art integrated CO2 refrigeration system for supermarkets: A comparative analysis". In: *International Journal of Refrigeration* 86 (Feb. 2018), pp. 239–257. ISSN: 0140-7007. DOI: 10.1016/J.IJREFRIG.2017.11.006.

[34] Minetto, S., Brignoli, R., Zilio, C., Marinetti, S., 2014. Experimental analysis of a new method for overfeeding multiple evaporators in refrigeration systems. International Journal of Refrigeration 38, 1–9.

[35] Gullo, P., Hafner, A., Cortella, G., 2017. Multi-ejector R744 booster refrigerating plant and air conditioning system integration – A theoretical evaluation of energy benefits for supermarket applications. International Journal of Refrigeration 75, 164–176. https://doi.org/10.1016/J.IJREFRIG.2016.12.009.

[36] Sawalha, S., 2008. Theoretical evaluation of trans-critical CO2 systems in supermarket refrigeration. Part II: System modifications and comparisons of different solutions. International Journal of Refrigeration 31, 525–534. https://doi.org/10.1016/J.IJREFRIG.2007.05.018.

[37] Gullo, P., Hafner, A., Banasiak, K., 2018. Transcritical R744 refrigeration systems for supermarket applications: Current status and future perspectives. International Journal of Refrigeration 93, 269–310. https://doi.org/10.1016/j.ijrefrig.2018.07.001.

[38] Bush, J., Beshr, M., Aute, V., Radermacher, R., 2017. Experimental evaluation of transcritical CO2 refrigeration with mechanical subcooling. Science and Technology for the Built Environment, 1-13.

[39] Bush, J., Aute, V., Radermacher, R., 2018. Transient simulation of carbon dioxide booster refrigeration system with mechanical subcooler in demand response operation. Science and Technology for the Built Environment 24, 687-699.

[40] Jesús Catalán-Gil et al. "Energy analysis of dedicated and integrated mechanical subcooled CO2 boosters for supermarket applications". In: *International Journal of Refrigeration* 101 (May 2019), pp. 11–23. ISSN: 0140-7007. DOI: 10.1016/J.IJREFRIG.2019.01.034.

[41] D'Agaro, P., Coppola, M.A., Cortella, G., 2020. Effect of dedicated mechanical subcooler size and gas cooler pressure control on transcritical CO2 booster systems. Applied Thermal Engineering, 116145.

[42] Gullo, P., Elmegaard, B., Cortella, G., 2016. Energy and environmental performance assessment of R744 booster supermarket refrigeration systems operating in warm climates. International Journal of Refrigeration 64, 61-79.

[43] Polzot A., Gullo P., D'Agaro P., Cortella G., 2016a. Performance evaluation of a R744 booster system for supermarket refrigeration, heating and DHW, Proceedings of the 12th IIR Gustav Lorentzen Natural

Working Fluids Conference, Edinburgh (UK), Paper ID 1022. doi: 10.18462/iir.gl.2016.1022 .

[44] Karampour, M., Sawalha, S., 2017. Energy efficiency evaluation of integrated CO 2 trans-critical system in supermarkets: a field measurements and modelling analysis. Int. J. Refrig. 82, 470–486. doi: 10.1016/j.ijrefrig.2017.06.002 .

[45] E. Oró et al. "Review on phase change materials (PCMs) for cold thermal energy storage applications". In: *Applied Energy* 99 (2012), pp. 513–533. ISSN: 0306-2619. DOI: https://doi.org/10.1016/j.apenergy.2012.03.058. URL: https://www.sciencedirect.com/science/article/pii/S0306261912002784.

[46] A. Polzot, P. D'Agaro, P. Gullo, G. Cortella, Water storage to improve the efficiency of CO2 commercial refrigeration systems., Proceedings of the 24th IIR International Congress of Refrigeration: Yokohama, Japan, August 16-22, 2015. (2015) 2765–2772. https://doi.org/10.18462/IIR.ICR.2015.0339.

[47] A. Polzot, P. D'Agaro, P. Gullo, G. Cortella, Water storage to improve the efficiency of CO2 commercial refrigeration systems., Proceedings of the 24th IIR International Congress of Refrigeration: Yokohama, Japan, August 16-22, 2015. (2015) 2765–2772. https://doi.org/10.18462/IIR.ICR.2015.0339.

[48] S. Sanaye, A. Shirazi, Four E analysis and multi-objective optimization of an ice thermal energy storage for air-conditioning applications, International Journal of Refrigeration. 36 (2013) 828–841. https://doi.org/10.1016/J.IJREFRIG.2012.10.014.

[49] Y.H. Yau, B. Rismanchi, A review on cool thermal storage technologies and operating strategies, Renewable and Sustainable Energy Reviews. 16 (2012) 787–797. https://doi.org/10.1016/J.RSER.2011.09.004.

[50] A. Beghi, L. Cecchinato, M. Rampazzo, F. Simmini, Energy efficient control of HVAC systems with ice cold thermal energy storage, J Process Control. 24 (2014) 773–781. https://doi.org/10.1016/J.JPROCONT.2014.01.008.

[51] J.A. Candanedo, V.R. Dehkordi, M. Stylianou, Model-based predictive control of an ice storage device in a building cooling system, Appl Energy. 111 (2013) 1032–1045. https://doi.org/10.1016/J.APENERGY.2013.05.081.

[52] Ju Hyok Kim, Jin Min Cho, and Min Soo Kim. "Cooling performance of several CO 2 /propane mixtures and glide matching with secondary heat transfer fluid". In: (). DOI: 10.1016/j.ijrefrig.2007.11.009.

[53] X. P. Zhang et al. "Determination of the optimum heat rejection pressure in transcritical cycles working with R744/R290 mixture". In: *Applied Thermal Engineering* 54 (1 May 2013), pp. 176–184. ISSN: 1359-4311. DOI: 10.1016/J.APPLTHERMALENG.2013.02.006.

[54] Dong Wang, Yuehong Lu, and Leren Tao. "Thermodynamic analysis of CO2 blends with R41 as an azeotropy refrigerant applied in small refrigerated cabinet and heat pump water heater". In: *Applied Thermal Engineering* 125 (Oct. 2017), pp. 1490–1500. ISSN: 1359-4311. DOI: 10.1016/J.APPLTHERMALENG.2017.07.009.

[55] Kumar, K., Kumar, P., 2019. Analysis of Propane + CO2 mixture as a working fluid in a vapor compression refrigeration system., 8th Conference on Ammonia and CO2 Refrigeration Technology. Proceedings: Orhid, North Macedonia, , 2019.

[56] Zhen Zhao et al. "Theoretical investigation and comparative analysis of the Linde–Hampson refrigeration system using eco-friendly zeotropic refrigerants based on R744/R1234ze(Z) for freezing process applications". In: *International Journal of Refrigeration* 145 (Jan. 2023), pp. 30–39. ISSN: 0140-7007. DOI: 10.1016/J.IJREFRIG.2022.09.036.

[57] Jintao Xie et al. "Numerical investigation on thermodynamic performance of CO 2-based mixed refrigerants applied in transcritical system". In: 147 (2022), pp. 6883–6892. DOI: 10.1007/s10973-021-11011-x. URL: https://doi.org/10.1007/s10973-021-11011-x.

[58] G. Vaccaro, A. Milazzo, and L. Talluri. "Thermodynamic assessment of trans-critical refrigeration systems utilizing CO2-based mixtures". In: *International Journal of Refrigeration* (Sept. 2022). ISSN: 0140-7007. DOI: 10.1016/J.IJREFRIG.2022.09.013.

[59] Tobaly P., Terrier M. F., Bouteiller P., 2018. CO2 + propane mixture as working fluid for refrigeration in hot climates. Experimental results of energy efficiency tests., 13th IIR Gustav Lorentzen Conference on Natural Refrigerants (GL2018). Proceedings. Valencia, Spain.

[60] Binbin Yu et al. "Performance improvements evaluation of an automobile air conditioning system using CO2-propane mixture as a refrigerant". In: *International Journal of Refrigeration* 88 (Apr. 2018), pp. 172–181. ISSN: 0140-7007. DOI: 10.1016/J.IJREFRIG.2017.12.016.

[61] Sánchez, D., Cabello, R., Llopis, R., Catalán, J., Nebot, L., Calleja, D., Gil, E., 2019. Energy improvements in a standalone transcritical refrigeration system using a low-GWP mixture of CO2/R1270, Refrigeration Science and Technology, pp. 2633-2640.

[62] Chengyu Li et al. "Thermodynamic analysis of CO2 blends for vehicle heat pump at cold ambient temperature". In: *Frontiers in Energy Research* 10 (Aug. 2022). ISSN: 2296598X. DOI: 10.3389/fenrg.2022.960600.

[63] Baomin Dai et al. "Energetic performance of transcritical CO2 refrigeration cycles with mechanical subcooling using zeotropic mixture as refrigerant". In: *Energy* 150 (May 2018), pp. 205–221. ISSN: 0360-5442. DOI: 10.1016/J.ENERGY.2018.02.111.

[64] ANNEX XV RESTRICTION REPORT – Per- and polyfluoroalkyl substances (PFASs) - PROPOSAL FOR A RESTRICTION (ECHA)-February 2023.

[65] Lemmon E. W., I.H., B., L., H.M., O., M.M., 2018. NIST Standard Reference Database 23: Reference Fluid Thermodynamic and Transport Properties-REFPROP, Version 10.0, National Institute of Standards and Technology.

[66] Ian H. Bell et al. *Survey of data and models for refrigerant mixtures containing halogenated olefins*. June 2021. DOI: 10.1021/acs.jced.1c00192.

[67] Ian H Bell and Eric W Lemmon. "Automatic Fitting of Binary Interaction Parameters for Multi-fluid Helmholtz-Energy-Explicit Mixture Models". In: (). DOI: 10.1021/acs.jced.6b00257. URL: https://pubs.acs.org/sharingguidelines.

[68] Lemmon, E. and McLinden, M. (2001), Method for Estimating Mixture Equation of State Parameters, Thermophysical Properties and Transfer Processes of New Refrigerants, Paderborn, -1 (Accessed September 6, 2023).

[69] P H Van Konynenburg and R L Scott. *Critical Lines and Phase Equilibria in Binary Van Der Waals Mixtures*. 1980. URL: https://about.jstor.org/terms.

[70] Niramol Juntarachat et al. "Experimental measurements and correlation of vapor-liquid equilibrium and critical data for the CO2 + R1234yf and CO2 + R1234ze(E) binary mixtures". In: *International Journal of Refrigeration* 47 (2014), pp. 141–152. ISSN: 01407007. DOI: 10.1016/j.ijrefrig.2014.09.001.

[71] Hakim Madani et al. "(Vapor + liquid) equilibrium data for (carbon dioxide + 1,1-difluoroethane) system at temperatures from (258 to 343) K and pressures up to about 8 MPa". In: *Journal of Chemical Thermodynamics* 40 (10 Oct. 2008), pp. 1490–1494. ISSN: 00219614. DOI: 10.1016/j.jct.2008.06.002.

[72] Ian H Bell and Ulrich K Deiters. "On the Construction of Binary Mixture p-x and T-x Diagrams from Isochoric Thermodynamics". In: *American Institute of Chemical Engineers AIChE J* 64 (2018), pp. 2745–2757. DOI: 10.1002/aic.16074. URL: https://aiche.onlinelibrary.wiley.com/doi/10.1002/aic.16074.

[73] Nebot-Andrés, L., Calleja-Anta, D., Sánchez, D., Cabello, R., Llopis, R., 2019. Thermodynamic analysis of a CO2 refrigeration cycle with integrated mechanical subcooling. Energies 13.

[74] Man Hoe Kim, Jostein Pettersen, and Clark W. Bullard. "Fundamental process and system design issues in CO2 vapor compression systems". In: *Progress in Energy and Combustion Science* 30 (2 Jan. 2004), pp. 119–174. ISSN: 0360-1285. DOI: 10.1016/J.PECS.2003.09.002.

[75] Rodrigo Llopis et al. "Experimental evaluation of zeotropic refrigerants in a dedicated mechanical subcooling system in a CO2 cycle; [Évaluation expérimentale des frigorigènes zéotropes dans un système à sous-refroidissement mécanique dédié dans un cycle au CO2]". In: *International Journal of Refrigeration* 128 (2021). Cited by: 10; All Open Access, Green Open Access, Hybrid Gold Open Access,

pp. 287–298. DOI: 10.1016/j.ijrefrig.2021.05.028. URL: https://www.scopus.com/inward/record.uri?eid=2-s2.0-85107729968&doi=10.1016%2fj.ijrefrig.2021.05.028&partnerID=40&md5=f4135e2db5a2cdfcc081a98ae56907e6.

[76] Vishaldeep Sharma, Brian Fricke, and Pradeep Bansal. "Comparative analysis of various CO2 configurations in supermarket refrigeration systems". In: *International Journal of Refrigeration* 46 (Oct. 2014), pp. 86–99. ISSN: 0140-7007. DOI: 10.1016/J.IJREFRIG.2014.07.001.

[77] Nilesh Purohit et al. "Integrated supermarket refrigeration for very high ambient temperature". In: *Energy* 165 (Dec. 2018), pp. 572–590. ISSN: 0360-5442. DOI: 10.1016/J.ENERGY.2018.09.097.

[78] Martinez-Angeles, M., Sicco, E., Toffoletti, G., Nebot-Andrés, L., Sánchez, D., Cabello, R., Cortella, G., Llopis, R., 2023. Evaluation of CO2-doped blends in single-stage with IHX and parallel compression refrigeration architectures.

[79] Dai, B., Liu, S., Sun, Z., Ma, Y., 2017. Thermodynamic Performance Analysis of CO2 Transcritical Refrigeration Cycle Assisted with Mechanical Subcooling. Energy Procedia 105, 2033-2038.

[80] Nebot-Andrés, L., Llopis, R., Sánchez, D., Catalán-Gil, J., Cabello, R., 2017. CO2 with Mechanical Subcooling vs. CO2 Cascade Cycles for Medium Temperature Commercial Refrigeration Applications Thermodynamic Analysis. Applied Sciences 7, 955.

[81] Lemmon, E.W., Huber, M.L., McLinden, M.O., 2013. REFPROP, NIST Standard Reference Database 23, v.9.1. National Institute of Standards, Gaithersburg, MD, U.S.A.

[82] Daniel Sánchez et al. "Energetic evaluation of a CO2 refrigeration plant working in supercritical and subcritical conditions". In: *Applied Thermal Engineering* 66 (1-2 May 2014), pp. 227–238. ISSN: 1359-4311. DOI: 10.1016/J.APPLTHERMALENG.2014.02.005.

[83] Laura Nebot-Andrés et al. "Experimental determination of the optimum intermediate and gas-cooler pressures of a commercial transcritical CO2 refrigeration plant with parallel compression". In: *Applied Thermal Engineering* 189 (May 2021), p. 116671. ISSN: 1359-4311. DOI: 10.1016/J.APPLTHERMALENG.2021.116671.

[84] R. J. Moffat. "Using Uncertainty Analysis in the Planning of an Experiment". In: *Journal of Fluids Engineering* 107.2 (June 1985), pp. 173–178. ISSN: 0098-2202. DOI: 10.1115/1.3242452. eprint: https://asmedigitalcollection.asme.org/fluidsengineering/article-pdf/107/2/173/5596024/173_1.pdf. URL: https://doi.org/10.1115/1.3242452.

[85] Riley B. Barta, Davide Ziviani, and Eckhard A. Groll. "Design and commissioning of a modular multi-stage two-evaporator transcritical CO2 test stand". In: *International Journal of Refrigeration* 130 (Oct. 2021), pp. 392–403. ISSN: 0140-7007. DOI: 10.1016/J.IJREFRIG.2021.05.033.

[86] Taylor, B.N., Kuyatt, C.E., 1994. NIST Technical Note 1297 1994 Edition, Guidelines for Evaluating and Expressing the Uncertainty of NIST Measurement Results. National Institute of Standards and Technology 1–20.

[87] Fang Liu, Yong Li, and Eckhard A. Groll. "Performance enhancement of CO2 air conditioner with a controllable ejector". In: *International Journal of Refrigeration* 35.6 (2012), pp. 1604–1616. ISSN: 0140-7007. DOI: https://doi.org/10.1016/j.ijrefrig.2012.05.005. URL: https://www.sciencedirect.com/science/article/pii/S0140700712001193.

[88] J. Kohler, C. Richter, W. Tegethoff, C. Tischendorf, Experimental and theoretical study of a CO2 ejector refrigeration cycle, in: Vortrag, VDA Winter Meeting, Saalfelden, 2007.

[89] Klein S.A, W.A. Beckman, J.A. Duffie, TRNSYS 17, A Transient System Simulation Program, Solar Energy Laboratory, University of Wisconsin, Madison, USA , (2010).

[90] London A.L., Seban R.A., Rate of Ice Formation. Transactions of the A.S.M.E., (1943) 771–778.

[91] A.H.W. Lee, J.W. Jones, Modeling of an ice-on-coil thermal energy storage system, Energy Convers Manag. 37 (1996) 1493–1507. https://doi.org/10.1016/0196-8904(95)00224-3.

[92] Fabio Giunta and Samer Sawalha. "Techno-economic analysis of heat recovery from supermarket's CO2 refrigeration systems to district heating networks". In: *Applied Thermal Engineering* 193 (July 2021), p. 117000. ISSN: 1359-4311. DOI: 10.1016/J.APPLTHERMALENG.2021.117000.

[93] Italian Regulatory Authority for Energy, Networks and Environment (ARERA), prices and tariffs, IV semester 2022, (n.d.).

[94] Aprea, C., de Rossi, F., Mastrullo, R., 1997. The uncertainties in measuring vapour compression plant performances. Measurement 21, 65-70.